CO – AXIAL CONDUCTING MATERIAL FOR SOLID OXIDE FUEL CELL

MANOP MASOMTOB

A THESIS SUBMITTED IN PARTIAL FULFILLMENT

OF THE REQUIREMENT FOR THE DEGREE OF

MASTER OF ENGINEERING IN AUTOMOTIVE ENGINEERING

(INTERNATIONAL PROGRAM)

INTERNATIONAL COLLEGE

KING MONGKUT'S INSTITUTE OF TECHNOLOGY LADKRABANG

2010

KMITL-2010-IC-M-004-003

Thesis Title	Co-Axial Conducting Material for Solid Oxide Fuel Cell
Student	Mr. Manop Masomtob
Student ID.	50061911
Degree	Master of Engineering
Program	Automotive Engineering (International Program)
Year	2010
Thesis Advisor	Assoc. Prof. Jarruwat Charoensuk
	Dr. Sumittra Charojrochkul
	Prof. Dr. Katsunori Hanamura

ABSTRACT

Solid Oxide Fuel Cells (SOFCs) have attracted a number of researchers due to their efficiency as alternative energy devices. Studies have been conducted to investigate different components in SOFCs to improve the performances. Current collecting wires are the components which have affected the overall performance. Since SOFCs are normally operated in the temperature range of 700-1000°C in dual atmospheres, the wiring material must be able to function at this condition. Currently, the material used to make the wires is platinum because of its high electrical conductivity, high melting point and oxidation resistant. However, platinum is expensive, especially for the practical operation of SOFCs. Silver could be an alternative choice due to its very high electrical conductivity. Nevertheless, the melting point of silver is rather low (900 - 960°C). In this thesis, modified current collecting wires, Ag_4625, Ag_4968, Au_4625 and Au_4968, have been used in the temperature range of 100-1000°C. Their conductivity curves have demonstrated higher performances in comparison with the systems employing Pt and gold wires. In addition, the cost is reduced approximately 800-1000 times from that of the traditional material used, and the behaviour of the contact interface between Ag and Au with SS 316L has been studied using SEM for microstructural investigation at the interface while the thermal stress of the contact interfaces were simulated using a finite element COMSOL program at each temperature.

In summary, the newly invented technique for the electric current conducting wire can be applied for use in a solid oxide fuel cell. According to experimental on electrical conductivity and the behaviour of contact interface, the conducting wires are not only capable of conducting electric current but also succeed in operating at high temperature.

ACKNOWLEDGEMENTS

This thesis could not be completed without the assistance of many persons to whom I would like to express my sincere appreciation.

First of all, I would like to sincerely thank my advisor, Dr. Sumittra Charojrochkul, who has given me many helpful suggestions, useful advice and fruitful discussion during the undertaken research. Also I would like to sincerely thank Assoc. Prof. Jarruwat Charoensuk and Prof. Dr. Katsunori Hanamura for kind advices, suggestions and helps.

I really appreciate National Science and Technology Development Agency (NSTDA) who provided the full scholarship for studying in the master program and National Metal and Materials Technology Center (MTEC), especially for providing laboratory equipments and instruments as well as financial support. Moreover, I would like to thank to all Electrochemical Materials and System Laboratory's members for helping me during the experiment.

Finally, I am very grateful to my family for all love, caring, understanding and motivation throughout my life.

Manop Masomtob

CONTENTS

CONTENTS (CONT.)

CONTENTS (CONT.)

LIST OF TABLES

LIST OF FIGURES

LIST OF FIGURES (CONT.)

LIST OF FIGURES (CONT.)

LIST OF FIGURES (CONT.)

LIST OF FIGURES (CONT.)

CHAPTER 1

INTRODUCTION

1.1 Significance and Background

At present, a large amount of energy is used in order to respond to various requirements of our lives. As for the world energy consumption, prices of petroleum and a number of emission gases such as NO_X, SO_2, and CO_2 have been increasing continuously. Fuel cells, which are electrochemical conversion devices, are one of the alternative energy used. They produce electricity, water and heat from fuel (on the anode side) and an oxidant (on the cathode side), which react in the presence of an electrolyte.

Based on the electrolyte materials, fuel cells can be typically classified into several types, i.e. Alkaline Fuel Cell (AFC), Proton Exchange Membrane Fuel Cell (PEMFC), Phosphoric Acid Fuel Cell (PAFC), Molten Carbonate Fuel Cell (MCFC), and Solid Oxide Fuel Cell (SOFC). SOFCs have a high power density and operate at relatively high temperatures at 800-1000°C which can be applied to be a power station and combined with other types of power generator to increase the efficiency.

One of the key components in SOFC system is an electric current conducting wire, which conducts electric current under high temperature. Most of electric conducting wires consist of platinum, silver and gold. They are very expensive and not durable when using them for a long time at high temperature.

This Thesis, therefore, focuses on an electric current conducting wire which is fabricated using a new technique. This technique is used with the conducting wire to increase the strength while maintaining high conductivity. In addition, this technique has still to be optimized for commercial application in the future.

1.2 Objectives

1.2.1 To study possibility of new technique to fabricate an electric conducting wire.

1.2.2 To study the behaviour at the contact interface of the electric conducting wire

1.3 Scopes

1.3.1 The first part was on the properties of materials comprising of gold, platinum, silver and stainless steel at high temperature.

1.3.2 The second part was to prove the new technique in fabricating the electric conducting wires.

1.3.3 The final part was to investigate the behaviour at the contact interface.

1.4 Expected Benefits

1.4.1 Understanding the process mechanism occurred at the contact interface of electric conducting wire.

1.4.2 Obtain an adequate electric conducting wire for an application in SOFC.

CHAPTER 2

THEORY AND LITERATURE REVIEW

2.1 Fuel Cells

A fuel cell is an energy conversion device which converts a gaseous fuel to electricity and heat in the presence of an oxidant. Because fuel cells have high energy efficiency and are environmentally friendly, they are potentially attractive in producing electricity. Moreover, they can be operated in a flexible and modular design since they do not suffer appreciably from problems of lubrication, wear, leakage and heat loss, which affect the reliability of traditional heat engines (Hirschenhofer *et al.*, 1998).

The fuel cell was invented in 1839 by Sir William Grove; however, the first real application was in the NASA space program onboard Apollo spacecraft in the 1960s when it was used to produce electricity and drinking water (Hirschenhofer *et al.*, 1998).

A fuel cell consists of an electrolyte sandwiched between two electrodes, called cathode and anode where the electrochemical reactions take place. The electrocatalytic oxidation of hydrogen at the anode and the reduction of oxygen at the cathode create a potential difference between these electrodes. This can be exploited if a gas-tight electrolyte between the electrodes allows for ionic mass and charge transport. In an actual application, fuel cells are connected in series to obtain a greater output potential. An interconnect plate is always installed to provide the electronic contact between the anode of one cell to the cathode of the adjacent cell (Hirschenhofer *et al.*, 1998).

Although the operational principles of a fuel cell are similar to those of a typical primary battery, they differ in several aspects. A battery is an energy storage device and the amount of energy available is determined by the amount of chemical reactant stored within the battery itself. The electrical energy produced decreases as the chemical reactant is consumed. A fuel cell, in contrast, can produce electrical energy continuously at a constant rate as long as the fuel and oxidant are supplied.

2.2 Types of Fuel Cells

Fuel cells are classified by the types of electrolyte. The characteristics of chemical reactions which occur in the fuel cell, the kind of catalysts required, the operating temperature

range, the fuel and the oxidizing agent required, affect the applications for which these cells are most suitable. Some of the popular fuel cells and their characteristics are listed in Table 2.1 [1].

Table 2.1 Types of fuel cells.

Fuel cell type	Electrolyte	Charge carrier	Operating temp.	Fuel	Electric efficiency	Application
AFC	KOH	OH^-	60 -120°C	Pure H_2	35-55%	<5kW military, space
PEMFC	Solid polymer	H^+	50 - 100°C	Pure H_2, tolerates CO_2	35-45%	5-250kW automotive, portable CHP
DMFC	Solid polymer	H^+	50 - 250°C	CH_3OH, C_2H_5OH,	35-45%	mobile application
PAFC	Phosphoric acid	H^+	~ 220°C	Pure H_2, tolerates CO_2	40%	200kW CHP
MCFC	Lithium and potassium carbonate	CO_3^{2-}	~ 650°C	H_2, CO, CH_4, tolerates CO_2	>50%	200kW-MW CHP and stand alone
SOFC	Yttria, Zirconia	O^{2-}	~ 1000°C	H_2, CO, CH_4, tolerates CO_2	>50%	2kW-MW CHP and stand alone

2.2.1 Alkaline Fuel Cells (AFCs)

An Alkaline fuel cell (AFC) is the first type used on spacecrafts to produce electrical energy and water. The electrolyte is a solution of potassium hydroxide in water. A variety of non-precious metals can be used as a catalyst at both the anode and cathode. High-temperature AFC operates at temperatures between 100°C and 250°C. However, recent designs of AFC operate at lower temperatures of roughly 23°C to 70°C.

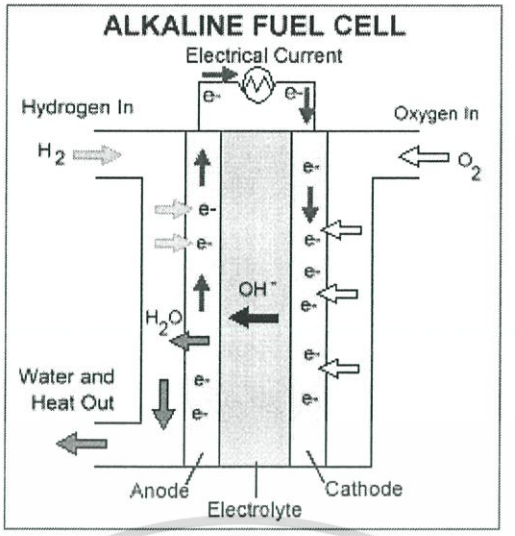

Figure 2.1 Alkaline fuel cell diagram (U.S. Department of Energy, 2008).

The chemical reactions which occur in the cell are responsible for high performance of AFC. They have also demonstrated efficiencies close to 60% in the space applications.

The disadvantage of this fuel cell type is that it is easily poisoned by carbon dioxide (CO_2). In fact, even a small amount of CO_2 in air affect this cell's operation, making it necessary to purify both hydrogen and oxygen used in the cell. This purification process is costly. Susceptibility to poisoning also affects the cell's lifetime, further adding to the cost.

Cost is less of a factor for remote locations, such as space or under the sea. However, effectively competing in most mainstream commercial markets, these fuel cells will have to become more cost-effective. AFC stacks have been shown to maintain sufficiently stable operation for more than 8,000 operating hours. To be economically viable in large-scale utility applications, these fuel cells need to reach operating times exceeding 40,000 hours, something that has not yet been achieved due to material durability issues. This obstacle is possibly the most significant in commercializing this fuel cell technology.

2.2.2 Polymer Electrolyte Fuel Cell (PEFC)

Polymer electrolyte fuel cell or proton exchange membrane fuel cell (PEMFC) delivers a high-power density and offers advantages of low weight and volume, compared with other fuel cells. PEM fuel cells use a solid polymer as an electrolyte and porous carbon electrodes containing platinum catalyst. They need only hydrogen, oxygen from air, and water to operate and do not require corrosive fluids like other fuel cells. They are typically fueled with pure hydrogen supplied from storage tanks or on-board reformers. For a system efficiency, a small 30

kW AC powerplants will likely be 35% fuel to electricity efficient, 200 kW units 40% and large units 45% (Ben Wiens, 2008).

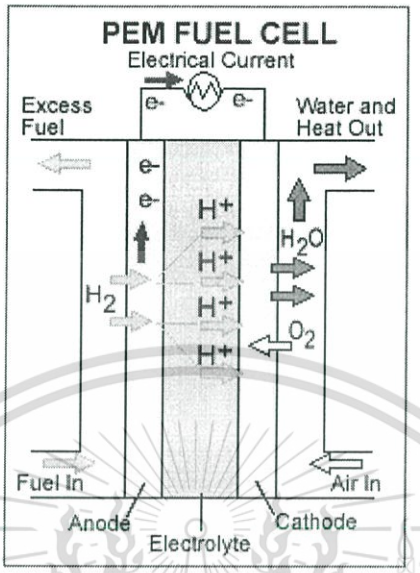

Figure 2.2 Polymer electrolyte membrane fuel cell (U.S. Department of Energy, 2008).

Polymer electrolyte fuel cells operate at relatively low temperatures, around 80°C. Low-temperature operation allows them to start quickly (less warm-up time) and results in less wear on system components, resulting in better durability. However, due to its operation in low temperature, it requires a noble-metal catalyst (typically platinum). The platinum catalyst is also extremely sensitive to carbon monoxide (CO) poisoning, making it necessary to employ an additional reactor to reduce CO in the fuel gas if hydrogen is derived from alcohol or hydrocarbon fuel. This also adds cost. Developers are currently exploring platinum/ruthenium catalysts which are more resistant to CO.

PEMFCs are used primarily for transportation applications and some stationary applications. Due to their fast start-up time, low sensitivity to orientation, and favourable power-to-weight ratio, PEMFCs are particularly suitable for use in passenger vehicles, such as cars and buses.

A significant barrier in using these fuel cells in vehicles is a hydrogen storage. Most fuel cell vehicles (FCVs) powered by pure hydrogen must store hydrogen on-board as a compressed gas in pressurized tanks. Due to the low-energy density of hydrogen, it is difficult to store enough hydrogen on-board to allow vehicles to travel the same distance as gasoline-powered vehicles before refuelling, typically 300–400 miles. Higher-density liquid fuels, such as methanol, ethanol,

natural gas, liquefied petroleum gas, and gasoline, can be used as a fuel, but the vehicles must have an on-board fuel processor to reform them to hydrogen. This requirement increases costs and maintenance. The reformer also releases carbon dioxide, though less than that emitted from current gasoline-powered engines.

2.2.3 Direct Methanol Fuel Cell (DMFC)

Most fuel cells are powered by hydrogen, which can be fed to the fuel cell system directly or can be generated within the fuel cell system by reforming hydrogen-rich fuels such as methanol, ethanol, and hydrocarbon fuels. However, direct methanol fuel cells are powered by pure methanol, which is mixed with steam and fed directly to the fuel cell anode.

Direct methanol fuel cells do not have many of the fuel storage problems typical of some fuel cells because methanol has a higher energy density than hydrogen—though less than gasoline or diesel fuel. Methanol is also easier to be transported and supplied to public using our current infrastructure because it is liquid, like gasoline.

Direct methanol fuel cell technology is relatively new compared with other types of fuel cells powered by pure hydrogen.

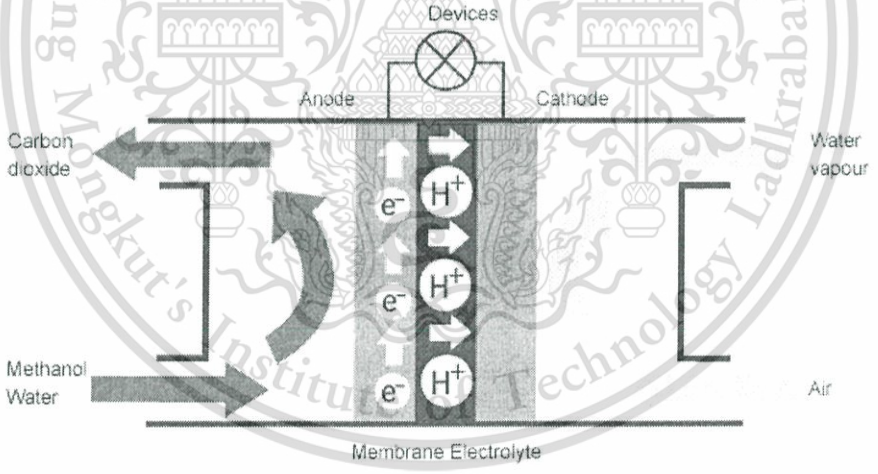

Diagram of a direct-methanol fuel cell

Figure 2.3 Direct methanol fuel cell (www.sfc.com, 2009).

2.2.4 Phosphoric Acid Fuel Cell (PAFC)

Phosphoric acid fuel cells use liquid phosphoric acid as an electrolyte, in which the acid is contained in a Teflon-bonded silicon carbide matrix, and porous carbon electrodes containing a platinum catalyst.

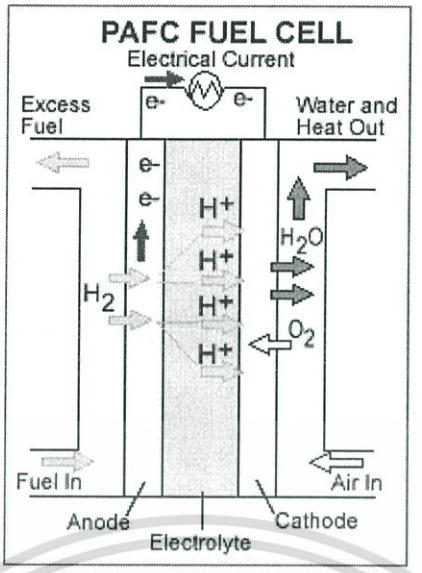

Figure 2.4 Phosphoric acid fuel cell (U.S. Department of Energy, 2008).

The phosphoric acid fuel cell (PAFC) is considered the "first generation" of modern fuel cells. This type of fuel cell is typically used for stationary power generation, but some PAFCs have been used to power large vehicles such as city buses.

PAFCs are more tolerant to impurities in fossil fuels that have been reformed into hydrogen than PEMFCs, which are easily "poisoned" by carbon monoxide because carbon monoxide binds to the platinum catalyst at the anode, hence decreasing the fuel cell's efficiency. They are 85% efficient when used for the co-generation of electricity and heat but less efficient when generating electricity alone (37%–42%). This is only slightly more efficient than combustion-based power plants, which typically operate at 33%–35% efficiency. PAFCs are also less powerful than other fuel cells, given the same weight and volume. As a result, these fuel cells are typically large and heavy. PAFCs are also expensive. Like PEM fuel cells, PAFCs require an expensive platinum catalyst, which raises the cost of the fuel cell.

2.2.5 Molten Carbonate Fuel Cell (MCFC)

Molten carbonate fuel cells are currently being developed for natural gas and coal-based power plants for electric utility, industrial, and military applications. MCFCs are high-temperature fuel cells that use an electrolyte composed of a molten carbonate salt mixture suspended in a porous, chemically inert ceramic lithium aluminium oxide ($LiAlO_2$) matrix. Because they operate at extremely high temperatures of 650°C and above, non-precious metals can be used as catalysts at the anode and cathode, thus reducing the costs.

Improved efficiency is another reason MCFCs offer significant cost reductions over phosphoric acid fuel cells. Molten carbonate fuel cells can reach efficiencies approaching 60%, considerably higher than the 37%–42% efficiencies of a phosphoric acid fuel cell plant. When the waste heat is captured and used, overall fuel efficiencies can be as high as 85%.

Unlike alkaline, phosphoric acid, and polymer electrolyte fuel cells, MCFCs do not require an external reformer to convert more energy-dense fuels to hydrogen. Due to the high temperatures at which MCFCs operate, these fuels are converted to hydrogen within the fuel cell itself by a process called internal reforming, which also reduces cost.

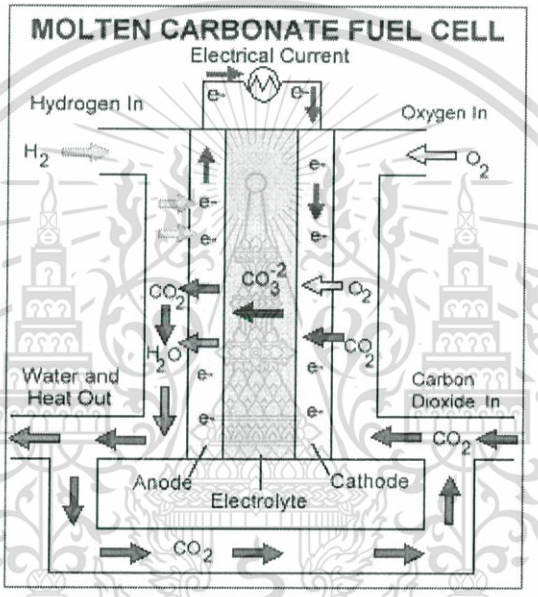

Figure 2.5 Molten carbonate fuel cell (U.S. Department of Energy, 2008).

Molten carbonate fuel cells are not prone to carbon monoxide or carbon dioxide poisoning, they can even use carbon monoxides as a fuel, making them more attractive for fuelling with gases made from coal. Because they are more resistant to impurities than other fuel cell types, scientists believe that they could even be capable of internal reforming of coal, assuming they can be made resistant to impurities such as sulphur and particulates that result from converting coal, a dirtier fossil fuel source than many others, into hydrogen.

The primary disadvantage of current MCFC technology is durability. The high temperatures at which these cells operate and the corrosive electrolyte used accelerate component breakdown and corrosion, decreasing cell life. Scientists are currently exploring corrosion-resistant materials for components as well as fuel cell designs which increase the cell life without decreasing the performance.

2.2.6 Solid Oxide Fuel Cell (SOFC)

Solid oxide fuel cells use a hard, non-porous ceramic compound as the electrolyte. Because the electrolyte is solid, the cells do not have to be constructed in the plate-like configuration typical of other fuel cell types. SOFCs are expected to be around 50% - 60% efficient at converting fuel to electricity. In applications designed to capture and utilize the system's waste heat (co-generation), overall fuel efficiencies could top 80%–85%.

SOFCs are also the most sulphur-resistant fuel cell type. They can tolerate several orders of magnitude more of sulphur than other cell types. In addition, they are not poisoned by CO, which can even be used as a fuel (K. Sasaki, 2002 and R. Suwanwarangkul, 2006) by using an internal reforming process. This property allows SOFCs to use gases from various hydrocarbon fuels such as natural gas, biogas, methanol and ethanol. However, these fuels must be reformed or gasified to produce synthesis gas mainly composing of H_2 and CO prior to entering an SOFC to increase the cell's efficiency.

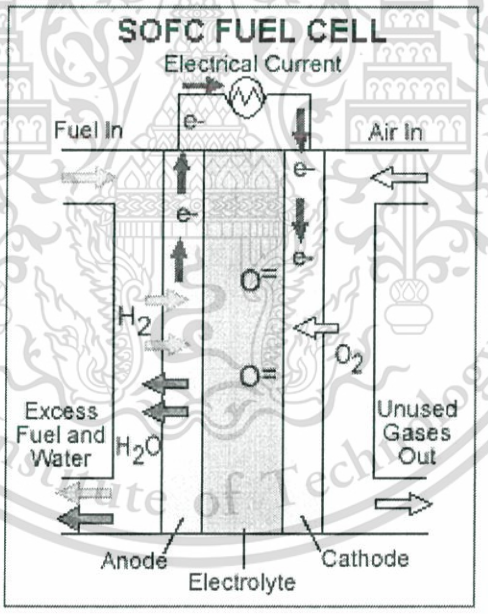

Figure 2.6 Solid oxide fuel cell (U.S. Department of Energy, 2008).

Solid oxide fuel cells operate at very high temperature around 1,000°C. High-temperature operation removes the need for precious-metal catalyst, thereby reducing cost. It also allows SOFCs to reform fuels internally, which enables the use of a variety of fuels and reduces the cost associated with adding a reformer to the system. Another advantage of high operating temperature is some of high temperature waste gases can be fed back to the system.

High-temperature operation has disadvantages. It results in a slow start up and requires significant thermal shielding to maintain heat and protect personnel, which may be acceptable for utility applications but not for transportation and small portable applications. The high operating temperatures also place stringent durability requirements on materials. The development of low-cost materials with high durability at the cell operating temperatures is the key technical challenge facing this technology.

Researchers are currently exploring the potential for developing lower-temperature SOFC operating at or below 800°C which are more durable and less costly. Lower-temperature SOFC produces less electrical power.

2.3 Material Properties

This part has presented properties of materials used in this thesis i.e. silver, gold, platinum and stainless steel. The material properties were set to be a function of temperature for use in simulation and other analyses.

2.3.1 Thermal Conductivity, *k*, is the property of a material which indicates its ability to conduct heat. It appears primarily in Fourier's Law for heat conduction. Thermal conductivity is measured in watts per Kelvin per metre ($W \cdot K^{-1} \cdot m^{-1}$).

Table 2.2 Thermal conductivity of metals as a function of temperature.

Materials	Equations	Range
Silver[6]	$TCS = -(5.786644).10^{-11}.T^4 + (2.109166).10^{-7}.T^3 - (2.937158).10^{-4}.T^2 + (9.979317).10^{-2}.T + 419.8682$	$(251\ K \leq T \leq 1235\ K)$
Gold[6]	$TCG = -(2.153620).10^{-11}.T^4 + (6.792908).10^{-8}.T^3 - (8.191375).10^{-5}.T^2 - (2.536626).10^{-2}.T + (330.6431)$	$(86\ K \leq T \leq 1338\ K)$
Platinum [6]	$TCP = -(2.748296).10^{-3}.T^5 + (0.2278691).10^{-1}.T^4 - (4.678988).T^3 + (18.16709).T^2 + (2.096991).10^2.T$ $TCP = (2.280531).10^{-5}.T^5 - (2.761393).10^{-3}.T^4 + (7.133190).10^{-2}.T^3 + (3.362113).T^2 - (2.011759).10^2.T + (2.978797).10^3$ $TCP = -(3.889706).10^{-7}.T^5 + (1.494028).10^{-4}.T^4 - (2.289560).10^{-2}.T^3 + (1.763533).T^2 - (69.25658).T + (1.212843).10^3$ $TCP = -(1.004522).10^{-10}.T^5 + (1.072687).10^{-7}.T^4 - (4.536814).10^{-5}.T^3 + (9.646914).10^{-3}.T^2 - (1.066855).T + (1.233886).10^2$ $TCP = -(6.133801).10^{-9}.T^3 + (2.646931).10^{-5}.T^2 - (1.557887).10^{-2}.T + 73.99627$	$(0\ K \leq T \leq 13K)$ $(14\ K \leq T \leq 50K)$ $(51\ K \leq T \leq 100K)$ $(101\ K \leq T \leq 285K)$ $(286\ K \leq T \leq 2045K)$

2.3.2 Specific Heat Capacity (J/kg.K), also known simply as specific heat, is the measurement of the heat energy required to increase the temperature of a unit quantity of a substance by a temperature interval.

Table 2.3 Specific heat capacity of metals as a function of temperature.

Materials	Equations	Range
Silver[7,8]	$SHS = -(1.768498).10^{-8}.T^3 + (5.007143).10^{-5}.T^2 + (1.705702).10^{-2}.T + 225.7065$	(301 K $\leq$ T $\leq$ 1235 K)
Gold[9]	$SHG = (1.148987).10^{2} + (3.228805).10^{-2}.T + (3.993522).10^{5}.T^{-2}$	(294 K $\leq$ T $\leq$ 1338 K)
Platinum [10,11]	$SHP = -(1.325633).10^{-6}.T^5 + (5.174165).10^{-5}.T^4 + (3.449445).10^{-4}.T^3 + (1.129466).10^{-3}.T^2 + (3.281349).10^{-2}.T$	(0 K $\leq$ T $\leq$ 19K)
	$SHP = -(3.445457).10^{-8}.T^5 + (1.359791).10^{-5}.T^4 - (2.010741).10^{-3}.T^3 + (0.1283953).T^2 - (1.986516).T + 10.30393$	(20 K $\leq$ T $\leq$ 119K)
	$SHP = -(2.455881).10^{-8}.T^4 + (2.453936).10^{-5}.T^3 - (9.418853).10^{-3}.T^2 + (1.721765).T + 0.4467027$	(120 K $\leq$ T $\leq$ 290K)
	$SHP = (7.556773).10^{-9}.T^3 - (1.836174).10^{-5}.T^2 + (3.986346).10^{-2}.T + 122.2187$	(291 K $\leq$ T $\leq$ 2000K)

2.3.3 Electrical Conductivity or specific conductivity is a measurement of an ability of material to conduct electric current. When an electrical potential difference is placed across a conductor, the flow of changes, gives rise to the electric current.

Table 2.4 Electrical conductivity of metals as a function of temperature.

Materials	Equations	Range
Silver[12]	$ECS = 1.0/\{(8.269045).10^{-18}.T^3 - (3.077059).10^{-15}.T^2 + (6.074742).10^{-11}.T - (1.812752).10^{-9}\}$	(201 K $\leq$ T $\leq$ 1235 K)
Gold[12]	$ECG = 1.0/\{(3.010164).10^{-14}.T^3 - (3.409278).10^{-13}.T^2 + (1.027514).10^{-12}.T + (2.194815).10^{-10}\}$	(1 K $\leq$ T $\leq$ 25 K)
	$ECG = 1.0/\{-(2.773737).10^{-14}.T^3 + (4.182944).10^{-12}.T^2 - (1.228888).10^{-10}.T + (1.390641).10^{-9}\}$	(26 K $\leq$ T $\leq$ 60 K)
	$ECG = 1.0/\{(6.950205).10^{-17}.T^3 - (4.632985).10^{-14}.T^2 + (9.057611).10^{-11}.T - (2.210068).10^{-9}\}$	(61 K $\leq$ T $\leq$ 400 K)
	$ECG = 1.0/\{(1.275961).10^{-17}.T^3 - (4.720065).10^{-16}.T^2 + (7.877041).10^{-11}.T - (1.145028).10^{-9}\}$	(401 K $\leq$ T $\leq$ 1338 K)
Platinum [11,13]	$ECP = 1.0/\{(3.513902).10^{-17}.T^5 - (7.414280).10^{-15}.T^4 + (5.545444).10^{-13}.T^3 - (1.305787).10^{-11}.T^2 + (1.415797).10^{-10}.T - (5.497611).10^{-10}\}$	(14 K $\leq$ T $\leq$ 47K)
	$ECP = 1.0/\{-(8.959380).10^{-19}.T^5 + (5.330375).10^{-16}.T^4 - (1.250757).10^{-13}.T^3 + (1.431636).10^{-11}.T^2 - (3.440080).10^{-10}.T + (1.845544).10^{-9}\}$	(48 K $\leq$ T $\leq$ 160K)
	$ECP = 1.0/\{-(4.447775).10^{-19}.T^4 + (6.694129).10^{-16}.T^3 - (4.107885).10^{-13}.T^2 + (5.233699).10^{-10}.T - (1.927892).10^{-8}\}$	(161 K $\leq$ T $\leq$ 600K)
	$ECP = 1.0/\{(2.814022).10^{-17}.T^3 - (1.600249).10^{-13}.T^2 + (5.552497).10^{-10}.T - (4.843579).10^{-8}\}$	(601 K $\leq$ T $\leq$ 2000K)

2.3.4 Thermal Expansion (1/K) is the tendency of matter to change in volume in response to a change in temperature. When a material is heated, its constituent particles move around more vigorously and by doing so generally maintain a greater average separation. Materials that contract with an increase in temperature are very uncommon; this effect is limited in size, and only occurs within limited temperature ranges. The degree of expansion divided by the change in temperature is called the material's coefficient of thermal expansion which usually varies with temperature

Table 2.5 Thermal expansion of metals as a function of temperature.

Materials	Equations	Range
Silver	$TES = (3.403595e).10^{-17}.T^5 - (4.019836).10^{-14}T^4 + (1.860200)10^{-11}.T^3 - (4.275991)10^{-9}.T^2 + (5.111237)10^{-7}.T - (8.786433)10^{-6}$	(30 K $\leq$ T $\leq$ 300 K)
Gold [16]	$TEG = (5.990814).10^{-13}.T^3 - (4.389255).10^{-10}.T^2 + (1.106436).10^{-7}.T + (4.040319).10^{-6}$ $TEG = -(5.528527).10^{-14}.T^2 + (5.169284).10^{-9}.T + (1.237291).10^{-5}$	(86 K $\leq$ T $\leq$ 200 K) (201 K $\leq$ T $\leq$ 1003K)

2.3.5 Density (ρ) is the ratio of its mass (m) to its volume (V), a measurement of how tightly the matter within it is packed together. Its SI units are kilograms per cubic metre (kg/m³). It is sometimes given in the cgs units of grams per cubic centimetre (g/cm³).

Table 2.6 Density of metals as a function of temperature.

Materials	Equations	Range
Silver [15-17]	$DS = (1.470941).10^{-10}.T^3 - (2.976784).10^{-7}.T^2 - (4.692536).10^{-4}.T + 10.65896$	(141 K $\leq$ T $\leq$ 873 K)
Gold[16]	$DG = (4.297982).10^{-11}.T^3 - (2.041944).10^{-7}.T^2 - (6.933844).10^{-4}.T + 19.50144$	(87 K $\leq$ T $\leq$ 1003 K)
Platinum [16, 18-21]	$DP = -(8.010422).10^{-12}.T^5 + (2.175230).10^{-9}.T^4 - (2.116082).10^{-7}.T^3 + (5.824972).10^{-6}.T^2 - (7.336997).10^{-5}.T + 21.51245$ $DP = -(1.883994).10^{-11}.T^4 + (1.502256).10^{-8}.T^3 - (4.701280).10^{-6}.T^2 + (1.433013).10^{-4}.T + 21.51032$ $DP = (4.698968).10^{-15}.T^4 - (3.171806).10^{-11}.T^3 - (1.752500).10^{-8}.T^2 - (5.675783).10^{-4}.T + 21.55719$	(0 K $\leq$ T $\leq$ 70 K) (71 K $\leq$ T $\leq$ 280 K) (281 K $\leq$ T $\leq$ 1973 K

2.3.6 Poisson's Ratio (ν), named after Simeon Poisson, is the ratio of the relative contraction strain, or transverse strain (normal to the applied load), divided by the relative extension strain, or axial strain (in the direction of the applied load). When a sample of material is stretched in one direction, it tends to contract (or rarely, expand) in the other two directions. Conversely, when a sample of material is compressed in one direction, it tends to expand (or rarely, contract) in the other two directions. Poisson's ratio (ν) is a measure of this tendency.

Table 2.7 Poisson's ratio of metals as a function of temperature.

Materials	Equations	Range
Silver [8,22]	$PRS = -(1.181682).10^{-15}.T^4 - (1.475466).10^{-11}.T^3 + (4.008534).10^{-8}.T^2 + (1.499369).10^{-5}.T + 36.02030$	$(1\ K \leq T \leq 1173\ K)$
Gold [24-27]	$PRG = (1.023495).10^{-11}.T^3 - (1.158876).10^{-8}.T^2 + (8.884688).10^{-6}.T + 0.4403494$	$(294\ K \leq T \leq 1280K)$
Platinum [28,29]	$PRP = -(5.685048).10^{-9}.T^2 - (1.897311).10^{-5}.T + 0.3516936$	$(0\ K \leq T \leq 70\ K)$

2.3.7 Young's Modulus (E) is a measure of the stiffness of a material. It is also known as the Young modulus, modulus of elasticity, elastic modulus (though the Young's modulus is actually one of several elastic moduli such as the bulk modulus and the shear modulus) or tensile modulus. It is defined as the ratio of stress over strain in the region in which Hooke's Law is obeyed for the material. This can be experimentally determined from the slope of a stress-strain curve created during tensile tests conducted on a sample of the material.

Young's modulus is named after Thomas Young, the 18th century British scientist. However, the concept was developed in 1727 by Leonhard Euler, and the first experiments that used the concept of Young's modulus in its current form were performed by the Italian scientist Giordano Riccati in 1782 -- predating Young's work by 25 years.

Table 2.8 Young's modulus of metals as a function of temperature.

Materials	Equations	Range
Silver [8, 22, 25]	$EMS = -(2.009828).10^{-11}.T^4 + (4.999535).10^{-8}.T^3 - (3.812331).10^{-5}.T^2 - (2.775728).10^{-2}.T + 91.43965$	$(1\ K \leq T \leq 1173\ K)$
Gold [25, 26, 27]	$EMG = -(8.937063).10^{-6}.T^2 - (2.049635).10^{-2}.T + 81.90431$ $EMG = (2.725845).10^{-11}.T^4 - (7.249967).10^{-8}.T^3 + (4.812792).10^{-5}.T^2 - (3.153455).10^{-2}.T + 82.49999$ $EMG = -(2.007007).10^{-5}.T^2 + (4.251872).10^{-4}.T + 77.36733$	$(0\ K \leq T \leq 93\ K)$ $(94\ K \leq T \leq 293\ K)$ $(294\ K \leq T \leq 1280\ K)$
Platinum [25, 28, 29]	$EMP = -(5.162897).10^{-8}.T^3 + (5.411562).10^{-5}.T^2 - (4.099535).10^{-2}.T + 166.7479$ $EMP = -(3.38).10^{-2}.T + 168.00$	$(93\ K \leq T \leq 293K)$ $(294\ K \leq T \leq 1480\ K)$

2.4 Electrical Theory [30]

The earliest accounts of electricity date from about 2,500 years ago, when it was discovered that static charge on a piece of amber was capable of attracting very light objects, such as feathers. The word itself--electricity--originated about 600 B.C.; comes from elektron, which was the ancient Greek word for amber. The true nature of electricity was not understood until much later, however. Following the work of Alessandro Volta and his invention of a copper-zinc battery, it was determined that the static electricity and the current that flows in metal wires connected to a battery are due to the same fundamental mechanism: the atomic structure of matter, consisting of a nucleus--neutrons and protons--surrounded by electrons. The fundamental electric quantity is charge, and the smallest amount of charge that exists is the charge carried by an electron, equal to

$$q_e = -1.602 \times 10^{-19} \quad C \tag{2.1}$$

The amount of charge associated with an electron is rather small. This, of course, has to do with the size of the unit used to measure charge, coulomb (C), named after Charles Coulomb. However, the definition of coulomb leads to an appropriate unit when electric current is defined, since current consists of the flow of very large number of charged particles. The other charge-carrying particle in an atom, the proton, is assigned a positive sign, and the same magnitude. The charge of a proton is

$$q_p = +1.602 \times 10^{-19} \quad C \tag{2.2}$$

2.4.1 Electric Current [30]

Electric current is defined as the rate of change passing through a predetermined area. Typically, this area is the cross-sectional area of a metal wire. Figure 2.7 depicts a macroscopic view of the flow of charge in a wire, where Δq units of charge flow through the cross-sectional area A in Δt units of time. The resulting current, i, is then given by

$$i = \frac{\Delta q}{\Delta t} \qquad \frac{C}{s} \tag{2.3}$$

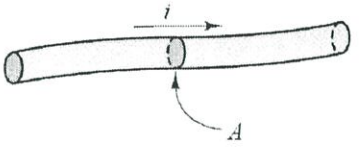

Figure 2.7 Current flow in an electric conductor.

The effect of the enormous number of elementary charges flow in which the relationship in differential form is:

$$i = \frac{dq}{dt} \quad \frac{C}{s} \tag{2.4}$$

The unit of electric current is called ampere (A), where 1 ampere = 1 coulomb/second. The name of the unit is a tribute to the French scientist Andr´e Marie Amp`ere. The electrical engineering convention states that the positive direction of current flow is that of positive charges. In metallic conductors, however, electric current is carried by negative charges. These charges are the free electrons in the conduction band, which are only weakly attracted to the atomic structure in metallic elements and are therefore easily displaced in the presence of electric fields.

2.4.2 Voltage [30]

Charge moving in an electric circuit gives rise to a current, as stated in the preceding section. Naturally, it must take some work, or energy, for the charge to move between two points in a circuit from point *a* to point *b*. The total work per unit charge associated with the motion of charge between two points is called voltage. Thus, the units of voltage are those of energy per unit charge; they have been called volts in honor of Alessandro Volta:

$$1\,volt = \frac{1\,joule}{coulomb} \tag{2.5}$$

The voltage, or potential difference, between two points in a circuit indicates the energy required to move charge from one point to the other. The direction, or polarity, of voltage is closely tied to whether energy is being dissipated or generated in the process. The seemingly abstract concept of work being done in moving charges can be directly applied to the analysis of electrical circuits; such as a simple circuit consisting of a battery and a light bulb. The circuit is drawn again for convenience in Figure 2.8, with nodes defined by the letters *a* and *b*. A series of carefully conducted experimental observations regarding the nature of voltages in an electric

circuit led Kirchhoff to the formulation of the second law, Kirchhoff's voltage law, or KVL. The principle underlying KVL is that no energy is lost or created in an electric circuit. In circuit terms, the sum of all voltages associated with sources must equal the sum of the load voltages, thus the net voltage around a closed circuit is zero. If this was not the case, it would need to find a physical explanation for the excess (or missing) energy not accounted for in the voltages around a circuit. Kirchhoff's voltage law may be stated in a form similar to that used for KCL:

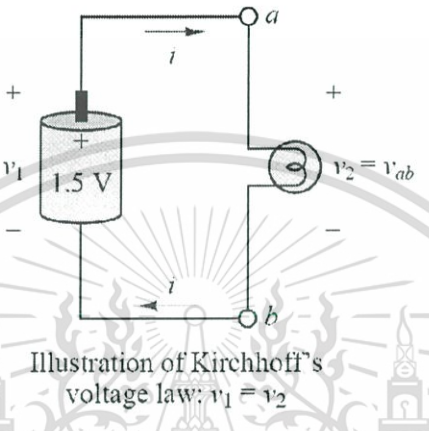

Figure 2.8 Voltages around a circuit

$$\sum_{n}^{N} v_n = 0 \quad \text{Kirchhoff's voltage law.} \tag{2.6}$$

Where the v_n are the individual voltages around the closed circuit. Making reference to Figure 2.8, it shows that it must follow from KVL that the work generated by the battery is equal to the energy dissipated in the light bulb to sustain the current flow and to convert the electric energy to heat and light:

$$v_{ab} = -v_{ba} \quad \text{or} \quad v_1 = v_2 \tag{2.7}$$

Another perspective may consider the work done in moving a charge from point *a* to point *b* and the work done in moving it back from *b* to *a* as corresponding directly to the voltages across individual circuit elements. Let Q be the total charge that moves around the circuit per unit time, giving rise to the current *i*. Then the work done in moving Q from *b* to *a* (i.e., across the battery) is

$$W_{ba} = Q \times 1.5V \tag{2.8}$$

The presence of voltage, v_2, across the open terminals a and b indicates the potential energy that enable the motion of charge, once a closed circuit is established to allow current to flow.

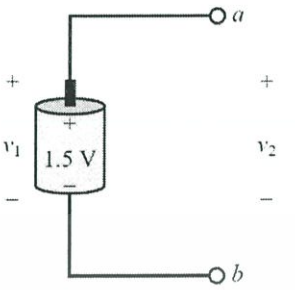

Figure 2.9 Concept of voltage as a potential difference

A symbolic representation of the battery–light bulb circuit of Figure 2.8.

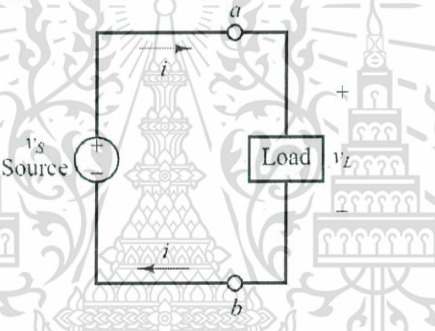

Figure 2.10 Sources and loads in an electrical circuit.

Similarly, work is done in moving Q from a to b, that is, across the light bulb. Note that the word potential is quite appropriate as a synonym of voltage, in that voltage represents the potential energy between two points in a circuit. If the light bulb is removed from its connections to the battery, there still exists a voltage across the (now disconnected) terminals b and a. This is illustrated in Figure 2.9. A moment's reflection upon the significance of voltage should suggest that it must be necessary to specify a sign for this quantity. Consider again, the same dry cell or alkaline battery, where, by virtue of an electrochemically induced separation of charge, a 1.5-Volt potential difference is generated. The potential generated by the battery may be used to move charge in a circuit. The rate at which charge is moved once a closed circuit is established (i.e., the current drawn by the circuit connected to the battery) depends now on the circuit element which is connected to the battery. Thus, while the voltage across the battery represents the potential in providing energy to a circuit, the voltage across the light bulb indicates the amount of work done in dissipating energy. In the first case, energy is generated; in the second, it is

consumed (note that energy may also be stored, by suitable circuit elements yet to be introduced). This fundamental distinction requires attention in defining the sign (or polarity) of voltages.

It can, in general, refer to elements which provide energy as sources, and to elements which dissipate energy as loads. Standard symbols for a generalized source-and-load circuit are shown in Figure 2.10.

2.4.3 Resistance and Ohm's Law [30]

When electric current flows through a metal wire or through other circuit elements, it encounters a certain amount of resistance, the magnitude of which depends on the electrical properties of the material. Resistance to the flow of current may be undesired--for example, in the case of lead wires and connection cable--or it may be exploited in an electric circuit in a useful way. Nevertheless, practically all circuit elements exhibit some resistance; as a consequence, current flowing through an element will cause energy to be dissipated in the form of heat. An ideal resistor is a device which exhibits linear resistance properties according to Ohm's law, which states that

$$V = IR \quad \text{Ohm's law} \tag{2.9}$$

That is, the voltage across an element is directly proportional to the current flow through it. R is the value of the resistance in units of ohms (Ω), where

$$1\Omega = 1V / A \tag{2.10}$$

The resistance of a material depends on a property called resistivity, denoted by the symbol ρ; the inverse of resistivity is called conductivity and is denoted by the symbol σ. For a cylindrical resistance element (shown in Figure 2.11), the resistance is proportional to the length of the sample, l, and inversely proportional to its cross-sectional area, A, and conductivity, σ.

$$v = \frac{l}{\sigma A} i \tag{2.11}$$

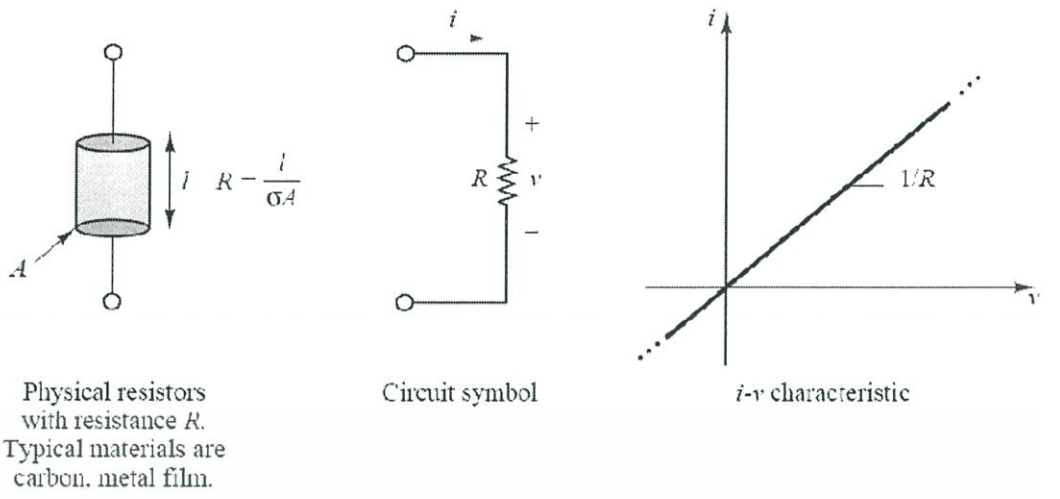

Figure 2.11 The resistance element.

It is often convenient to define the conductance of a circuit element as the inverse of its resistance. The symbol used to denote the conductance of an element is G, where

$$G = \frac{1}{R}\ siemens(S) \qquad where \quad 1S = 1A/V \tag{2.12}$$

Thus, Ohm's law can be restated in terms of conductance as:

$$I = GV \tag{2.13}$$

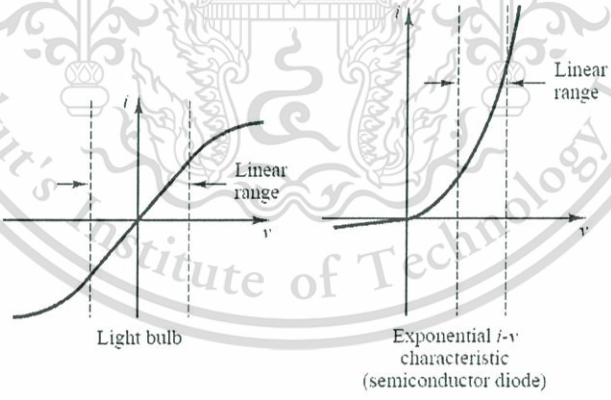

Figure 2.12 The linear resistance concept may apply to elements with nonlinear *i-v* characteristics.

Ohm's law is an empirical relationship that finds widespread application in electrical engineering, because of its simplicity. It is, however, only an approximation of the physics of electrically conducting materials. Typically, the linear relationship between voltage and current in electrical conductors does not apply at very high voltages and currents. Further, not all electrically conducting materials exhibit linear behaviour even for small voltages and currents. It is usually

true, however, that for some range of voltages and currents, most elements display a linear *i-v* characteristic. Figure 2.12 illustrates how the linear resistance concept may apply to elements with nonlinear *i-v* characteristics, by graphically defining the linear portion of the *i-v* characteristic of two common electrical devices: the light bulb, which we have already encountered, and the semiconductor diode.

2.4.4 Two Point Probe [31]

Ohmmeter measurements are normally made with just a two-point measurement method. However, when measuring very low values of ohms, in the milli-ohm or micro-ohm range, the two-point method is not satisfactory because the test lead resistance becomes a significant factor. A similar problem occurs when making ground resistance tests, because a long lead length of up to 1000 feet is used. In this research, the lead resistance, due to long lead length, will affect the measurement results.

Figure 2.13 Ohmmeter measurements of a two-point measurement method.

2.4.5 Four Point Probe [31]

The four-point resistance measurement method eliminates lead resistance. Instruments based on the four-point measurement work on the following principle:

- Two current leads, C1 and C2, comprise a two-wire current source which circulates current through the resistance under testing.
- Two potential leads, P1 and P2, provide a two-wire voltage measurement circuit which measures the voltage drop across the resistance under testing.
- The resistance is computed from the measured values of current and voltage.

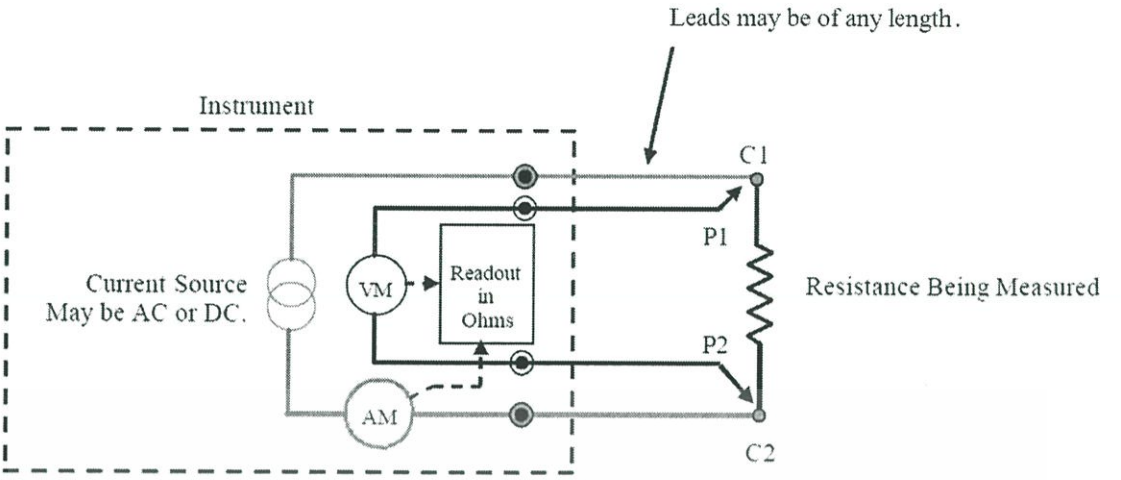

Figure 2.14 Four point measurement diagram [Kilowatt Classroom, LLC].

The purpose of the 4-point probe measurement is to measure the resistivity of any semiconductor material. It can measure either bulk or thin film specimen, each of which consists of a different expression. The 4-point probe setup used in Figure 2.15 consists of four equally spaced tungsten metal tips with finite radius. Each tip is supported by springs on the other end to minimize sample damage during probing. The four metal tips are part of an auto-mechanical stage which travels up and down during measurements. A high impedance current source is used to supply current through the outer two probes; a voltmeter measures the voltage across the inner two probes (See Figure 2.15) to determine the sample resistivity. Typical probe spacing $s \approx 1\,mm$

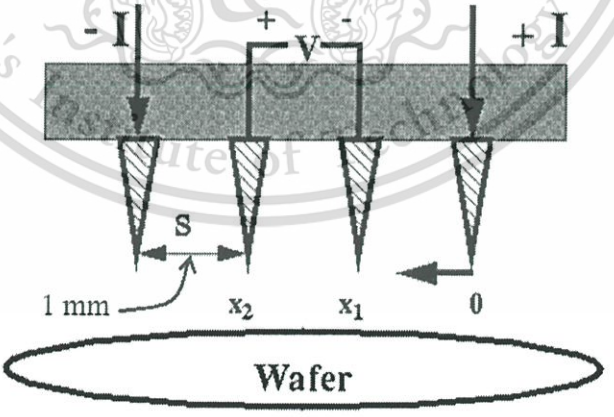

Figure 2.15 Schematic of 4-point probe configuration [EECS 143, Microfabrication Technology].

2.4.5.1 Bulk Sample [32]

In our derivations for this section, we assume that the metal tip is infinitesimal and samples are semi-infinite in lateral dimension. For bulk samples where the sample thickness $t >> s$, the probe spacing, we assume a spherical protrusion of current emanating from the outer probe tips. The differential resistance:

$$\Delta R = \rho\left(\frac{dx}{A}\right) \tag{2.14}$$

This is integrated between the inner probe tips (where the voltage is measured):

$$R = \int_{x_1}^{x_2} \rho \frac{dx}{2\pi x^2} = \frac{\rho}{2\pi}\left(-\frac{1}{x}\right)\Bigg|_{x_1}^{x_2} = \frac{1}{2s}\frac{\rho}{2\pi} \tag{2.15}$$

Where probe spacing is uniformly s. Due to the superposition of current at the outer two tips, $R = V/2I$. Thus, we arrive at the expression for bulk resistivity:

$$\rho = 2\pi s\left(\frac{V}{I}\right) \tag{2.16}$$

2.4.5.2 Thin Sheet [32]

For a very thin layer (thickness $t << s$) use current rings are used instead of spheres. Therefore the expression for the area $A = 2\pi xt$. The derivation is as follows:

$$R = \int_{x_1}^{x_2} \rho \frac{dx}{2\pi xt} = \int_{S}^{2S} \frac{\rho}{2\pi t}\frac{dx}{x} = \frac{\rho}{2\pi t}\ln(x)\Big|_{S}^{2S} = \frac{\rho}{2\pi t}\ln 2 \tag{2.17}$$

Consequently, for R = V/2I, the sheet resistivity for a thin sheet is:

$$\rho = \frac{\pi t}{\ln 2}\left(\frac{V}{I}\right) \tag{2.18}$$

Note that this expression is independent of the probe spacing s. Furthermore, this latter expression is frequently used for characterization semiconductor layers, such as a diffused N+ region in a p-type substrate. In general, the sheet resistivity $R_S = \rho/t$ can be expressed as:

$$Rs = k\left(\frac{V}{I}\right) \tag{2.19}$$

Where the factor k is a geometric factor. In the case of a semi-infinite thin sheet, $k = 4.53$, which is just $\pi/\ln 2$ from the derivation. The factor k will be different for non-ideal samples.

2.4.6 Three-Point Resistance Measurements

The three-point method, a variation of the four-point method, is usually used when making ground (earth) resistance measurements. With the three-point method (Figure 2.14), the C1 and P1 terminals are tied together at the instrument and connected with a *short* lead to the ground system being tested. This simplifies the test in that only three leads are required instead of four. Because this common lead is kept short, when compared to the length of the C2 and P2 leads, its effect is negligible. Some ground testers are only capable of the three-point method, so are equipped with only three test terminals.

In summary, the four-point probe measurement was a measuring instrument used to identify the electrical resistance of specimen in this thesis. The current source which is DC circulates through the specimen from one end to another end and different voltage is measured using a digital voltmeter at position 1 and position 2 as shown in Figure 2.16. The resistance of specimen is calculated from electric current and electric voltage, and then the electrical conductivity is determined using the resistance value, cross section area and length of specimen.

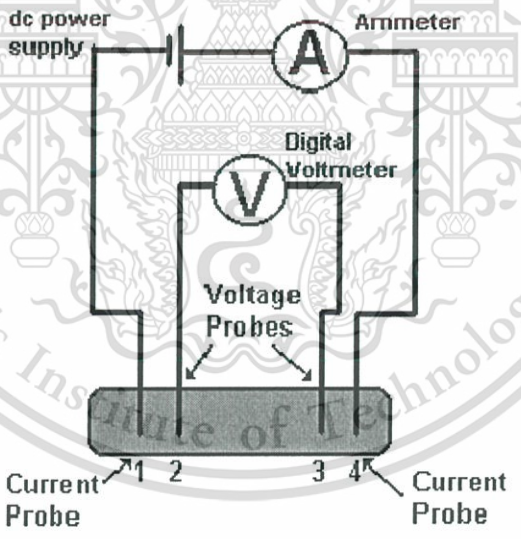

Figure 2.16 Schematic of Four-Point Probe.

From equation 2.14 $$\Delta R = \rho\left(\frac{dx}{A}\right)$$

Where $A = \frac{\pi d^2}{4}$, cross section area of specimen circular

$$R = \int_{x_1}^{x_2} \rho \frac{dx}{\frac{\pi}{4} d^2} = \frac{4\rho}{\pi d^2} x \Big|_{x_1}^{x_2} = \frac{4\rho}{\pi d^2} L$$

$\Delta x = x_2 - x_1 = L$, which is the length from point 2 to point 3.

$$\rho = \frac{\pi R d^2}{4L} \tag{2.20}$$

Electrical conductivity or specific conductance is a measure of a material's ability to conduct electric current. When electrical potential difference is placed across a conductor, its movable charges flow, giving rise to the electric current .Conductivity is the reciprocal (inverse) of electrical resistivity, ρ, and has the SI units of Siemens per metre ($S \cdot m^{-1}$) and CGSE units of inverse second (s^{-1}):

$$\sigma = \frac{1}{\rho} = \frac{4L}{\pi R d^2} \tag{2.21}$$

2.5 Diffusion

Diffusion in alloys is always an interdiffusion of all the atoms of the solid and depends on the tracer diffusivity of each component. The models of tracer diffusion and interdiffusion in binary alloys are well established [33-37]. At a concentration x of component B the coefficient $B(x)$ of interdiffusivity in a binary alloy is given by [5]

$$D(x) = \left\{ x D_A^*(x) + (1-x) D_B^*(x) \right\} \gamma(x) \tag{2.22}$$

$$D(x) = D_{B \text{ in } A}^*(x) \quad x \ll 1$$

$$D(x) = D_{A \text{ in } B}^*(x) \quad x \cong 1$$

Interdiffusion depends on the tracer diffusivities $D_A^*(x)$ and $D_B^*(x)$ of the components A and B, as well as on the thermodynamic factor $\gamma(x)$.

At small concentrations of component B, x will be close to 0 and the thermodynamic factor equals unity, $\gamma(x) = 1$. Interdiffusion will then be equivalent to the impurity diffusion of tracer B in the nearly pure A metal. For very large concentrations, x will be close to 1, $\gamma(x)$ again equals one and interdiffusion is equal to impurity diffusion of tracer A in the nearly pure B metal. At all other concentrations, x , interdiffusion is equivalent to an effective impurity diffusion.

The Kirkendall effect is the migration of markers that occurs when markers are placed at the interface between an alloy and a metal, and the whole is heated to a temperature where diffusion is possible; the markers will move towards the alloy region. For example, using molybdenum as a marker between copper and brass (a copper-zinc alloy), molybdenum atoms will migrate towards brass. This is explained by assuming that the zinc diffuses more rapidly than the copper, and thus diffuses out of the alloy down its concentration gradient. Such a process is impossible if the diffusion is by direct exchange of atoms.

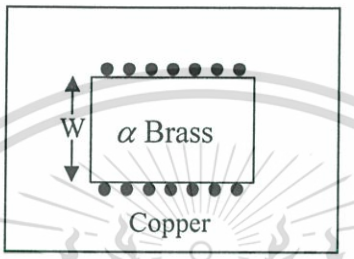

Figure 2.17 An experimental arrangement to show the Kirkendall effect.[45]

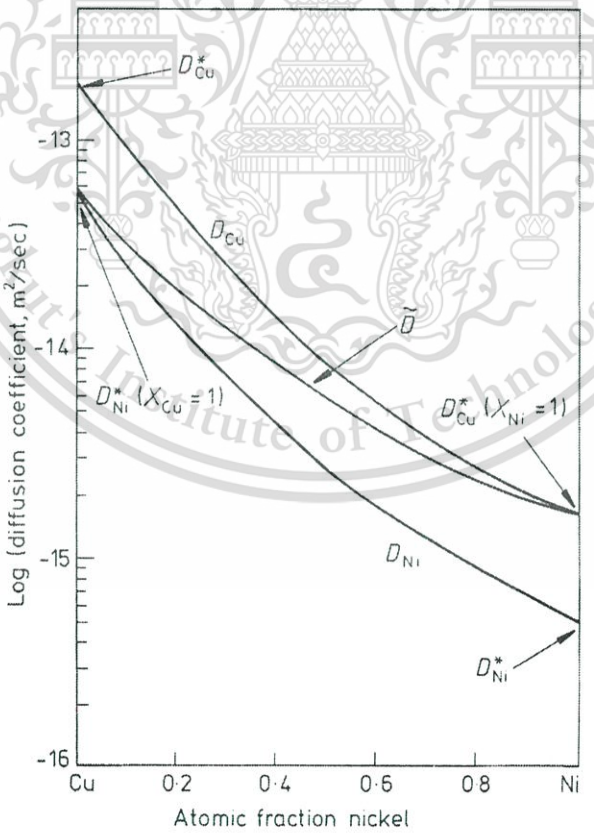

Figure 2.18 The relationship between the various diffusion coefficients in the Cu-Ni system at 1000°C (After A.G. Guy, Introduction to Material Science, McGraw-Hill, New York, 1971.)

For example of an experiment [44], a block of α -brass (Cu-30% Zn) was wound with molybdenum wire and encapsulated in a block of pure Cu, as shown in Figure 2.17. After annealing at a high temperature it was found that the separation of the markers (w) had decreased. This is because $D_{Zn} > D_{Cu}$ and the zinc atoms diffuse out of the central block faster than they are replaced by copper atoms diffusing in the opposite direction. Similar effects have since been demonstrated in many other alloy systems. In general, it is found that in any given couple, atoms with the lower meting point process a higher D. The exact value of D, however, varies with the composition of alloy. Thus in Cu-Ni alloys, D_{Cu}, D_{Ni} and $\tilde{D}$ are all composition dependent, increasing as X_{Cu} increases, Figure 2.18

2.5.1 Diffusion Coefficients of Iron, Cobalt and Nickel in Silver [38]

Diffusion coefficients of iron, cobalt and nickel in silver have been determined over the temperature range 600–850°C using radioactive tracers and the residual-activity technique. The results are as follows (in units of cm^2/sec):

$$D_{Fe/Ag} = 9.4\times10^{-7} \exp(-29{,}600/RT) \quad (2.23)$$

$$D_{Co/Ag} = 3.0\times10^{-7} \exp(-29{,}700/RT) \quad (2.24)$$

$$D_{Ni/Ag} = 8.5\times10^{-7} \exp(-28{,}700/RT) \quad (2.25)$$

The frequency factors and activation energies are quite small relative to those for self-diffusion in silver. It appears that the extremely low solid solubilities of iron, cobalt and nickel in silver reduce the flux through the lattice to the point where diffusion along dislocation short-circuiting paths becomes the controlling mechanism.

Table 2.9 Diffusivity of iron, cobalt and nickel in silver [38].

Temperature (°C)	Diffusion coefficient (cm^2/sec) Fe^{59}	Co^{60}	Ni^{63}
601	3.59×10^{-14}	1.06×10^{-14}	6.59×10^{-14}
647	7.60×10^{-14}	2.95×10^{-14}	1.04×10^{-13}
698	2.51×10^{-13}	6.76×10^{-14}	2.82×10^{-13}
744	4.47×10^{-13}	9.82×10^{-14}	6.81×10^{-13}
788	8.08×10^{-13}	2.63×10^{-13}	1.02×10^{-12}
843	1.27×10^{-12}	4.53×10^{-13}	2.03×10^{-12}

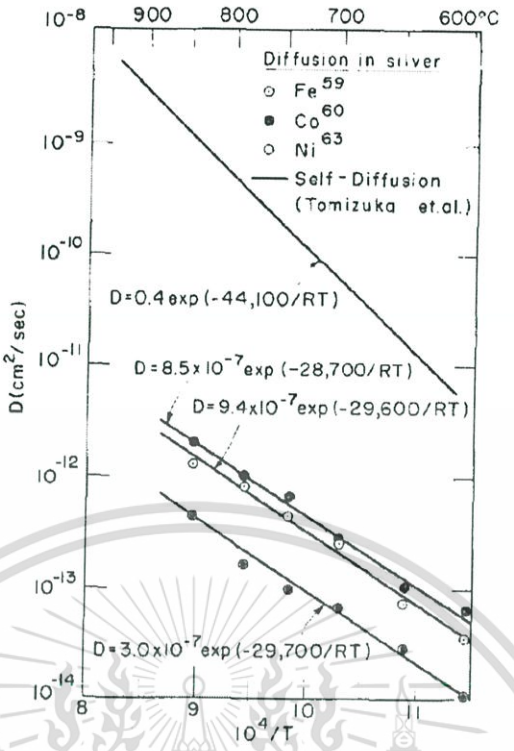

Figure 2.19 Temperature dependence of diffusivities in silver [38].

2.51 Diffusion Coefficients of Iron, Cobalt and Nickel into Otherwise Pure Gold [39]

The diffusivities of iron, cobalt and nickel into otherwise pure gold were determined by the residual-activity technique, after checking this procedure against the better-known sectioning method for self-diffusion in gold. The results may be summarized as follows (in units of cm^2 sec).

Table 2.10 Temperature dependence of diffusion coefficients [39].

Tracer	Temperature range (°C)	D_0(cm² sec)	Q(cal/mol)
Au^{198}	702–899	0.117	42,100
Fe^{59}	701–948	0.082	41,600
Co^{60}	702–948	0.068	41,600
Ni^{63}	702–988	0.034	42,000

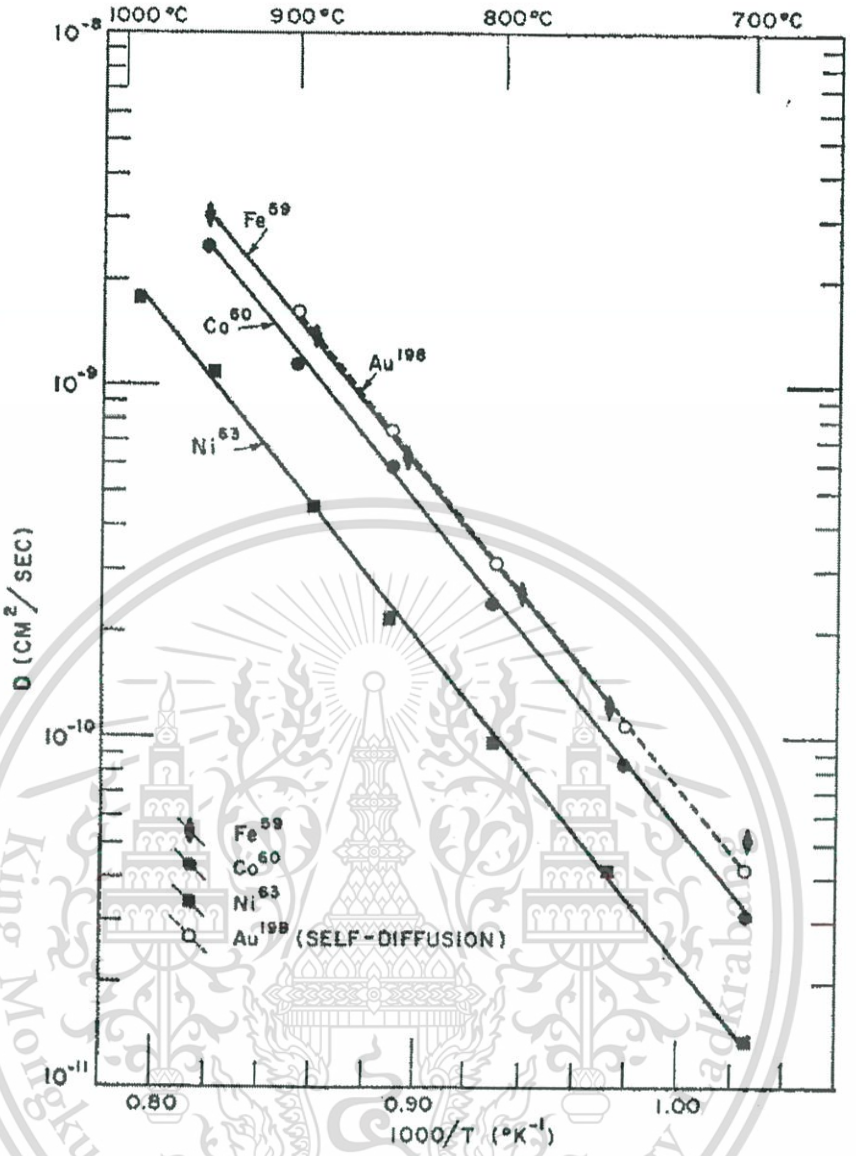

Figure 2.20 Temperature dependence of diffusivities in gold [39].

$$D_{Au} = 0.117 \exp(-42{,}100/RT) \tag{2.26}$$

$$D_{Fe/Au} = 0.082 \exp(-41{,}600/RT) \tag{2.27}$$

$$D_{Co/Au} = 0.068 \exp(-41{,}600/RT) \tag{2.28}$$

$$D_{Ni/Au} = 0.034 \exp(-42{,}000/RT) \tag{2.29}$$

The frequency factors and activation energies for the diffusion of the transition elements into gold are quite normal relative to the values for self-diffusion in gold, and suggest that the lattice diffusion is operative, in contrast to the corresponding situation for the diffusion of these elements into aluminum where short circuiting paths appear to be operative. This difference in behavior is explained in terms of the marked difference in solid solubilities in the two series.

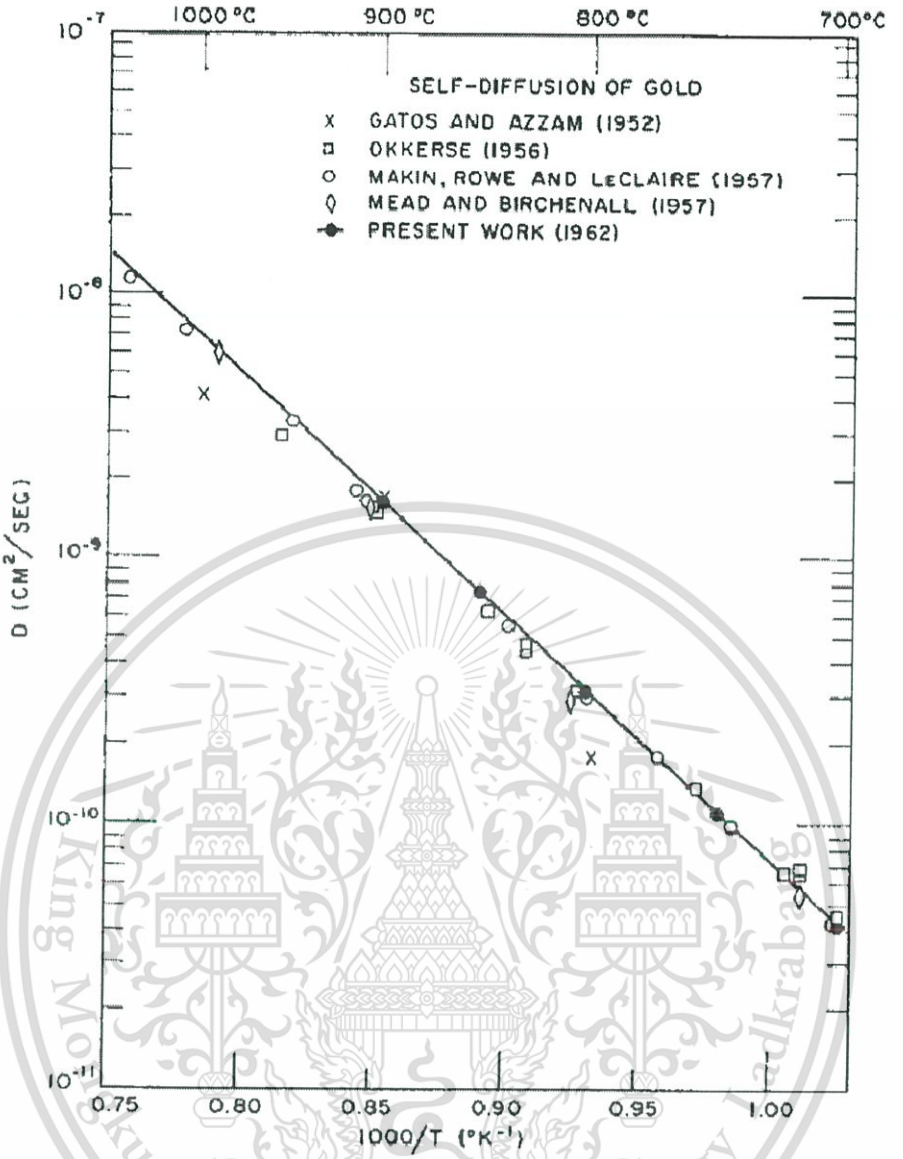

Figure 2.21 Comparison of the self-diffusion investigations on gold [39].

From Figure 2.20 – Figure 2.21, the diffusion coefficients of iron, cobalt and nickel in gold is higher than the diffusion coefficients of iron, cobalt and nickel in silver. Temperature also has a direct effect on diffusion coefficient; the higher temperature, the greater diffusion coefficient is. In addition, the self-diffusion of silver is a little lower than the self-diffusion of gold.

J. Mimkes and M. Wuttig (1996) have studied the relationship between diffusion and phase diagram which is discussed in more detail for Ag-Au and Au-Ni alloys. For each alloy tracer diffusion and interdiffusion data have been compared with the corresponding phase diagram. Tracer diffusion is related to the solid-liquid phase transition. Ag and Au D*(x) in Ag-Au alloys and melting temperature $T_m(x)$ of Ag-Au show opposite curvatures. Tracer diffusivities of Au and Ni in Au-Ni alloys and indicates a vacancy diffusion mechanism. An interdiffusion depends on the critical temperature of the solid-solid phase transition of the phase diagram. The curvature of interdiffusivity D(x) is determined by the sign of T,(x) or the interaction energy E of the regular alloy. The calculations agree well with the experimental data.

2.6 Pressure-Temperature Phase Diagrams [23]

The simplest phase diagrams are pressure-temperature diagrams of a single simple substance. The axes correspond to the pressure and temperature. The phase diagram shows, in pressure-temperature space, the lines of equilibrium or phase boundaries between the three phases of solid, liquid, and gas.

The Figure 2.22 shows an example of a pressure-temperature phase diagram, which summarizes the effect of temperature and pressure on a substance in a closed container. Every point in this diagram represents a possible combination of temperature and pressure for the system. The diagram is divided into three areas, which represent the solid, liquid, and gaseous states of the substance.

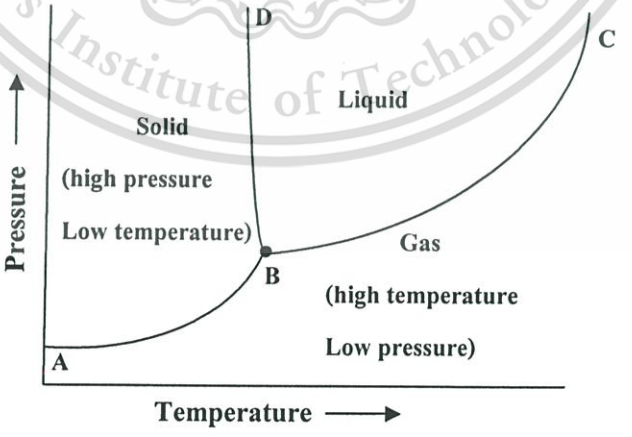

Figure 2.22 Pressure-Temperature Diagram.

Low temperatures and high pressures favor the formation of a solid. Gases, on the other hand, are most likely to be found at high temperatures and low pressures. Liquids lie between these extremes. When a solid is heated at constant pressure, it melts to form a liquid, which eventually boils to form a gas.

The points along the line connecting points A and B in the phase diagram in figure 2.22 represent all combinations of temperature and pressure at which the solid is in equilibrium with the gas. At these temperatures and pressures, the rate at which the solid sublimes to form a gas is equal to the rate at which the gas condenses to form a solid.

Along *AB* line:

rate at which solid sublimes to form a gas = rate at which gas condenses to form a solid

The solid line between points B and C is identical to the plot of temperature dependence of the gas pressure of the liquid. It contains all of the combinations of temperature and pressure at which the liquid boils. At every point along this line, the liquid boils to form a gas and the gas condenses to form a liquid at the same rate.

Along *BC* line:

rate at which liquid boils to form a gas = rate at which gas condenses to form a liquid

The solid line between points B and D contains the combinations of temperature and pressure at which the solid and liquid are in equilibrium. At every point along this line, the solid melts at the same rate at which the liquid becomes solid.

Along *BD* line:

rate at which solid melts to form a liquid = rate at which liquid freezes to form a solid

The *BD* line is almost vertical because the melting point of a solid is not very sensitive to changes in pressure. For most compounds, this line has a small positive slope, as shown in the Figure 2.22. The slope of this line is slightly negative for water, however. As a result, water can melt at temperatures near its freezing point when subjected to pressure. The ease with which ice skaters glide across a frozen pond can be explained by the fact that the pressure exerted by their skates melts a small portion of the ice that lies beneath the blades.

Point B in this phase diagram represents the only combination of temperature and pressure at which a pure substance can exist simultaneously as a solid, a liquid, and a gas. It is therefore called the triple point of the substance, and it represents the only point in the phase diagram in which all three states are in equilibrium. Point C is the critical point of the substance, which is the highest temperature and pressure at which a gas and a liquid can coexist at equilibrium.

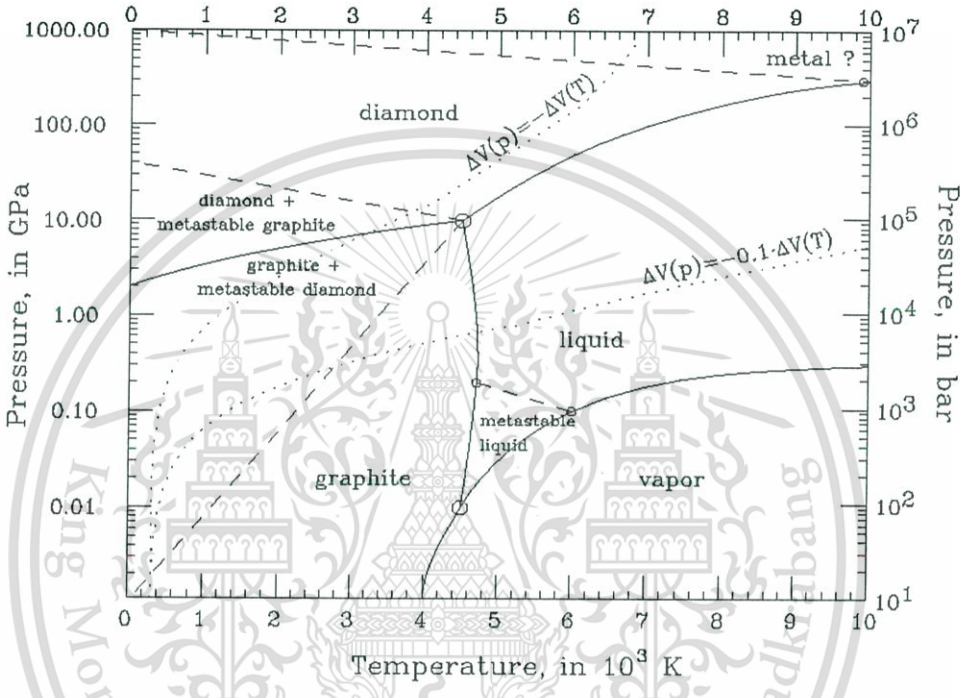

Figure 2.23 Pressure-temperature phase diagram of graphite.

Although the material in Figure 2.23 is not gold and silver, but it helps to understand the changing behaviour that pressure has an effect on changing phases from solid to liquid. When pressure is increased, the temperature is increased to change phases from solid to liquid.

Figure 2.24 shows a phase diagram of Au-Ni. These materials have a chance to combine to alloy when the specimen made of gold and SUS316L is heated at high temperature (700-900°C). Ni and Cr are the main composition in SUS316L as shown in table 2.11.

Table 2.11 Composition in 316L stainless steels.[43]

Grade		C	Mn	Si	P	S	Cr	Mo	Ni	N
316L	Min	-	-	-	-	-	16.0	2.00	10.0	-
	Max	0.03	2.0	0.75	0.045	0.03	18.0	3.00	14.0	0.10

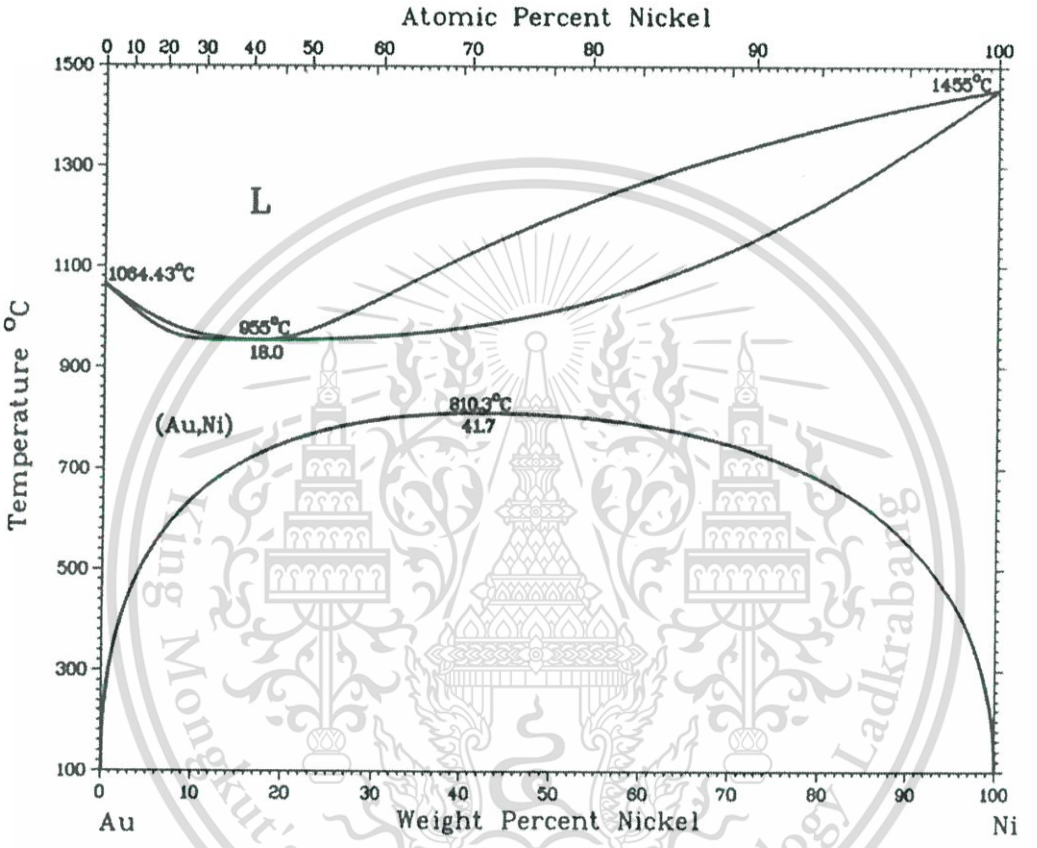

Figure 2.24 Au-Ni phase diagram.[]

2.7 Function of Stainless Steel at High Temperature [43]

Stainless steel is most commonly used for its corrosion resistance. The second most common reason stainless steel is used is for the high temperature properties; stainless steels can be found in applications where high temperature oxidation resistance is necessary and in other applications where high temperature strength is required. The high chromium content which is so beneficial to the wet corrosion resistance of stainless steel is also highly beneficial to their high temperature strength and resistance to scaling at elevated temperatures, as shown in Figure 2.25.

2.7.1 Scaling Resistance

Resistance to oxidation, or scaling, is dependent on the chromium content in the same way as the corrosion resistance is, as shown in the graph below. Most austenitic steels, with chromium contents of at least 18%, can be used at temperatures up to 870°C and Grades 309, 310 and 2111HTR (UNS S30815) even higher. Most martensitic and ferritic steels have lower resistance to oxidation and hence lower useful operating temperatures. An exception to this is the ferritic grade 446 - which contains approximately 24% chromium, and can be used to resist scaling at the temperature up to 1100°C.

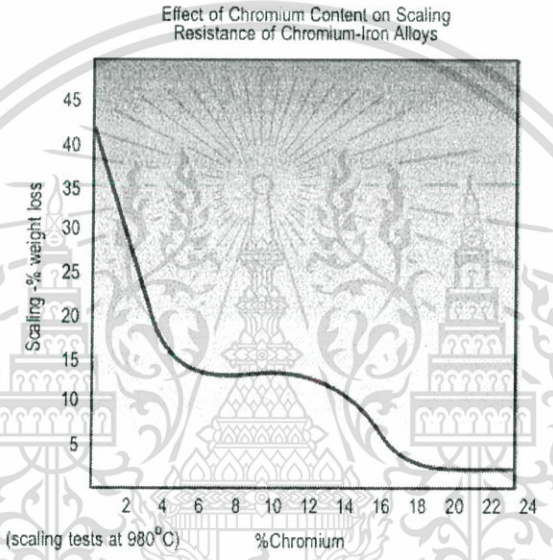

Figure 2.25 Effect of chromium content on scaling resistance

Table 2.25 shows the approximate maximum service temperatures at which the various grades of stainless steels can be used to resist oxidation in dry air. Note that these temperatures depend very much on the actual environmental conditions, and in some instances substantially lower temperatures will result in destructive scaling.

2.7.2 Creep Strength

The high temperature strength of materials is generally expressed in terms of their "creep strength" - the ability of the material to resist distortion over long term exposure to a high temperature. In this regard the austenitic stainless steel is particularly good. Design codes such as Australian Standard AS1210 "Pressure Vessels" and AS4041 "Pressure Piping" (and corresponding codes from ASME and other bodies) also stipulate allowable working stresses of each grade at a range of temperature. The low carbon version of the standard austenitic grades

(Grades 304L and 316L) have reduced strength at high temperature thus are not generally used for structural applications at elevated temperatures. "H" versions of each grade (eg 304H) have higher carbon contents for these applications, which results in significantly higher creep strengths. "H" grades are specified for some elevated temperature applications.

Table 1. Maximum service temperatures in dry air, based on scaling resistance (ref: ASM Metals Handbook)

Grade	Intermittent (°C)	Continuous (°C)
304	870	925
309	980	1095
310	1035	1150
316	870	925
321	870	925
410	815	705
416	760	675
420	735	620
430	870	815
2111HTR	1150	1150

Although the duplex stainless steels have good oxidation resistance due to their high chromium contents, they suffer from embrittlement if exposed to temperatures above about 350°C, so they are restricted to applications below this.

Both martensitic and precipitation hardening families of stainless steels have high strengths achieved by thermal treatments; exposure of these grades at temperatures exceeding their heat treatment temperatures will result in permanent softening, so again these grades are seldom used at elevated temperatures.

2.7.3 Structural Stability

The problem of grain boundary carbide precipitation was discussed under intergranular corrosion. This same phenomenon occurs when some stainless steels are exposed in service to temperatures of 425 to 815°C, resulting in a reduction of corrosion resistance which may be significant. If this problem is to be avoided, the use of stabilised grades such as Grade 321 or low carbon "L" grades should be considered.

A further problem that some stainless steels have in high temperature applications is the formation of sigma phase. The formation of sigma phase in austenitic steels is dependent on both time and temperature and is different for each type of steel. In general, Grade 304 stainless steel is practically immune to sigma phase formation, but not so for those grades with higher chromium contents (Grade 310) with molybdenum (Grades 316 and 317) or with higher silicon contents (Grade 314). These grades are all prone to sigma phase formation if exposed for long periods to a temperature of about 590 to 870°C. Sigma phase embrittlement refers to the formation of a precipitate in the steel microstructure over a long period of time within this particular temperature range. The effect of the formation of this phase is to make the steel extremely brittle and failure can occur because of brittle fracture. Once the steel has become embrittled with sigma, it is possible to reclaim it by heating the steel to a temperature above the sigma formation temperature range, however this is not always practical. Because sigma phase embrittlement is a serious problem with the high silicon grade 314, this is now unpopular and largely replaced by high nickel alloys or by stainless steels resistant to sigma phase embrittlement, particularly 2111HTR (UNS S30815). Grade 310 is also fairly susceptible to sigma phase formation in the temperature range 590 to 870°C, so this "heat resistant" grade may not be suitable for exposure at this comparatively low temperature range and Grade 321 is often a better choice.

2.7.4 Environmental Factors

Other factors which can be important in the use of steels for high temperature applications are carburisation and sulphidation resistance. Sulphur bearing gases under reducing conditions greatly accelerate the attack on stainless alloys with high nickel contents. In some instances, Grade 310 has given reasonable service. In others grade (S30815), with a lower nickel content is better, but in others a totally nickel-free alloy is superior. If sulphur bearing gases are present under reducing conditions, it is suggested that pilot test specimens be first run under similar conditions to determine the best alloy.

Localized stresses from expansion during heating and cooling can contribute to stress corrosion cracking in an environment which would not normally attack the metal. These applications require design to minimise the adverse effects of temperature differentials such as the use of expansion joints to permit movement without distortion and the avoidance of notches and abrupt changes of section.

CHAPTER 3

ELECTRICAL CONDUCTIVITY

This chapter presents experimental setups for the electrical conductivity study of electric conducting wires for SOFC system. The resistance of each specimen was measured using a four-point probe approach. The electrical conductivities were calculated from the resistance results. In addition, the manufacturing costs of the electric conducting wires have been presented in final part of this chapter.

3.1 Experimental Setup

Generally, the resistance of electric current conducting wires was measured using a two-point or four-point probe approach. In this thesis, the resistance of conducting wire was about measured using a four-point probe as shown in Figure 3.1 because of all the reason presented in chapter 2. The current was set from fifty to five hundreds mA and the voltage across the specimen was measured using a voltmeter. In addition, the temperature was varied from 100 to 1,000°C as shown schematically in Figure 3.1 and Figure 3.2. Before collecting the data, the wire was heated up at the rate of 2.5°C.min^{-1}.

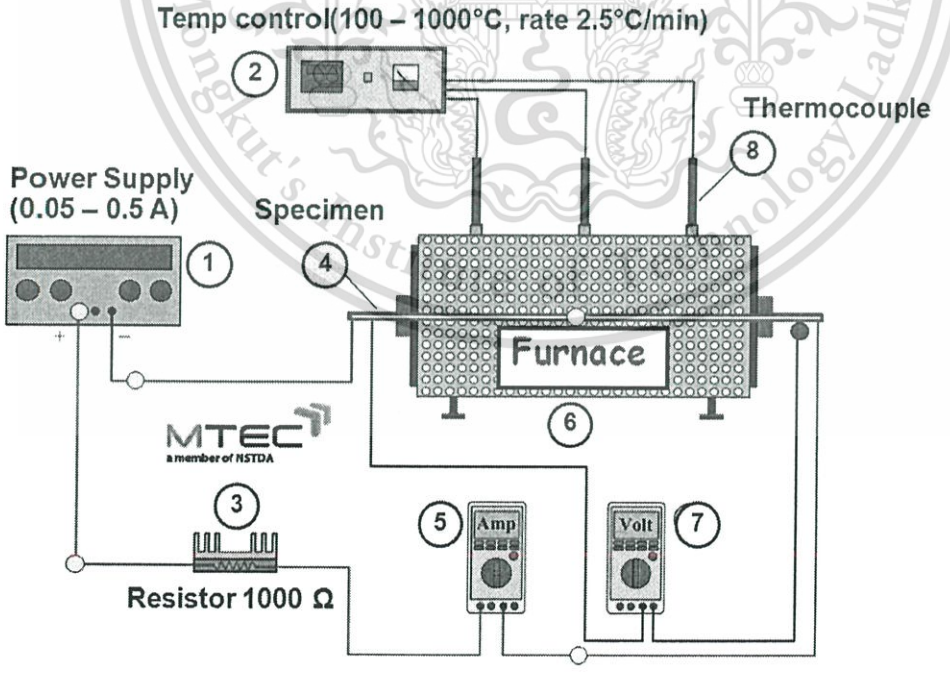

Figure 3.1 Schematic of equipment for a four-point probe measurement.

Table 3.1 Laboratory component specifications

Equipment/Devices	Descriptions
1. DC Power Supply	Adjustable range of electric current from 50 to 500 mA
2. Temperature Control	To control the temperature in the electric furnace from 100 to 1000°C
3. Resistor	A 1000 Ohm resistor is installed in this system to protect the short circuit because the resistance of specimens are very low.
4. Wire Specimens	They are new products which are shown in table 3.2
5. Amp Meter	For measuring the electric current generated from the DC power supply.
6. Volt Meter	Volt meter is used to measure the voltage between two ends of the specimen.
7. Electric Furnace	It has the maximum temperature capacity at 1000 °C by using a temperature control.
8. Thermocouple	The temperature at three locations in the furnace was monitored using three separate thermocouples.

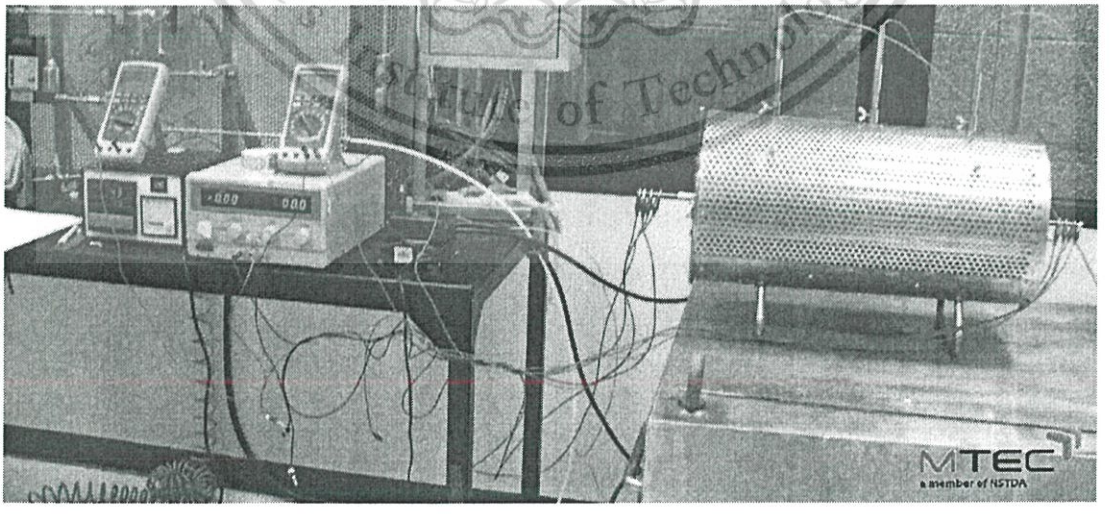

Figure 3.2 Equipment set up for a four-point probe measurement.

3.2 Preparation Specimens

The geometries similar to a cylindrical tube were assembled from two materials including silver sheathed with SUS316L and gold sheathed with SUS316L. The length of SUS316L tubes was 610 mm, silver and gold rods were 650 mm as shown in Figure 3.3 and Figure 3.4. The outer diameter and inner diameters of SUS316L were shown in Figure 3.4 and the specific data were shown in Table 3.2.

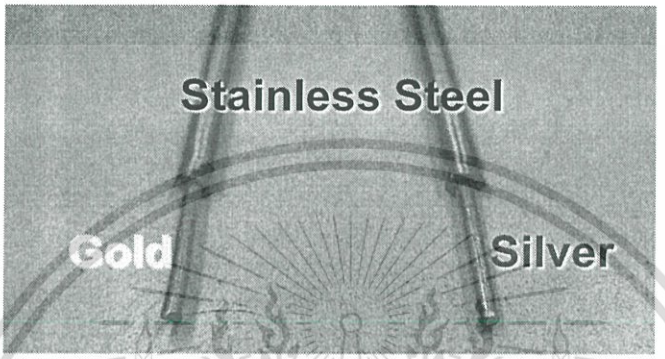

Figure 3.3 Geometries of specimen.

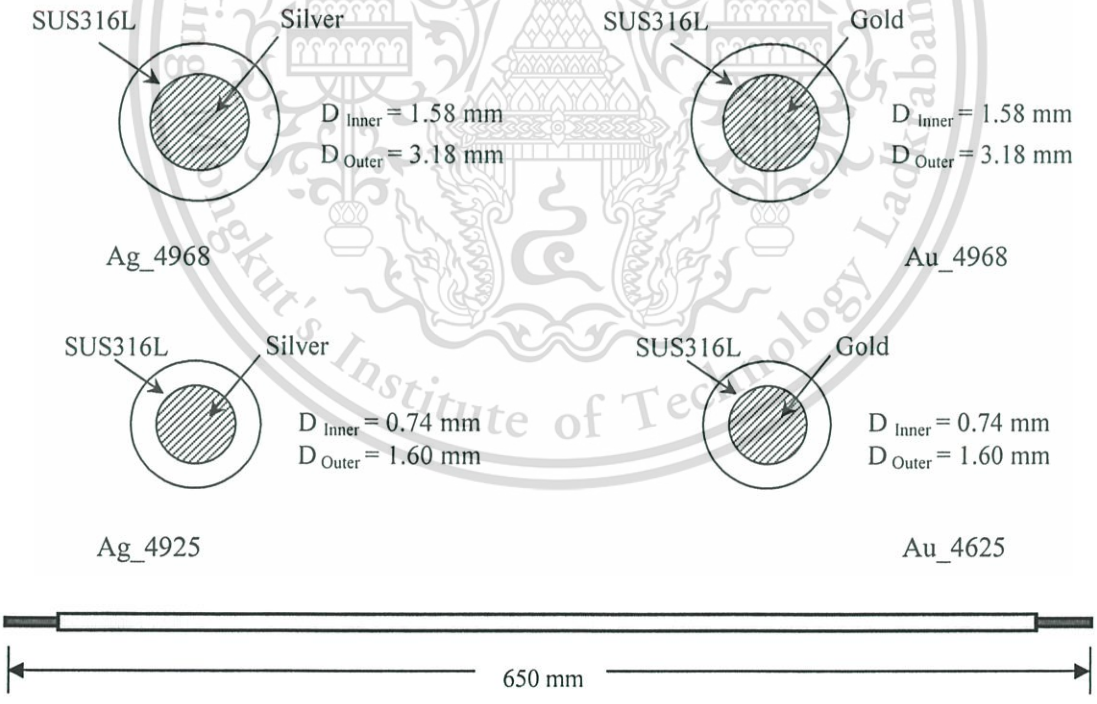

Figure 3.4 Cross sections and side view of the specimens.

Table 3.2 Specific data of specimens

Model	Gold	Silver	Stainless Steel (SUS316L)	Area Ratio
Ag_4625	-	Ø 0.72 mm	$Ø_{in}$ 0.74mm $Ø_{out}$ 1.60mm	0.2721
Ag_4968	-	Ø 1.56 mm	$Ø_{in}$ 1.58mm $Ø_{out}$ 3.18mm	0.3277
Au_4625	Ø 0.72 mm	-	$Ø_{in}$ 0.74mm $Ø_{out}$ 1.60mm	0.2721
Au_4968	Ø 1.56 mm	-	$Ø_{in}$ 1.58mm $Ø_{out}$ 3.18mm	0.3277

In assembly, the gap between inner material and outside material was 0.01 - 0.05 mm because the inner material of some model cannot be sheathed easily. Therefore, the inner material had to be rubbed with sand paper to decrease its diameter. Ag_4968 and Au_4968 can be assembled easier than Ag_4625 and Au_4625 because silver and gold are high strength due to large cross section area. However, a new method will be presented in topic 5.2.2

3.3 Experimental Conditions

In this experiment, the specimens were heated in a furnace at normal air. The temperature was set at 200, 400, 600, 700, 800, 900 and 1000°C, each of which was held for half an hour before the data of each specimen were collected. The electric current from the DC power supply was varied from 0.05 to 0.5 A (0.05A/step) for each temperature. Therefore, there are 63 conditions for each specimen as shown in Figure 3.5.

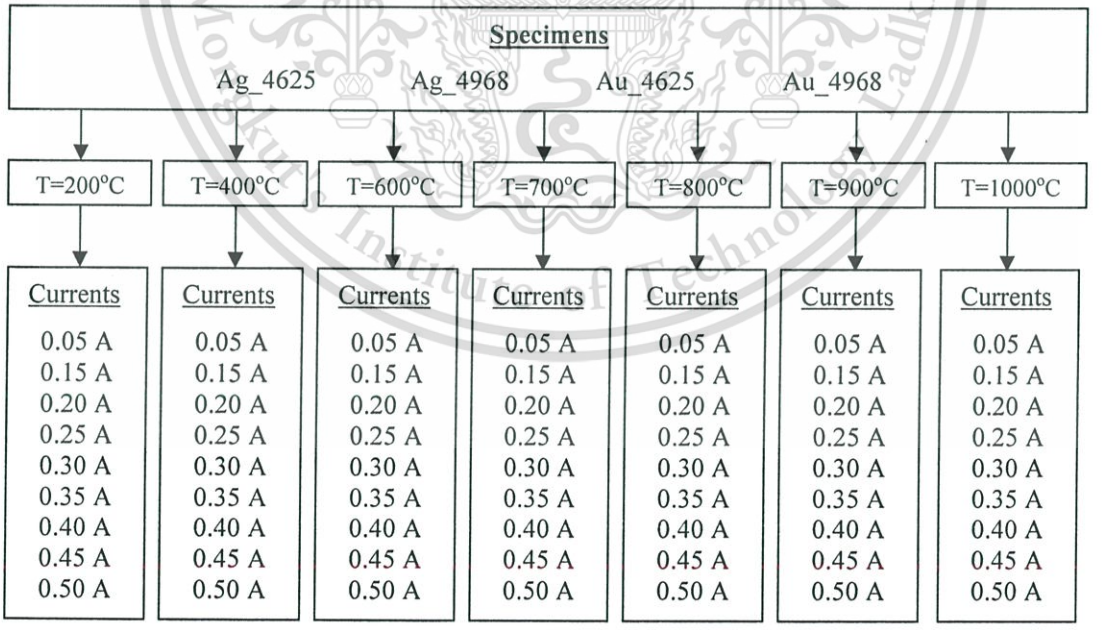

Figure 3.5 The 252 conditions for measuring electrical conductivity.

In addition, more conditions were measured to map the four patterns for measuring a four-point probe measurement which will be explained in the next topic.

3.4 Four-Point Probe Measurement

In this experiment, each specimen was measured using 4 patterns shown in Figure 3.6. The four patterns of measurement are based on the technique of four-point probe. The specimens allow electric current to flow through from one end to another end, depending on each pattern as shown in Figure 3.6.

In Figure 3.6, the material in which locates point 3 and point 4 for all the patterns were stainless steel but the inner material which locates point 1 and point 2 were silver or gold depending on the models.

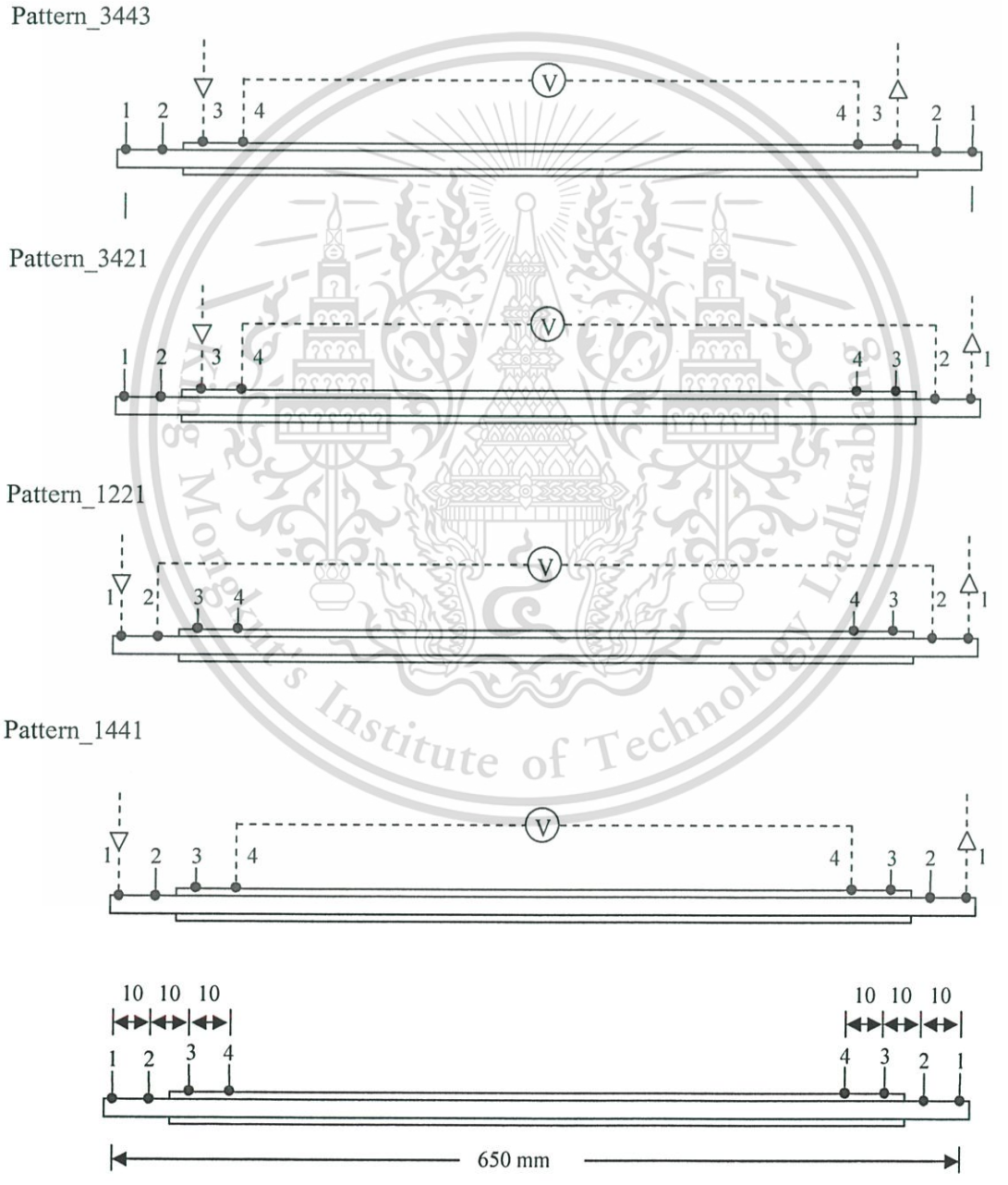

Figure 3.6 Positions for four-point probe measurement.

In measuring Pattern_3443, the electric current was varied from 0.05 to 0.50 A flows through from one end at point 3 to another end at point 3 and the voltmeter measured the difference in electric voltage from one end at point 4 to another end at point 4. Results from the measurement were plotted to find a slope which was the electric resistance of each specimen. Several patterns were measured because the electric resistance for each pattern is different.

3.5 Electrical Conductivity Calculation

Four patterns of measurement were used to calculate the relationship between the voltage drop and electric current of each model. For example, Ag_4625 model measured using four-point probe measurement was demonstrated in Figure 3.7 which presents the relationship between voltage drop and electric current of the model. The slope was an electric resistance. The electrical conductivity can be calculated from the slope of electric resistance from the plot, cross section and length of specimen.

Table 3.3 Data from the specimen Ag_4625 in pattern_3443 at 400°C.

Current(Amp)	Voltage(mV)
0.0560	7.9
0.1000	14.3
0.1500	21.3
0.2010	28.6
0.2540	36.2
0.3020	43.3
0.3550	50.6
0.4070	58.6
0.4540	65.3
0.5050	72.7

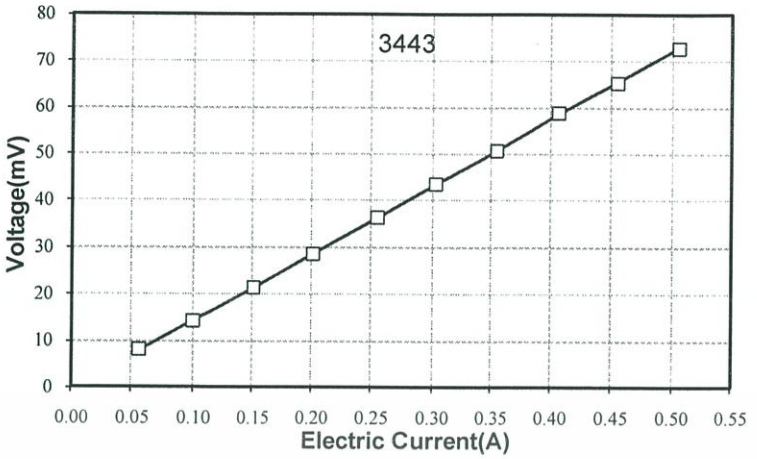

Figure 3.7 The relationship between voltage and electric current of pattern_3443 of Ag_4625.

The slope in Figure 3.7 was fitted with a least square to calculate the electric resistance. Form linear question $y = A + Bx$, B is the electrical resistance of the specimen.

$$\begin{bmatrix} n & \sum x \\ \sum x & \sum x^2 \end{bmatrix} \begin{Bmatrix} A \\ B \end{Bmatrix} = \begin{bmatrix} \sum y \\ \sum xy \end{bmatrix} \quad 3.1$$

Table 3.4 Data generated from Table 3.3 for Ag_4625 in pattern_3443 at 400°C

	x	y	x^2	xy
1	0.056000	0.007900	0.003136	0.000442
2	0.100000	0.014300	0.010000	0.001430
3	0.150000	0.021300	0.022500	0.003195
4	0.201000	0.028600	0.040401	0.005749
5	0.254000	0.036200	0.064516	0.009195
6	0.302000	0.043300	0.091204	0.013077
7	0.355000	0.050600	0.126025	0.017963
8	0.407000	0.058600	0.165649	0.023850
9	0.454000	0.065300	0.206116	0.029646
10	0.505000	0.072700	0.255025	0.036714
$\sum$	2.784000	0.398800	0.984572	0.141260

Where A = -0.000296 and B = 0.144312, the electric resistance of the specimen Ag_4625 of pattern_3443 is 0.1444312 Ohm.

From equation 2.21, the electrical conductivity was calculated from this equation.

$$\sigma = \frac{1}{\rho} = \frac{4L}{\pi Rd^2}$$

Where L=650 mm, d = 0.0016 m

$$\sigma = \frac{1}{\rho} = \frac{4L}{\pi Rd^2} = \frac{4 \times (0.650)}{\pi \times (0.1444312) \times (0.0016)^2} = 2238321.624 \quad S\,m^{-1}$$

Thus, the electrical conductivity of Ag_4625 for pattern_3443 at 400°C is 2238321.624 $S\,m^{-1}$.

3.6 Results and Discussion

3.6.1 Effect of Measurement Patterns

Measurement patterns have several effects on the specimens such as flow direction of the electric current and voltage in which the electrical conductivity is calculated from. Therefore, the resistance model of each pattern shown in Figure 3.8 – Figure 3.11 is invented to explain the behaviour of voltage and direction of electric current.

In case of pattern_3443, most electricity flows through the specimen from the third point of one end to the other third point on the other end via the flow direction of I1 because the sum of resistance of this direction is lower than the sum of resistance of the flow direction of I2 as shown in Figure 3.8. The material of the flow direction of I2 is 316L stainless steel. On the contrary, most materials of the flow direction of I2 are silver and gold. Therefore, the different voltages measured from the fourth point of one end to the other fourth point of this pattern were on the other end higher than other patterns.

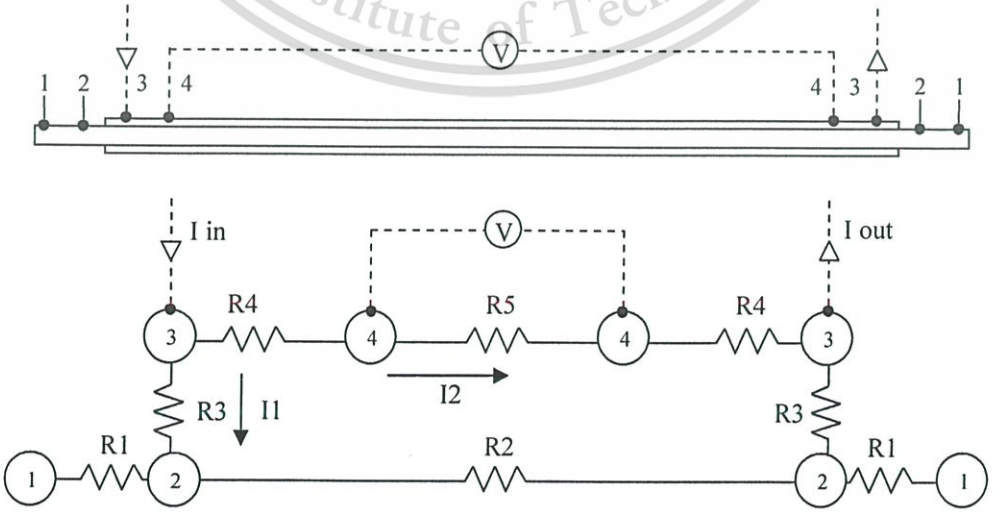

Figure 3.8 The model of resistance for measuring pattern_3443.

For pattern_3421 as shown in Figure 3.9, the resistance model of this pattern is similar to the model resistance of pattern_3443 but this pattern is different from pattern_3443 in that the outlet electric current channel is point 1 of the right side, and the measurement points of measured voltage are between point 4 of the left side and point 2 of the right side. The voltage of this pattern is less than that from pattern_3443 as a result of most electric current flowing through to I1.

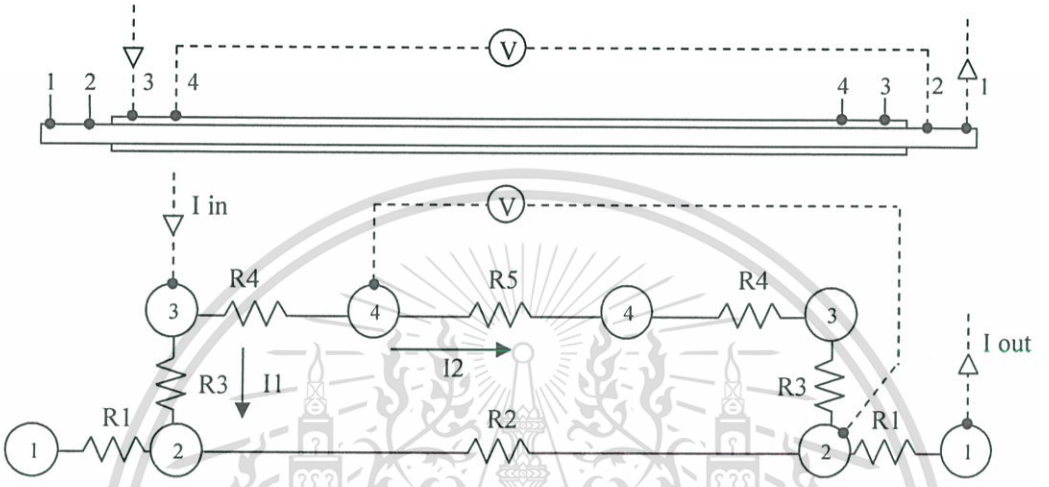

Figure 3.9 The model of resistance for measuring pattern _3421.

For pattern_1221 as shown in Figure 3.10, almost all of the electricity flow from point 1 of the left side, inlet current, to point 1 of the other side, outlet current, using the flow direction of I1 due to low resistance of R2 of gold and silver. Therefore, the different voltages measured in this pattern are lower than pattern_3443 and pattern_3421. It may imply that the voltages of this pattern seem to be from the voltage drop occurring between both ends of R2.

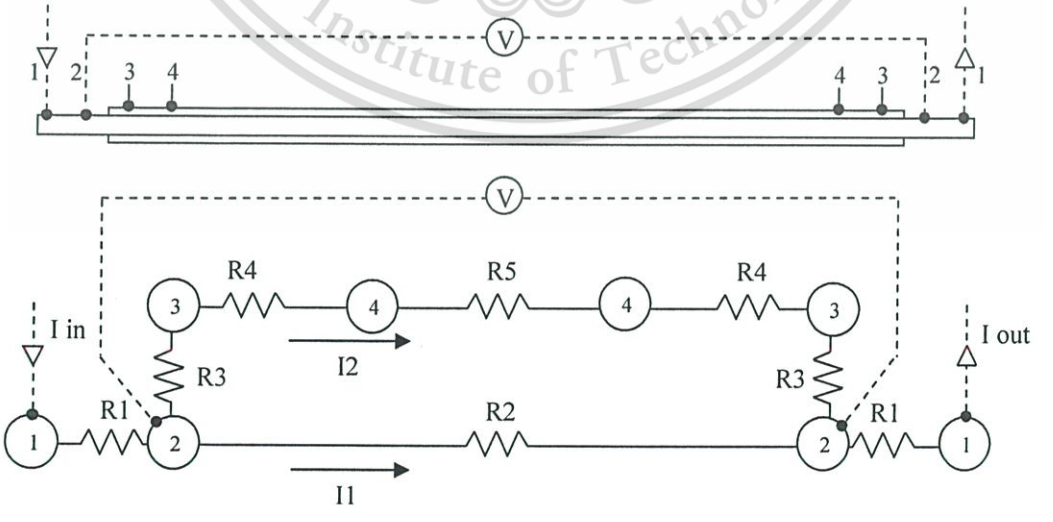

Figure 3.10 The model of resistance for measuring pattern _1221.

In case of pattern_1441 as shown in Figure 3.11, the different voltages of this pattern are the least of other patterns. In the same way, the flow direction of electricity of this pattern is similar to the pattern_1221 which flows through the direction I1. The voltage of this pattern was measured at point 4 of both two points which are connected through both ends of R7 blocked by R3. The difference of the voltage drop at R7 is the same as R5 because of both resistances of R3 which is resistance of contact interface between two materials. Therefore, the different voltages of this pattern are voltage drop occurring between two ends of R7 (R7<R2).

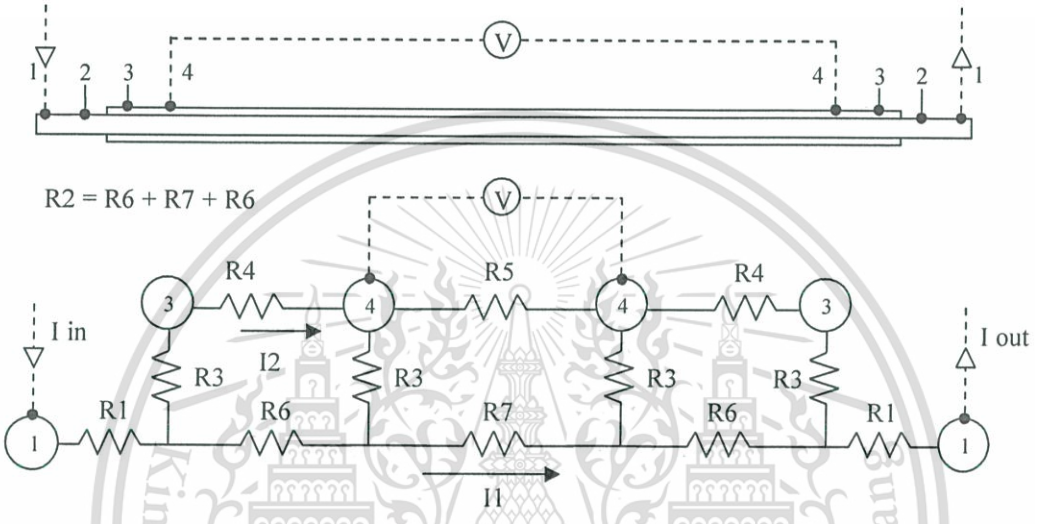

Figure 3.11 The model of resistance for measuring pattern _1441.

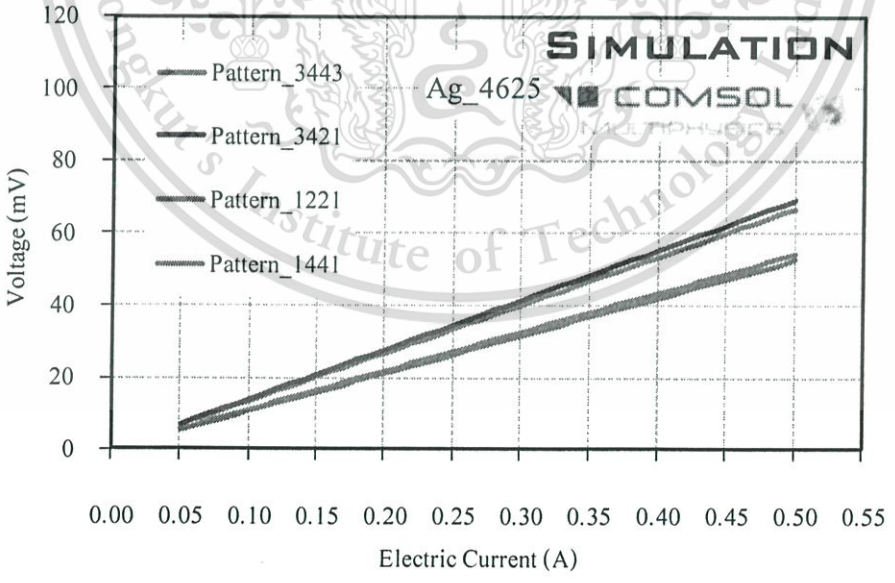

Figure 3.12 The voltage drop of each pattern as a function of electric current for Ag_4625 at 400°C from simulation.

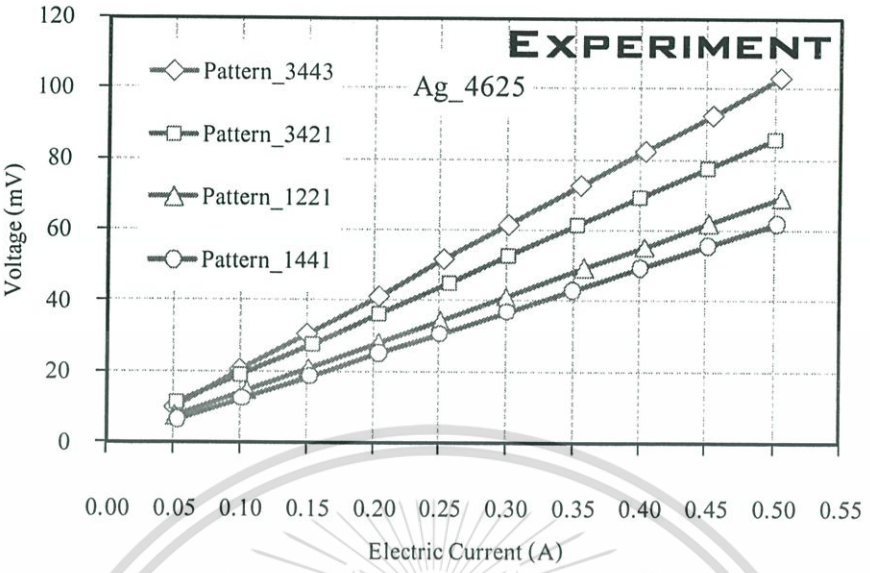

Figure 3.13 The voltage drop of each pattern as a function of electric current for Ag_4625 at 400°C from experimental.

Figure 3.13 is an example of the measured voltage from Ag_4625 at 400°C. The voltage of every pattern has the same tendency. The higher the electric current flows through the specimen, the higher the voltage drop occurs. The voltage of pattern_3443 is higher than other patterns and the least voltage is from pattern_1441.

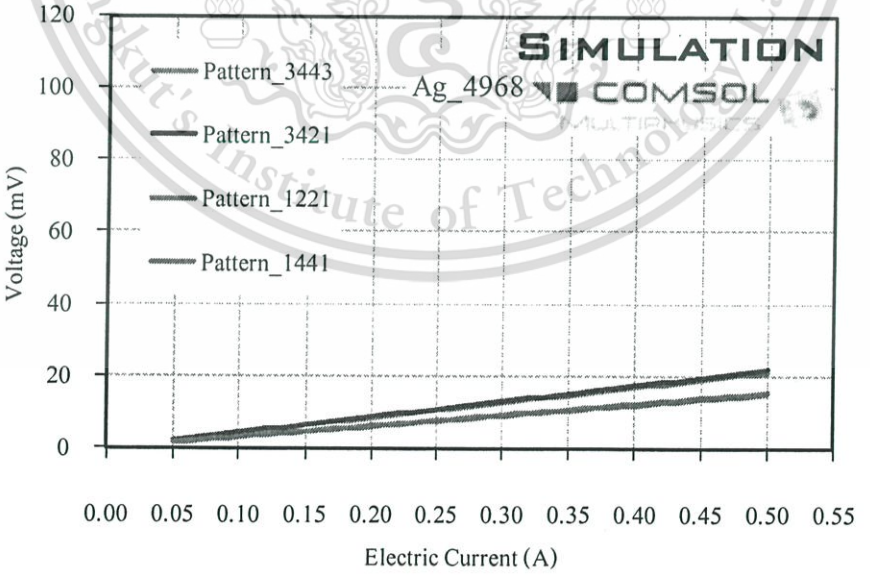

Figure 3.14 The voltage drop of each pattern as a function of electric current for Ag_4968 at 400°C from simulation.

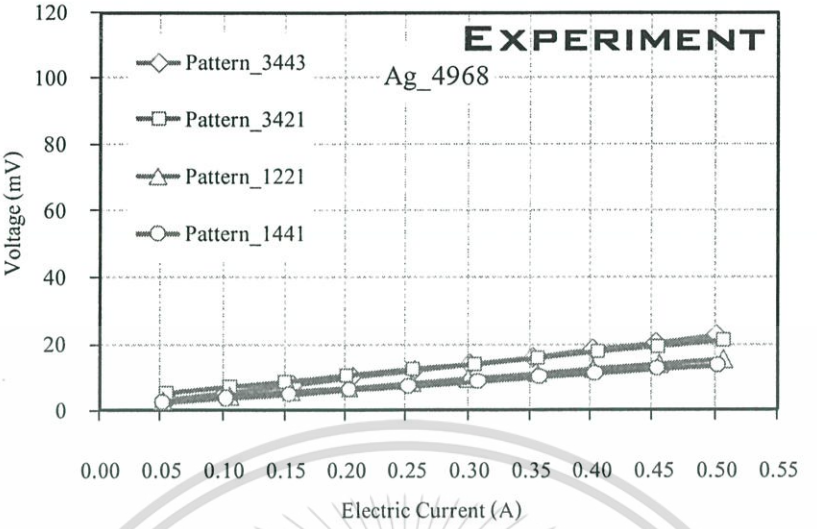

Figure 3.15 The voltage drop of each pattern as a function of electric current for Ag_4968 at 400°C from experimental.

Figure 3.16 Cross-section area of Ag_4968 (a) and Ag_4625 (b).

Figure 3.15 is the result of measured voltage from Ag_4968 at 400°C. The voltage of every pattern has the same tendency. Even though Ag_4968 was made of the same materials like Ag_4625 but the proportion of cross – section area of Ag_4968, 0.2721 (silver/SUS316L), is greater than the proportion of cross – section area of Ag_4625, 0.3277 (silver/SUS316L). In addition, the sum of cross – section area of Ag_4968 both silver and SUS316L is larger than the sum of cross-section area of Ag_4625 as shown in Figure 3.16. Consequently, the voltage of every pattern of Ag_4968 is lower than Ag_4625 due to the lower resistance of Ag_4968.

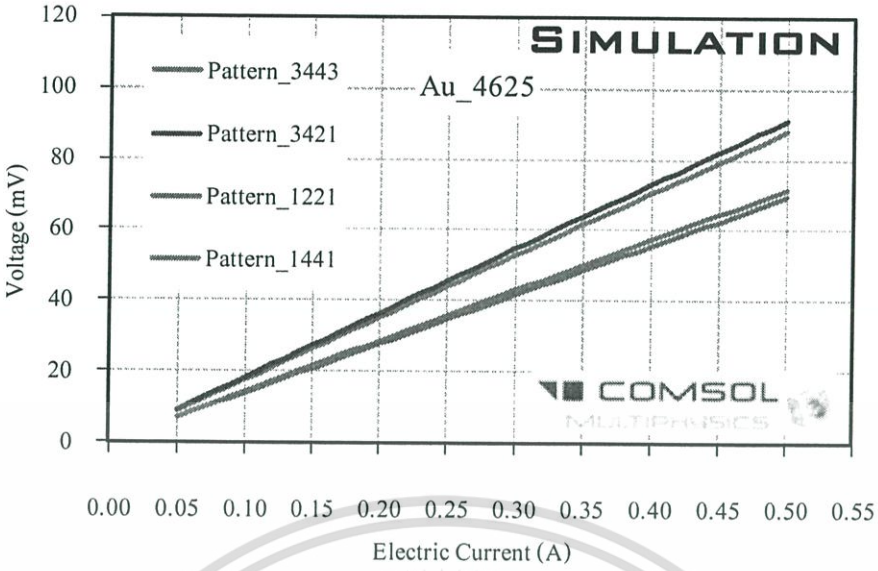

Figure 3.17 The voltage drop of each pattern as a function of electric current for Au_4625 at 400°C from simulation.

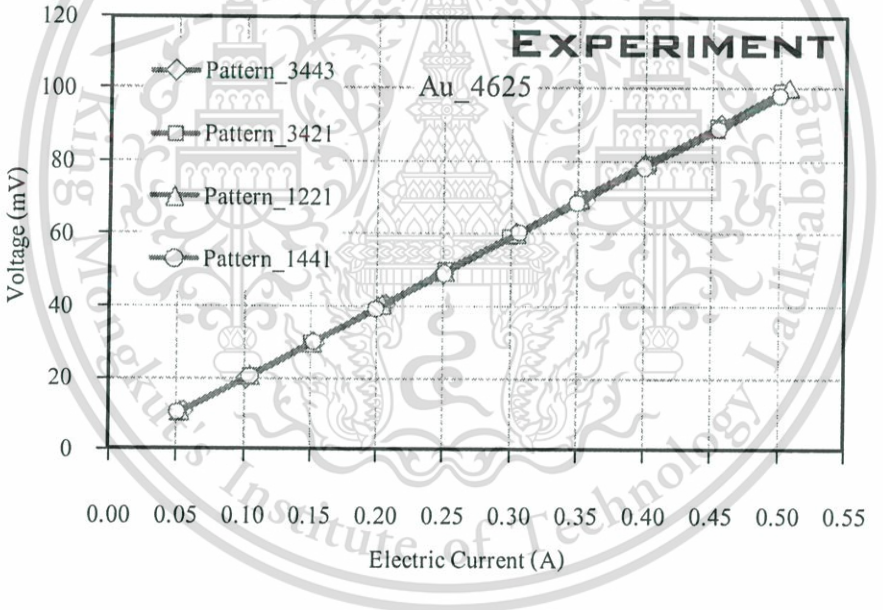

Figure 3.18 The voltage drop of each pattern as a function of electric current for Au_4625 at 400°C from experiment.

From Figure 3.18, the measurement patterns have a little effect on Au_4625. The difference of resistance per meter of gold and SUS316L are almost identical if they are compared with each model as shown in Table 3.5. The inner resistance per meter of Au_4625 is the highest of models and the different resistance ratio of Au_4625, (outside – inner)/total, is less than other models. Therefore, flowing pattern of electric current of Au_4625 is in parallel circuit; the amount of electric current flow through both gold and SUS316L.

Table 3.5 Resistance of inner material and outside material of specimen (at room temperature)

Model	Geometry of specimen	Ain	Aout	Electrical Conductivity(S/m)		Resistance(Ohm/m)		
		(mm^2)	(mm^2)	Inside	Outside	Inside	Outside	Total
Ag_4625	$Ø_{in}$ 0.74mm $Ø_{out}$ 1.60mm	0.43	1.5805	24877000	1019923	0.09348	0.62035	0.0812407
Ag_4968	$Ø_{in}$ 1.58mm $Ø_{out}$ 3.18mm	1.96	5.981	24877000	1019923	0.02051	0.16393	0.0182285
Au_4625	$Ø_{in}$ 0.74mm $Ø_{out}$ 1.60mm	0.43	1.5805	18000400	1019923	0.12920	0.62035	0.1069272
Au_4968	$Ø_{in}$ 1.58mm $Ø_{out}$ 3.18mm	1.96	5.981	18000400	1019923	0.02834	0.16393	0.0241657

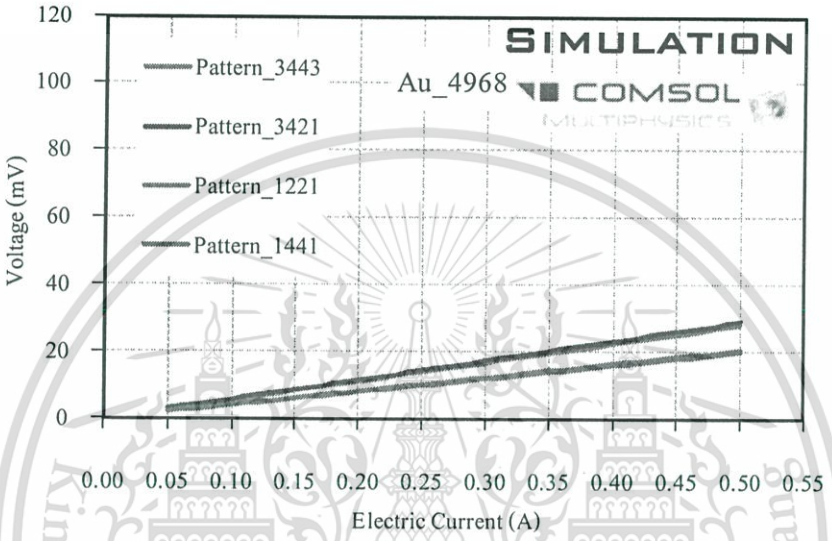

Figure 3.19 The voltage drop of each pattern as a function of electric current for Au_4968 at 400°C from simulation.

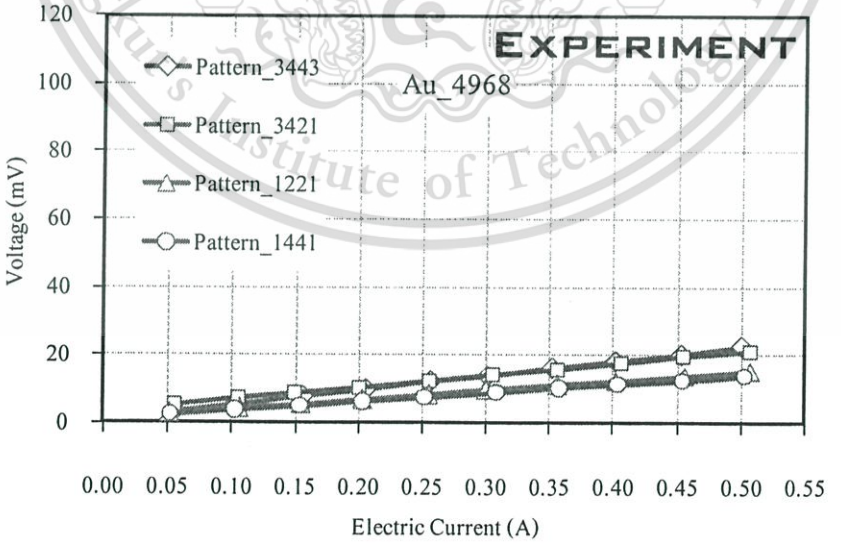

Figure 3.20 The voltage drop of each pattern as a function of electric current for Au_4968 at 400°C from experimental.

Figure 3.20 is the result of measured voltage from Au_4968 at 400°C. The result of the measurement pattern of Au_4968 is almost the same as Ag_4625 because they are almost the same resistance both inner and outside. However, the effect of measurement patterns of Au_4968 is also lower than that of Ag_4625.

In summary, this is an example of the measurement patterns at 400°C only. They have a little effect on Ag_4968, Au_4625 and Au_4968. However, it is not in the critical point because the unit of voltage, mV, is insignificant when it is calculated in term of electrical conductivity. For Ag_4625, although its measurement patterns have impact on the voltage but it is still able to conduct electricity better than Au_4625. In fact, the pattern_1221 is the pattern to be used in SOFC The inner material is directly in contact with the interconnect of SOFC, hence the electricity can flow through the inner material very well.

3.6.2 Effect of Temperature

The Change in temperature has a direct impact on the properties of materials which were referred to in chapter 2. The electrical resistance is a variable which depends on temperature. When specimens, Ag_4625, Ag_4968, Au_4625 and Au_4968, are heated up, their total resistances are increased. It seems that the temperature would be obstacle to developing almost all parts of SOFC. However, every model of electric conducting wire still can be operated until 1000°C even though the results of the total resistance of the specimen have changed.

Ag_4625

From Figure 3.21 to 3.24, the relationship between voltage and electric current for each of the measured patterns of Ag_4625 has a tendency to be linear equation at every temperature. It is clear that the change of voltage may rise as long as the electric current is increased. In addition, the higher temperature has an impact on the voltage in every measurement pattern. When the temperature is raised, the voltage or voltage drop is higher.

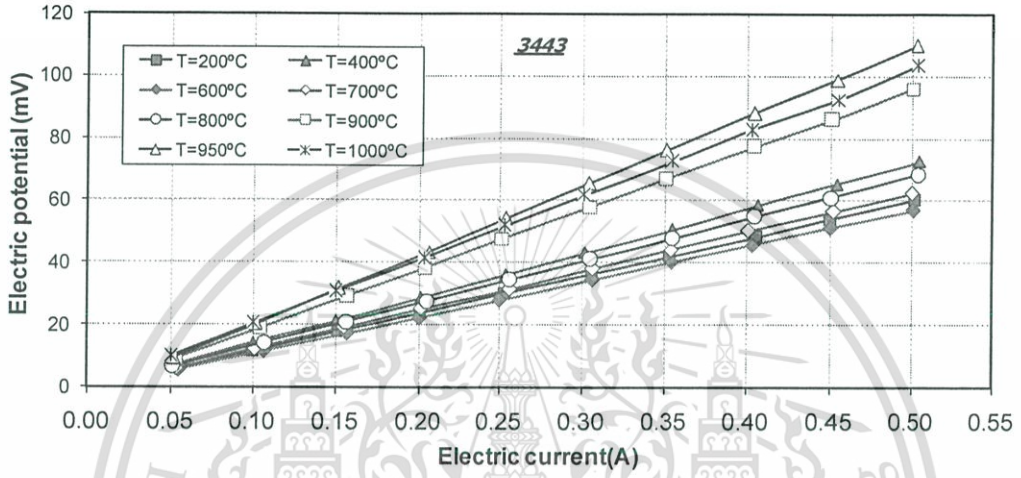

Figure 3.21 The relationship between voltage and electric current of Ag_4625 for pattern_3443.

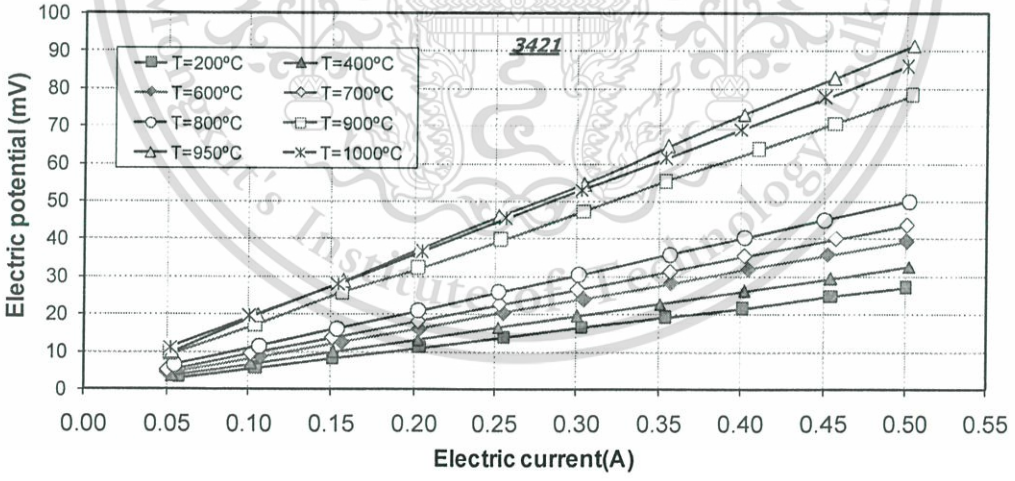

Figure 3.22 The relationship between voltage and electric current of Ag_4625 for pattern_3421.

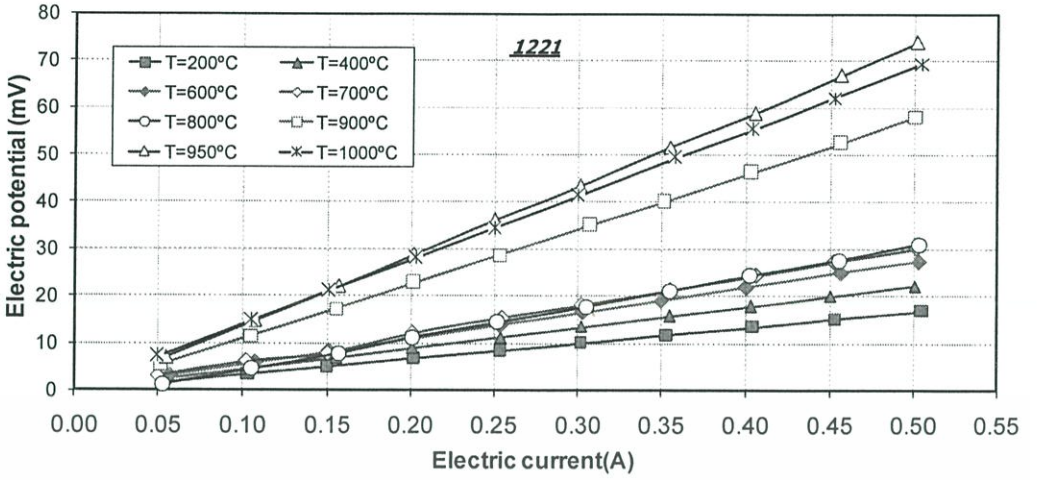

Figure 3.23 The relationship between voltage and electric current of Ag_4625 for pattern_1221.

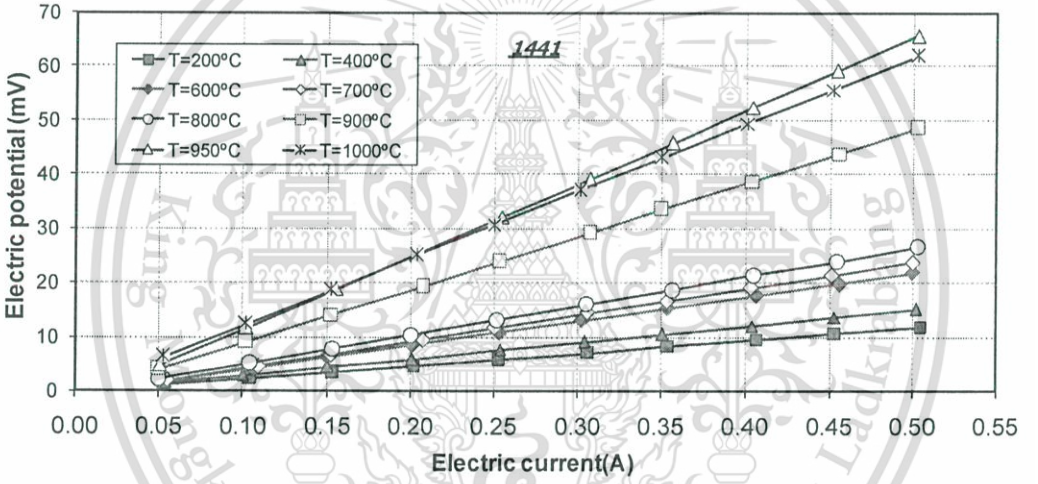

Figure 3.24 The relationship between voltage and electric current of Ag_4625 for pattern_1441.

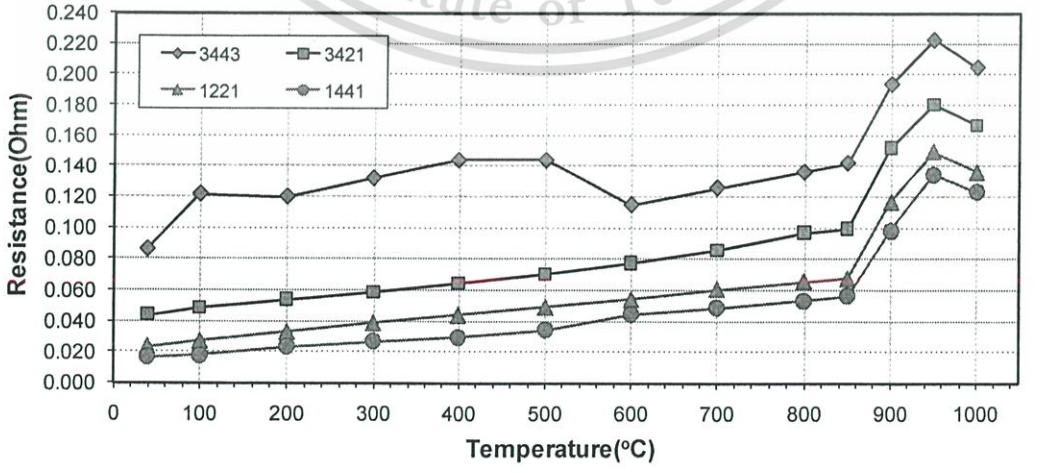

Figure 3.25 The resistance of Ag_4625 as a function of temperature of each measurement pattern.

From Figure 3.25, the resistance as a function of temperature is calculated form slopes of relationship between voltage and electric current from Figures 3.21 to 3.24. The resistances of pattern_3421, pattern_1221 and pattern_1441 have the same tendency from room temperature to 1000°C whereas the resistance of pattern_3443 oscillates at the initial step of temperature until 600°C then the tendency of resistance turns to be similar to other patterns until 900°C. At 1000°C, the resistance of every pattern is lower than the resistance at 900°C because of the change phase of silver from solid to liquid; the melting point of silver is 961.93°C [41].

Ag_4968

The result of the relationship between voltage and electric current for each of the measurement pattern of Ag_4968 is shown in Figures 3.26 to 3.29. The increase of voltage has a tendency to be linear like Ag_4625 when electric current was raised.

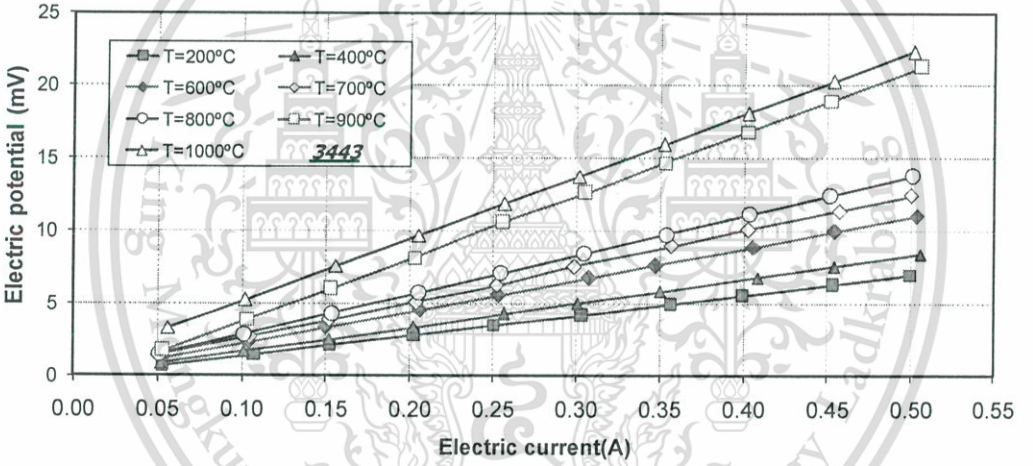

Figure 3.26 The relationship between voltage and electric current of Ag_4968 for pattern_ 3443.

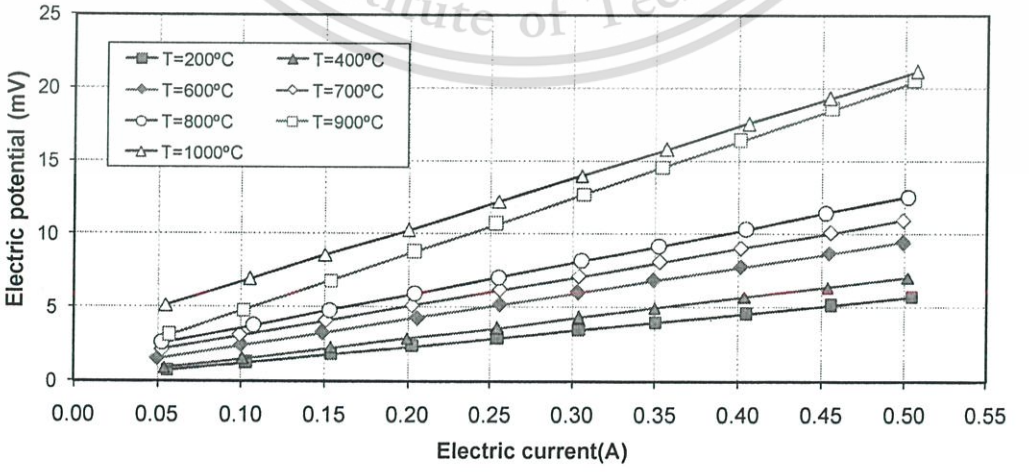

Figure 3.27 The relationship between voltage and electric current of Ag_4968 for pattern_ 3421.

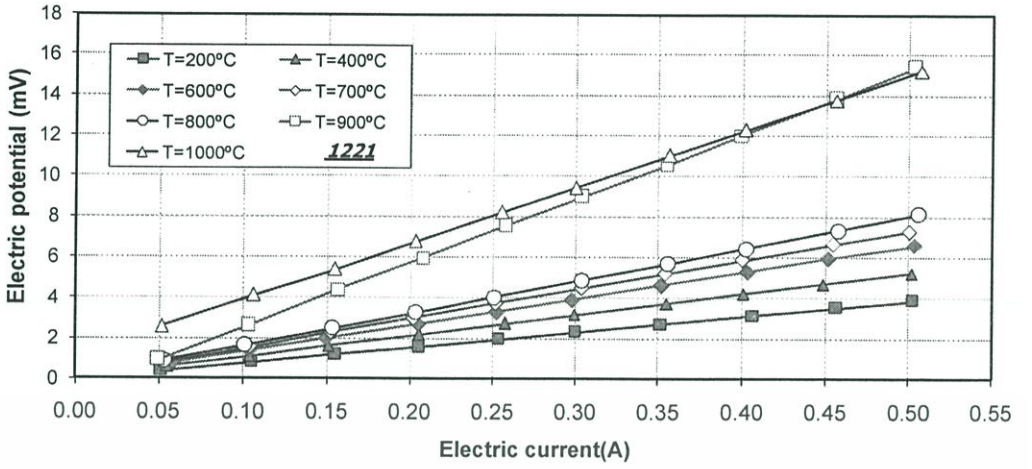

Figure 3.28 The relationship between voltage and electric current of Ag_4968 for pattern_ 1221.

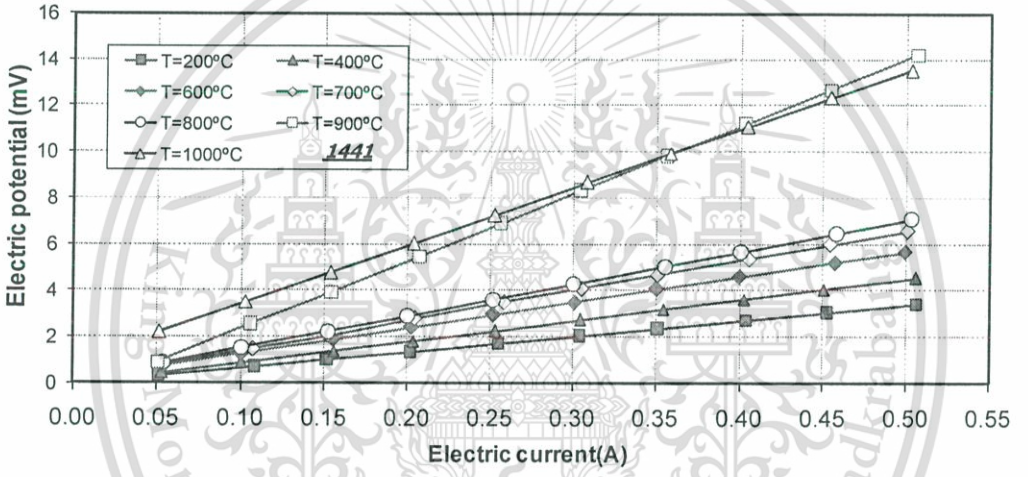

Figure 3.29 The relationship between voltage and electric current of Ag_4968 for pattern_ 1441.

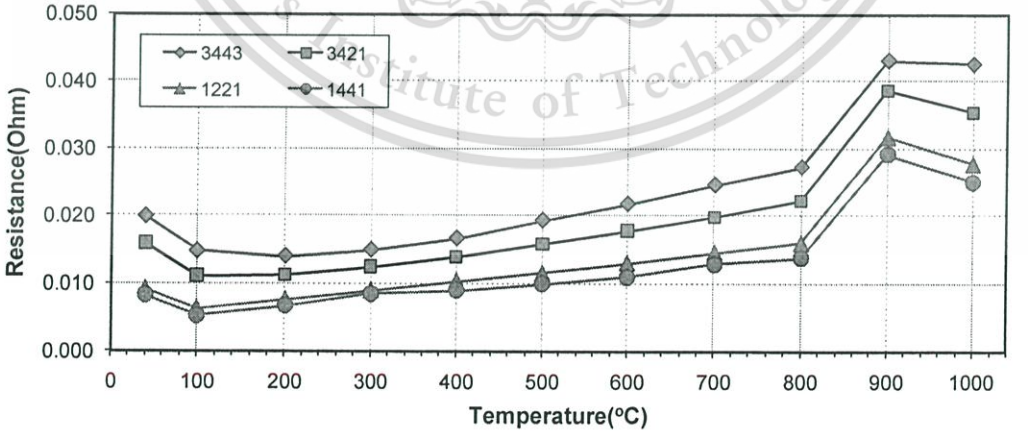

Figure 3.30 The resistance of Ag_4968 as a function of temperature of each measurement pattern.

The result of resistance calculated from Figures 3.26 to 3.29 belongs to Ag_4968 is shown in Figure 3.30. The resistances of every measurement pattern have the same tendency from room temperature to 1000°C. The resistance at initial temperature is higher than the resistance at 100°C; it might have an effect from the gap between inner and outside materials which is not contacted at the initial temperature. However, this effect was not concerned in this thesis because SOFC does not operate at this temperature. The behaviour of resistances from 800°C to 1000°C shoots up and comes down. The reason of this effect is the same as with Ag_4625 which is the melting effect of silver.

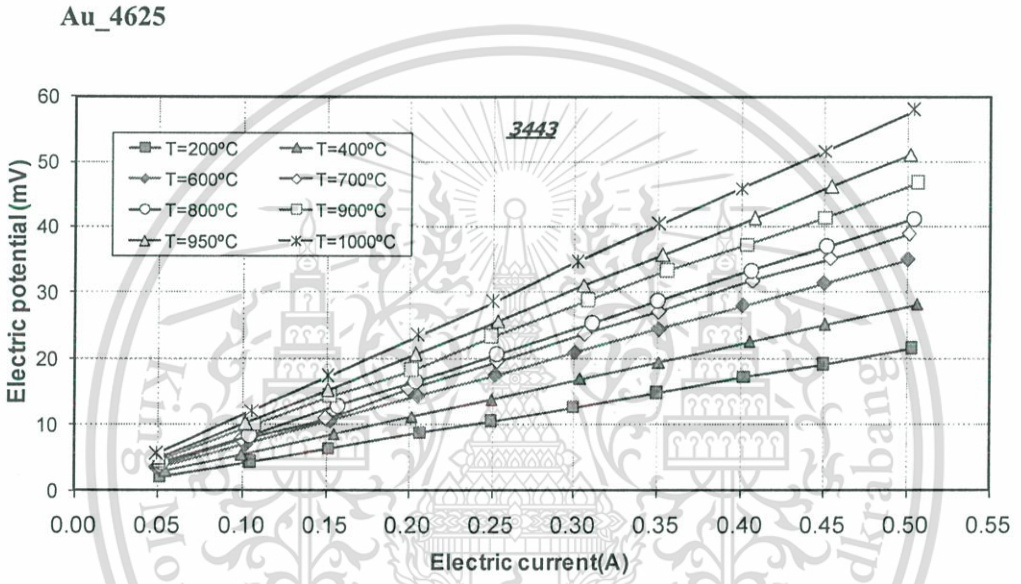

Figure 3.31 The relationship between voltage and electric current of Au_4625 for pattern_3443.

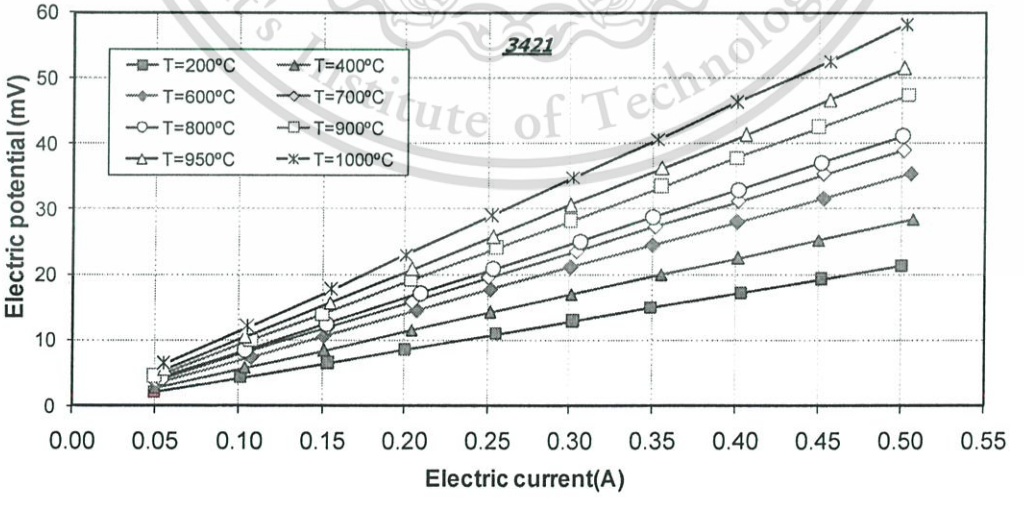

Figure 3.32 The relationship between voltage and electric current of Au_4625 for pattern_3421.

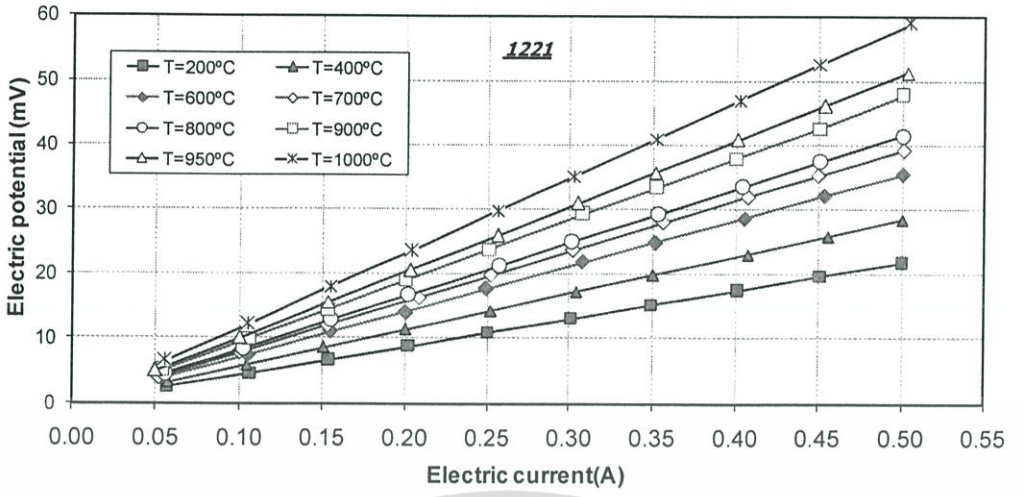

Figure 3.33 The relationship between voltage and electric current of Au_4625 for pattern_1221.

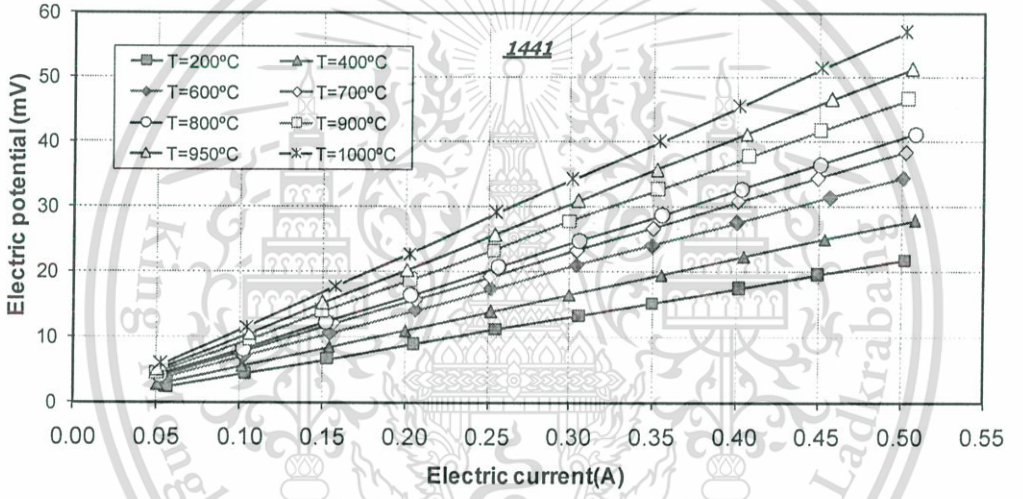

Figure 3.34 The relationship between voltage and electric current of Au_4625 for pattern_1441.

The result of the relationship of Au_4625 between voltage and electric current for each of the measured pattern are shown in Figure 3.31 to Figure 3.34. An increase of voltage has a tendency like Ag_4625 and Ag_4968. When electric current was raised and this specimen was heated up, the voltage is increased.

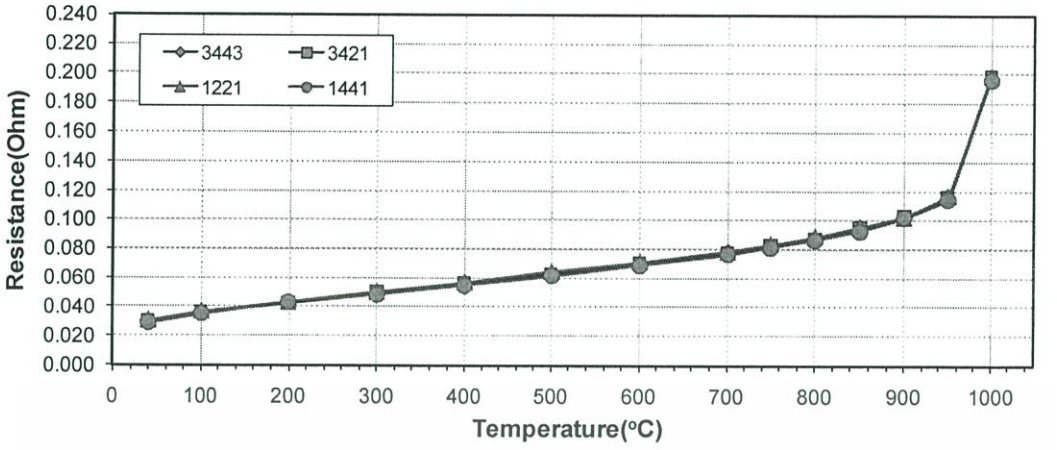

Figure 3.35 The resistance of Au_4625 as a function of temperature of each measured pattern.

In Figure 3.35, this graph shows the resistance for each of the measured pattern for model Au_4625 as a function of temperature. The temperature effect of Au_4625 has a little effect on resistance in each measured pattern when it is compared with the resistance result of Ag_4625. The reason why it has a little effect from temperature is due to the diffusion effect at contact interface between gold and SUS316L that will be shown in chapter 4.

Au_4968

The relationship between voltage and electric current in each of the measured pattern of Au_4625 are shown in Figures 3.36 to 3.39. An increase in voltage also has the tendency like every previous model. However, the melting point of gold, 1064.18°C [41], also makes an impact on the voltage at 950°C and 1000°C.

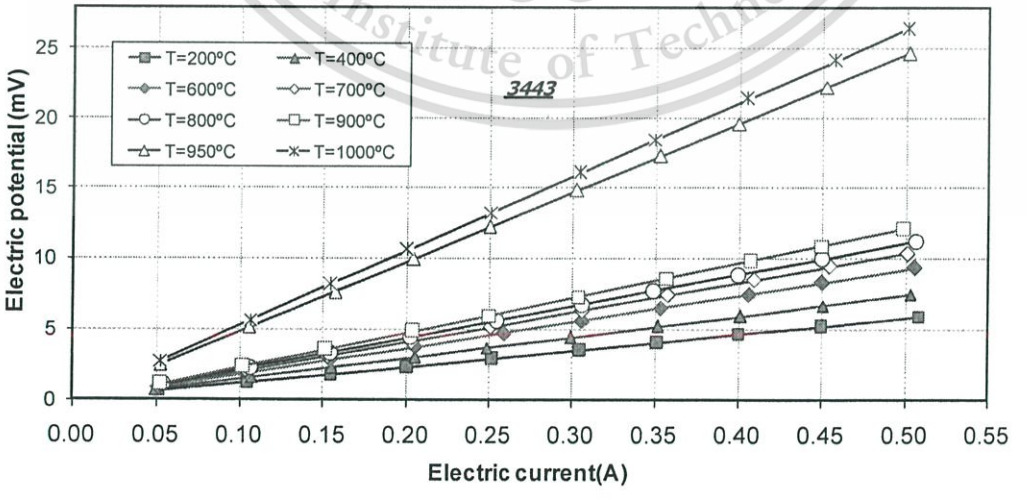

Figure 3.36 The relationship between voltage and electric current of Au_4968 for pattern_ 3443.

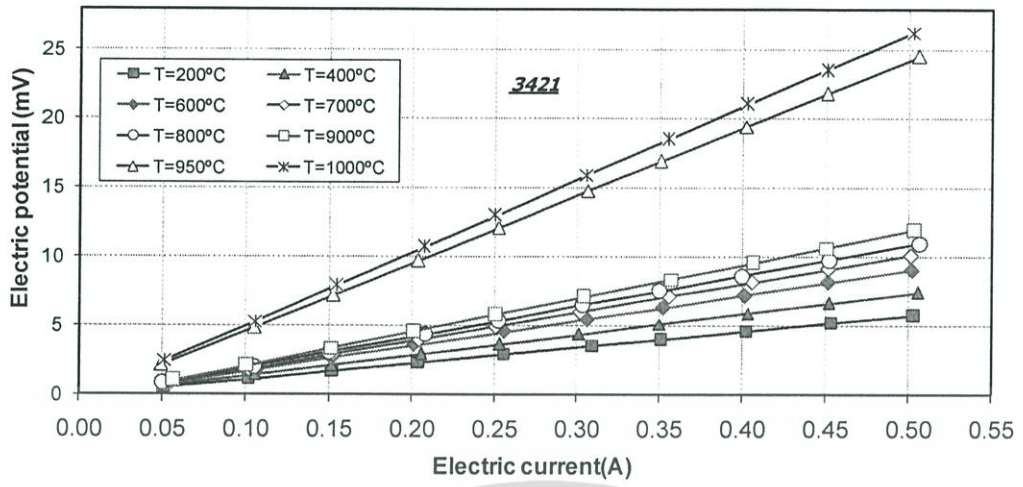

Figure 3.37 The relationship between voltage and electric current of Au_4968 for pattern_ 3421.

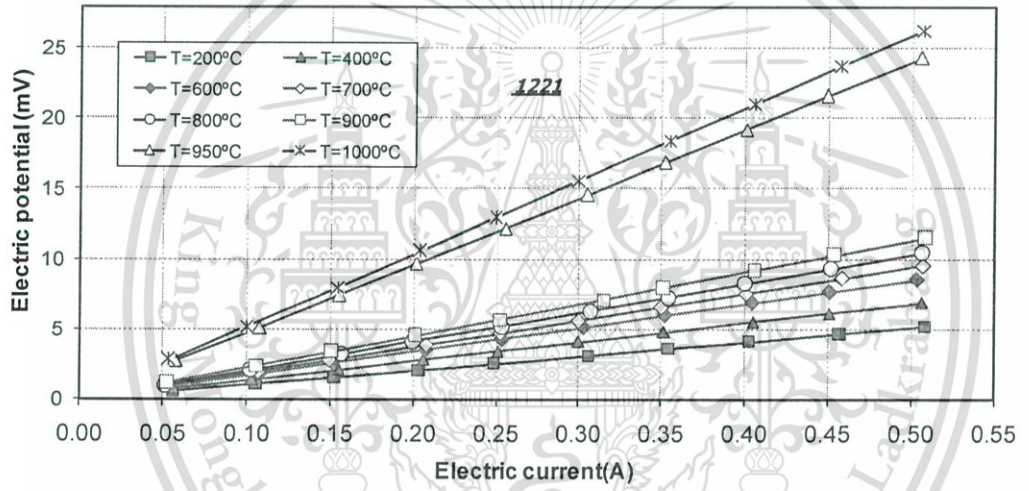

Figure 3.38 The relationship between voltage and electric current of Au_4968 for pattern_ 1221.

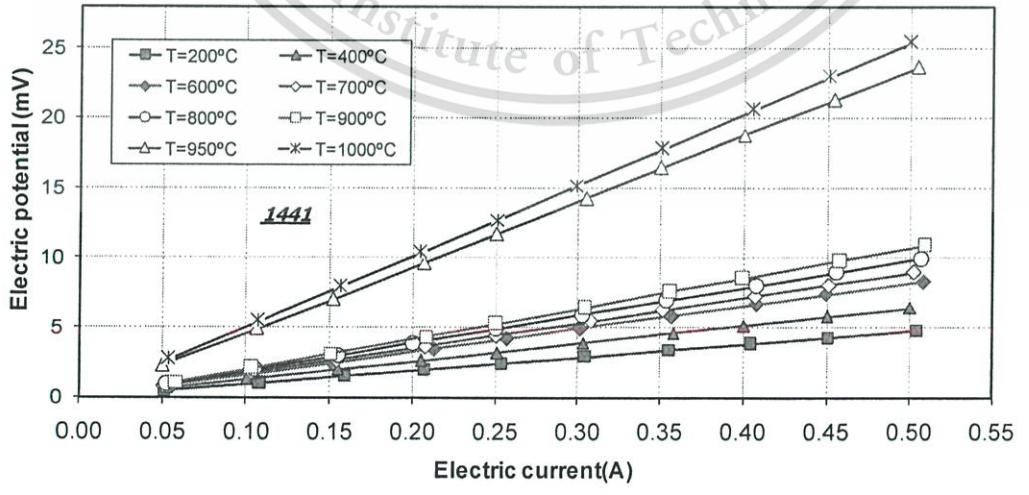

Figure 3.39 The relationship between voltage and electric current of Au_4968 for pattern_ 1441.

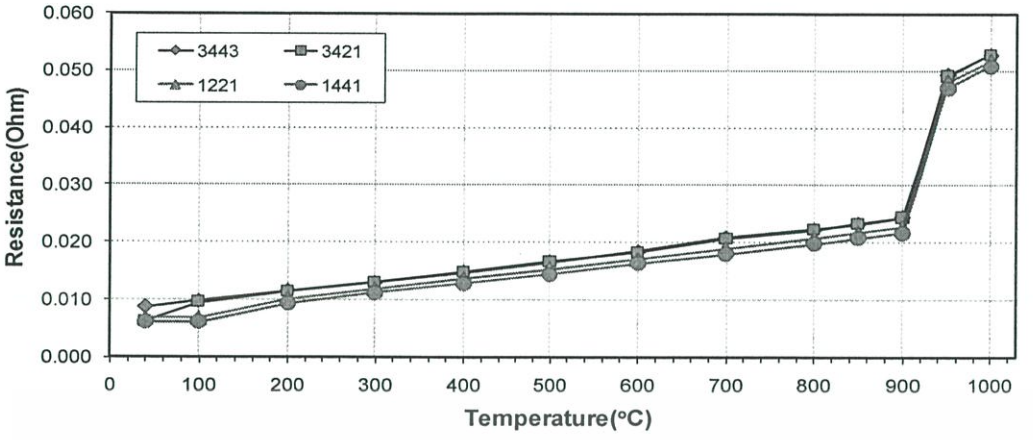

Figure 3.40 The resistance of Ag_4968 as a function of temperature of each measurement pattern.

In Figure 3.40, this graph shows the resistances for each of the measurement patterns for model Ag_4968 as a function of temperature. Every resistance in this graph has a tendency to be more adjacent together than the resistances of model Au_4968. Moreover, when the plot is compared with the plot of Ag_4625 shown in Figure 3.25, the gaps of resistance in each measurement pattern of Figure 3.40 are a closer than that in Figure 3.35.

In summary, the temperature effect has a direct impact on electrical resistance of models Ag_4625 and Ag_4968 whereas it has little impact on electrical resistance of models Au_4625 and Au_4968. In addition, the cross-section area for both silver and gold expands more than the contraction of the cross-section area of SUS316L from the temperature effect. Finally, they are practical to used in SOFC at high temperature

3.6.3 Electrical Conductivity

The electrical conductivity of composite material can be calculated from I-V curves and plotted to compare with commercial materials (Ag [12], Au [12] and Pt [13, 14]) as a function of temperature shown in Figure 3.41 – Figure 3.44. The cross-section area used for calculating the electrical conductivity of Au_4625, Au_4968, Ag_4625 and Ag_4968 is the sum between inner cross-section area and outside cross-section area.

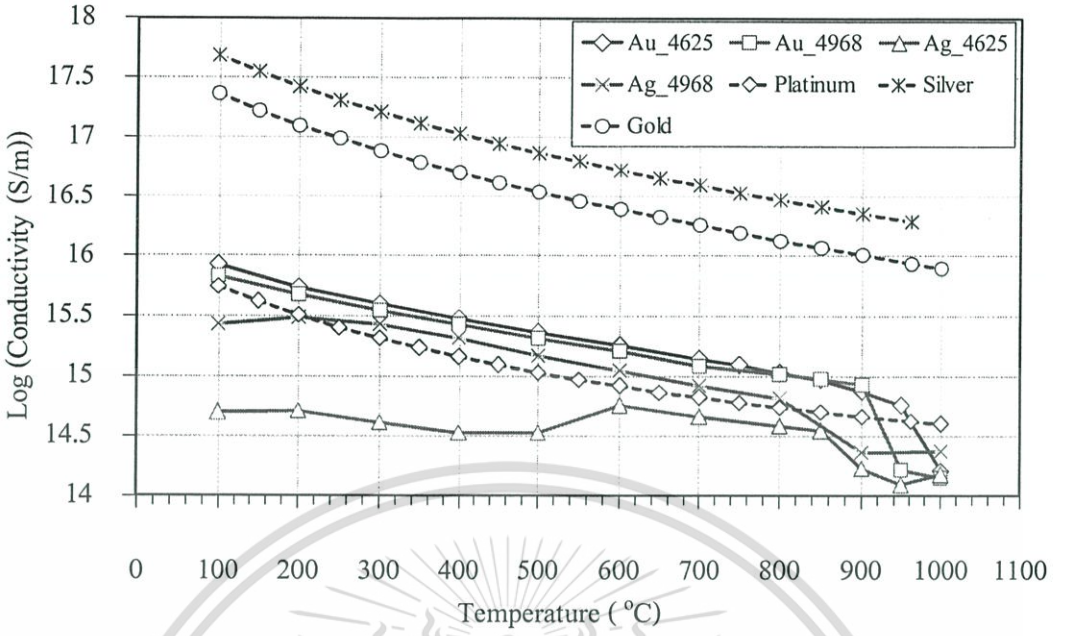

Figure 3.41 Electrical conductivity as a function of temperature in pattern_3443.

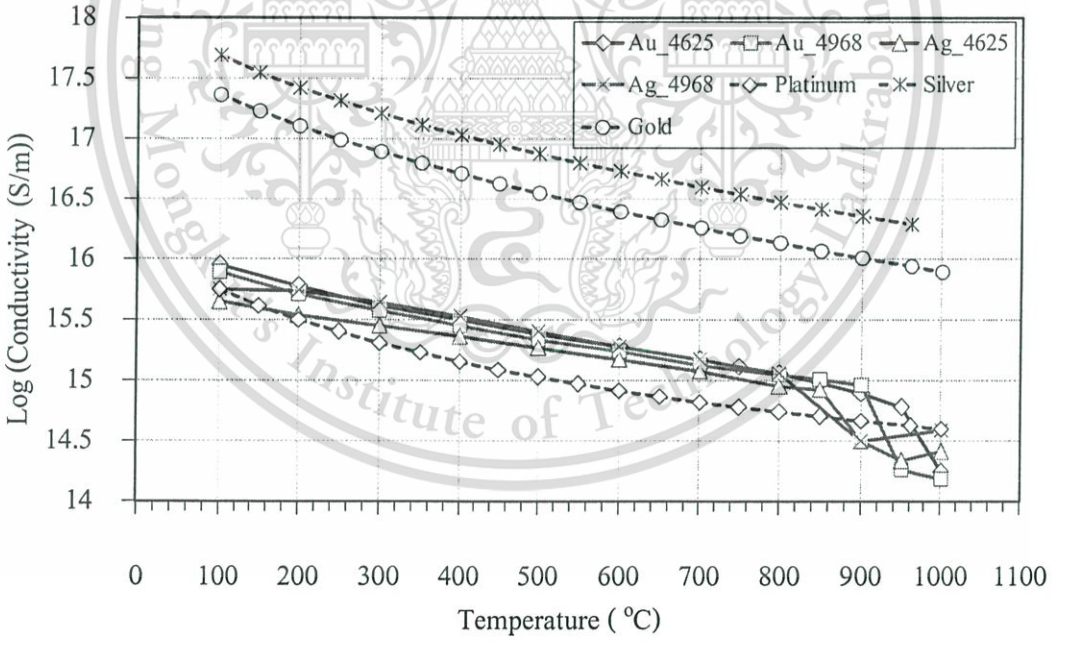

Figure 3.42 Electrical conductivity as a function of temperature in pattern_3421.

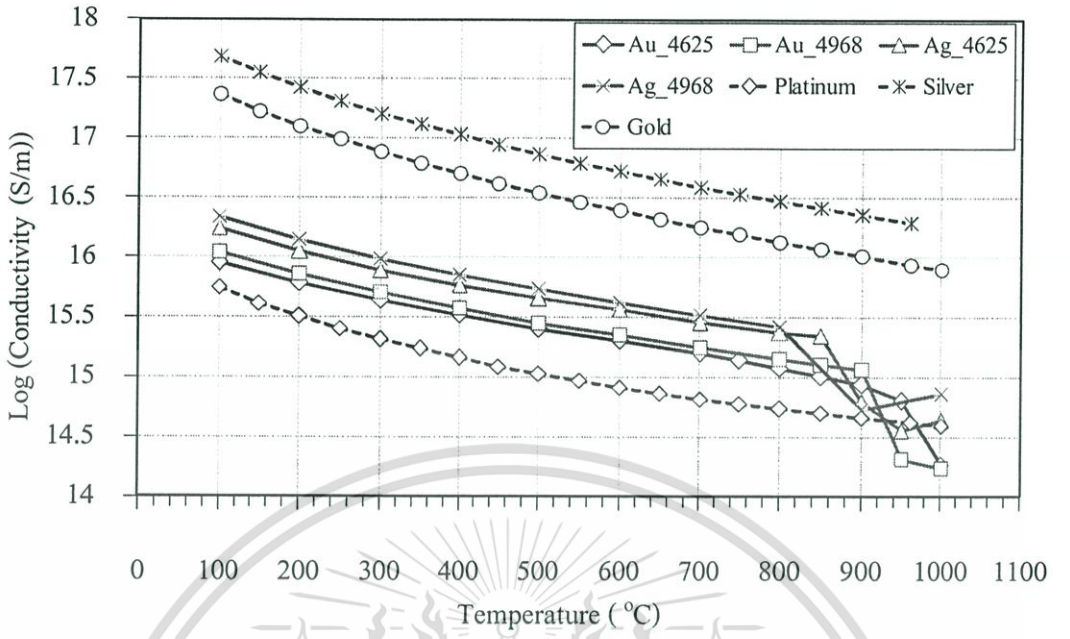

Figure 3.43 Electrical conductivity as a function of temperature in pattern_1221.

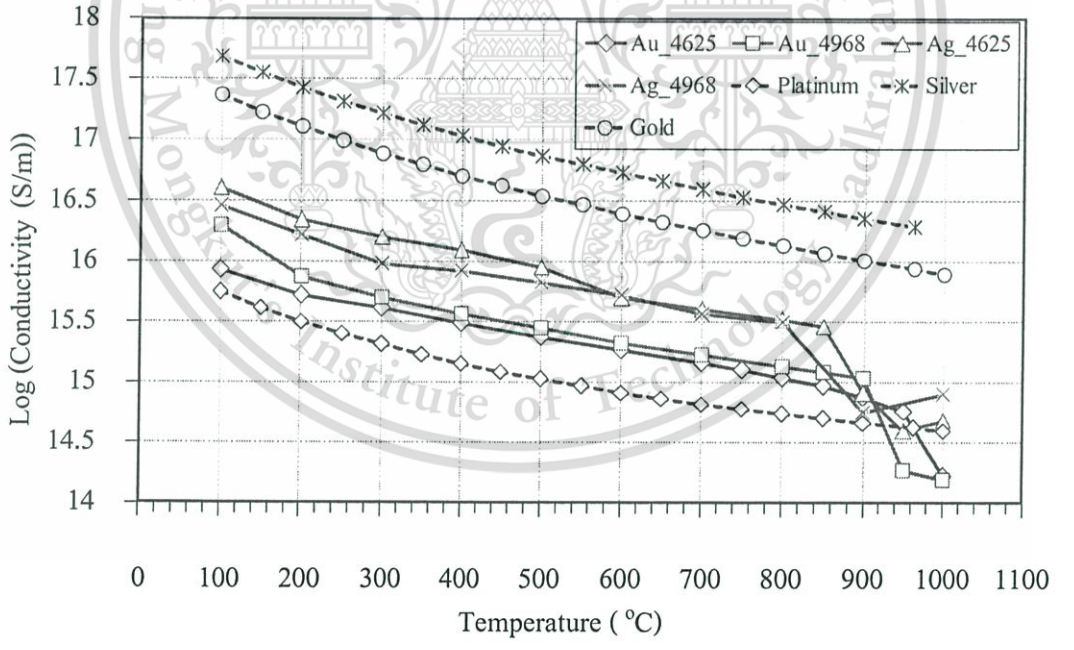

Figure 3.44 Electrical conductivity as a function of temperature in pattern_1441.

Form Figures 3.41 – 3.44, the conductivities of composite materials; Au_4625, Au_4968, Ag_4625 and Ag_4968 are lower than silver and gold at every temperature. The effect of measurement pattern has a direct impact on the electrical conductivity of Ag_4625 as shown in Figure 3.41 in which pattern_3443 shows the lowest among other models and other commercial materials. According to the measurement pattern in previous topic (3.61), pattern_1221 and pattern_1441 are practical for use in SOFC because electricity directly flow through the inner materials, silver and gold. Figure 3.43 (pattern_1221) and Figure 3.44 (pattern_1441) show that the electrical conductivity of Au_4625, Au_4968, Ag_4625 and Ag_4968 are higher than that of platinum from room temperature to 900°C. When they are heated up to 950°C, their electrical conductivities go down next to the electrical conductivity of platinum. The rapid downturn of electrical conductivity of models made of silver begins at about 800 – 850°C because their temperatures are near to the melting point of silver. In the same way with gold, the electrical conductivity quickly decreases at about 900°C as the melting point of gold is 1064.18°C. Wire in every model can conduct electricity despite the fact that both silver and gold are close to their melting points. In addition, most materials are low in mechanical strength when they are operated at high temperature [41]. Therefore, silver may have a chance to deform or damage at as high temperature as 850°C

In summary of electrical conductivity, the conductivity of Ag is higher than other materials at every range of operating temperature. In practice, it cannot be used in SOFC because of deformation from low melting point and low strength at high temperature. Ag_4625 and Ag_4968 were designed to prevent from the deformation from the low melting point of silver and to enhance a mechanical strength of a current conducting wire. In addition, this method can also prevent the oxidation of silver wire. From Figure 3.41, Ag_4625 and Ag_4968 can be used at high temperature. Gold is a material which has both high electrical conductivity and high strength at operating temperature of SOFC, but if is still expensive like platinum, which is going to be presented in the next topic. In addition, the main reason why the electrical conductivities Au_4625, Au_4968, Ag_4625 and Ag_4968 are lower than Ag and Au although they are made of Ag and Au because their electrical conductivity were calculated by using cross-section areas both the inner material, which is Ag and Au, and the outside material which is SUS316L. The electrical conductivity of SUS316L is the lowest among other materials considered in thesis. However, the main duties of SUS316L are prevention oxidation and improve strength of every model.

3.6.4 Cost

Silver, gold and platinum are commercially available materials. Ag_4625, Ag_4968, Au_4625 and Au_ 4968 are composite materials used in this thesis. The cost per gramme of each material has been calculated as shown in Table 3.6.

Table 3.6 Cost of materials [42]

Materials Cost	(USD/g)
Silver 99.99% (Ag)	0.542
Gold 99.99% (Au)	28.404
Platinum 99.99% (Pt)	61.792
Composite of sliver 0.4625 (Ag 4625)	0.657*
Composite of sliver 0.4968 (Ag 4968)	0.675*
Composite of gold 0.4625 (Au 4625)	34.479*
Composite of gold 0.4968 (Au 4968)	35.415*

www.kitco.com April 1, 2008

* calculated from material and production cost

Figure 3.45 shows the cost of material at various operating temperatures compared at a constant resistance of 0.2 Ω/m. The cost estimated for each model consists of material cost [42] and manufacturing cost, compared with the commercial materials, silver, gold and platinum. The cost of each material is approximately 2-3 times different between pure metal and its composite while at high temperature the result from current collecting wire is increased at the cross-section area for keeping constant resistance of 0.2 Ω/m.

In comparison between silver composite (Ag_4625 and Ag_4968) and gold composite (Au_4625 and Au_4968), the cost of composite silver is cheaper than composite gold and the conductivity of composite silver is greater than that of composite gold.

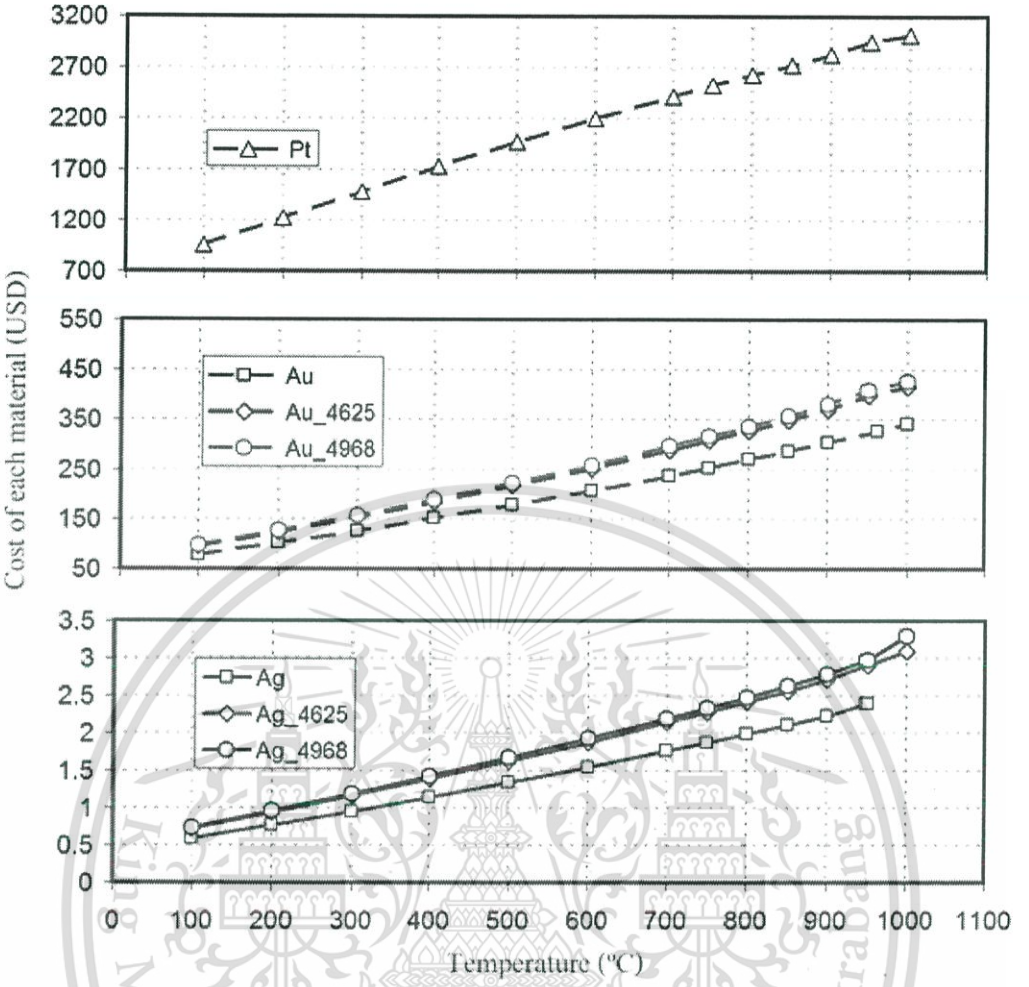

Figure 3.45 Cost of materials at various operating temperatures, compared at constant resistance of 0.2 Ω/m.

The cost of Pt is higher than the cost of Ag, Ag_4625 and Ag_4968 approximately 1200-1300 times at low temperature and 900-1000 times at high temperature. The cost of gold is higher than the cost of Ag, Ag_4625 and Ag_4968 about 100-150 times.

In summary, Ag_4625 and Ag_4968 are good choices for using at high temperature because they are relatively inexpensive and mechanically strength. In addition, they are still electrically conductive at high temperature.

CHAPHER 4

CONTACT INTERFACE

In this chapter, the behaviour of the contact interface between Ag and Au with SUS316L at high temperature (600 to 1000°C) has been studied when using the electric conducting wire at high temperature. The behaviours at each temperature of the specimens were investigated using SEM for microstructural investigation at the interface while the thermal stress of the contact interfaces were simulated using a finite element COMSOL program at each temperature (600 to 900°C).

The behaviours of the contact interface for metals are important for an application in Solid Oxide Fuel Cells (SOFCs) because a high electrical conductivity at high temperature (900°C to 1000°C) is desired. Metals of our interest for using in SOFCs are platinum, gold, silver and stainless steel. They were selected because of their high electrical conductivity and potential for an application at high temperature. The contact behaviour of metals such as gold and silver sheathed in stainless steel (SUS316L) has been studied. The properties of material from the simulation work are temperature dependent, i.e., thermal conductivity, thermal expansion coefficient, density, Poisson's ratio and Young's modulus.

4.1 Behaviour at the Contact Interface Using SEM

Experiments were conducted in these sequences.

4.1.1 Preparation of Specimens

The geometries of investigated tube specimens were shown in Figure 4.1. Silver and gold were sheathed in SUS316L. The outer diameter and inner diameter of SUS316L were 3.18 mm and 1.58 mm, respectively. The gap of about 0.05 mm was observed at the interfacial contacts.

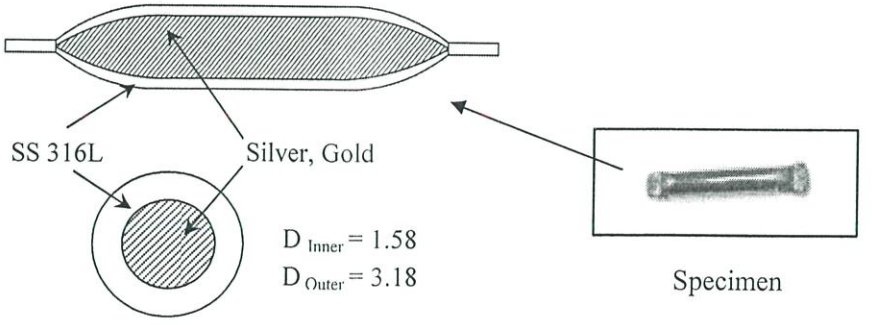

Figure 4.1 Geometries of investigated specimen.

4.1.2 Heating and Quenching Specimen

The specimens were heated in a furnace at 600°C, 650°C, 700°C, 750°C, 800°C, 850°C, 900°C, 950°C, 975°C and 1000°C and held at each temperature for 30 minutes in air as shown in Figure 4.2 and then quenched in water at room temperature.

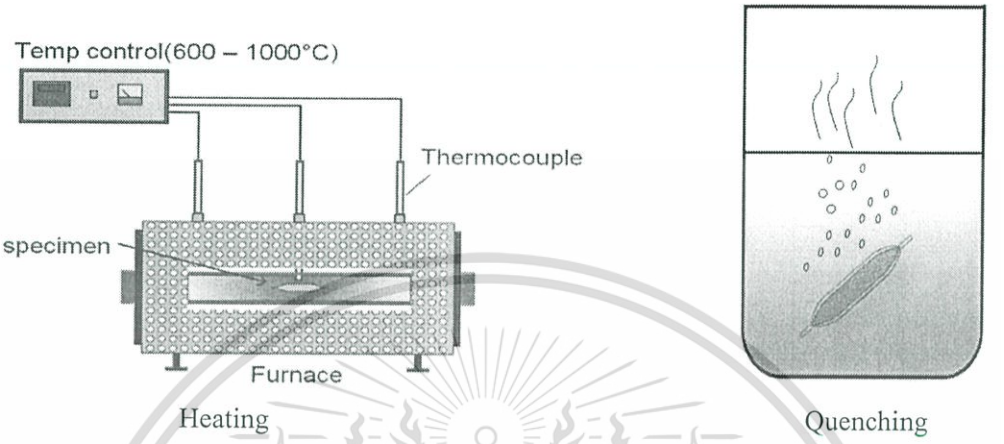

Figure 4.2 Heating and quenching specimen.

The quenching process was also simulated by using COMSOL program in order to indentify the quenching time of the contact interface for both silver and gold sheathed in SUS316L. The heat transfer convection coefficient and temperature of water were the two parameters which hypothesized. The heat convection coefficient of water [42] was varied from 500 to 2000 $W/m^2.°C$ in the simulation process and temperature of water was set at 30°C. Some specimens in the experiment at 900°C, 950°C, 975°C and 1000°C were simulated because of abundant diffusion effect at these temperatures more than at other temperatures.

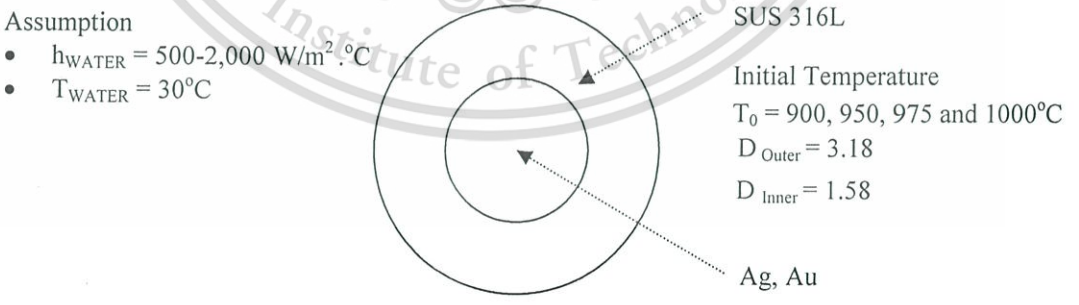

Figure 4.3 Condition of specimen used in studying the quenching time.

The boundary condition for simulation is shown in Figure 4.3 containing 9952 elements as shown in Figure 4.4. In this case, the results focus on the quenching time at the contact interface. The elements used were triangle meshes because they could be generated to cover all

the area of a circle. However, a triangle mesh is less accurate than a square mesh. The number of element is a choice to increase the precision of result using the triangle mesh.

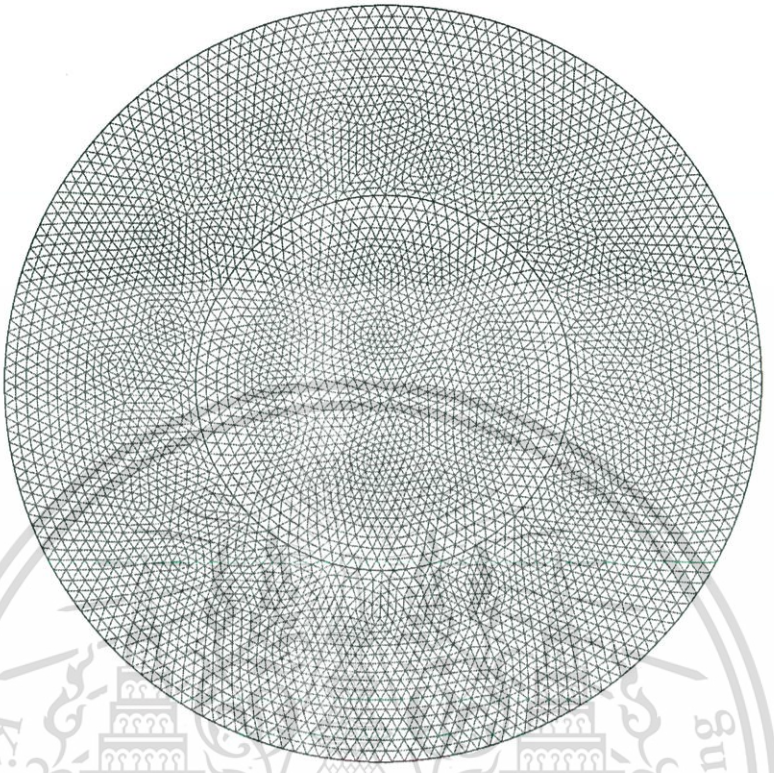

Figure 4.4 9952 elements used for simulation.

The results of simulation in Figure 4.5 to Figure 4.8 show the quenching time versus temperature of the electric conducting wire of silver sheathed in SUS316L. The heat transfer convection coefficient plays an important role with the cooling rate; the cooling rate at high heat convection coefficient quickly decreases higher than the cooling rate at low heat transfer convection coefficient. The quenching time is not over 14 second in each of the heat transfer convection coefficient from initial temperature to room temperature (30°C). The quenching time of heat transfer convection coefficient at 2000 $W/m^2.°C$ took around 8 seconds from 900-1000°C to room temperature which is the least time required for this heat transfer convection coefficient. However, the heat transfer convection coefficients set in the simulation are trends to find the quenching time between 500-2000 $W/m^2.°C$ which are the lowest range of the heat transfer convection coefficient of water.

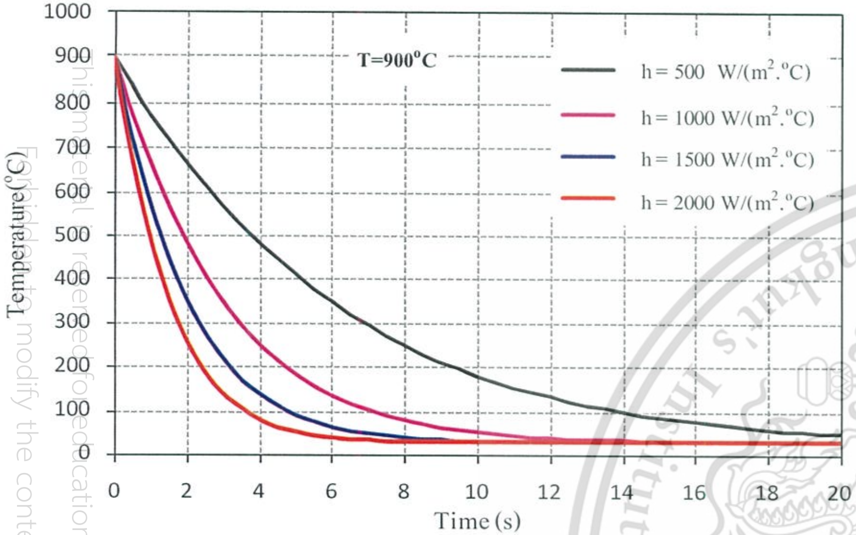

Figure 4.5 Quenching time of silver sheathed in SUS316L from 900°C in water.

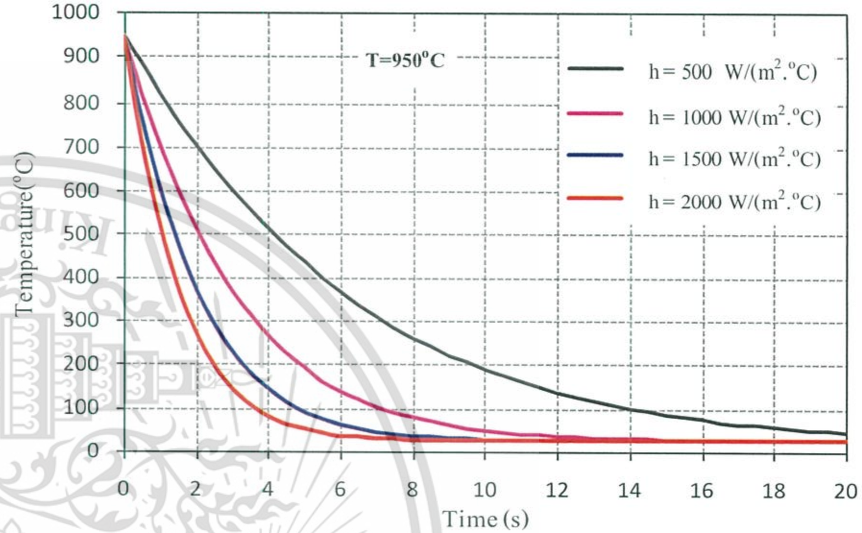

Figure 4.6 Quenching time of silver sheathed in SUS316L from 950°C in water.

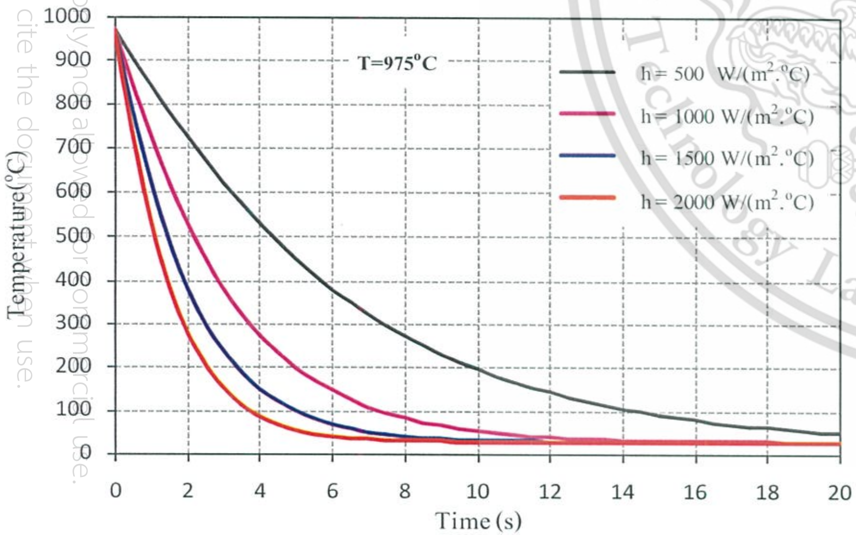

Figure 4.7 Quenching time of silver sheathed in SUS316L from 975°C in water.

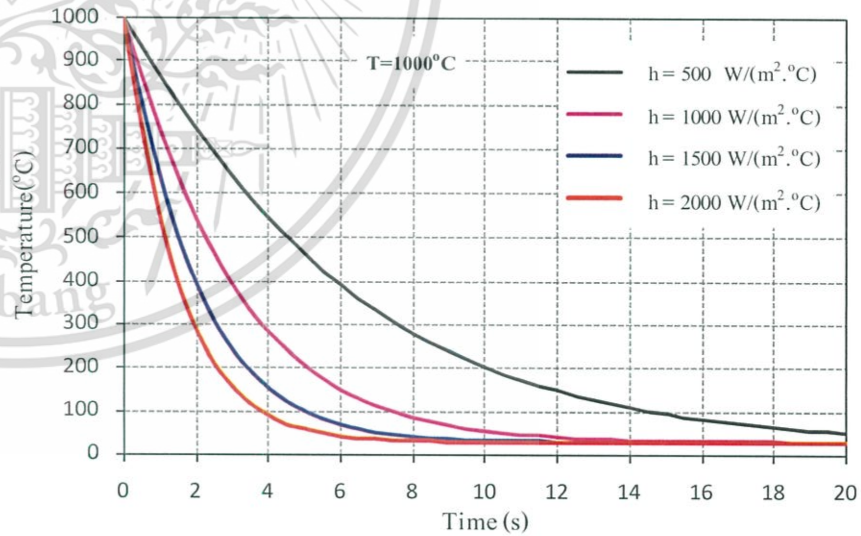

Figure 4.8 Quenching time of silver sheathed in SUS316L from 1000°C in water.

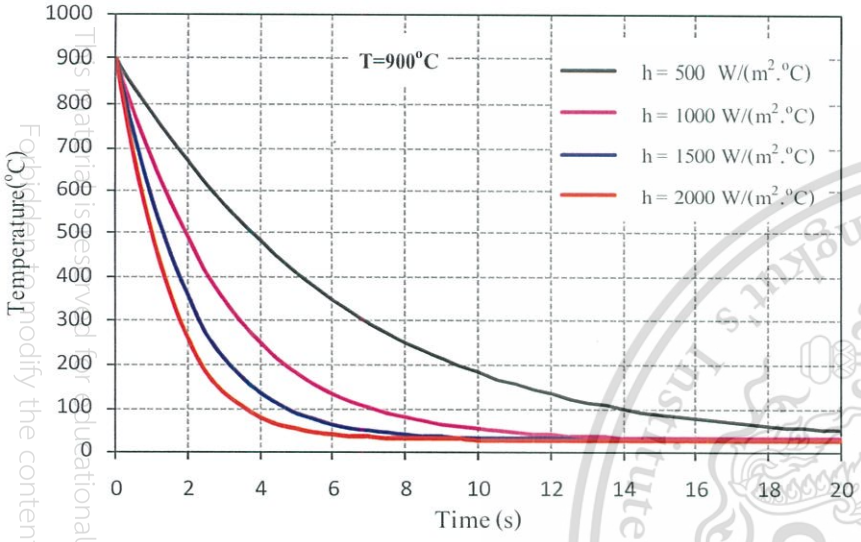

Figure 4.9 Quenching time of gold sheathed in SUS316L from 900°C in water.

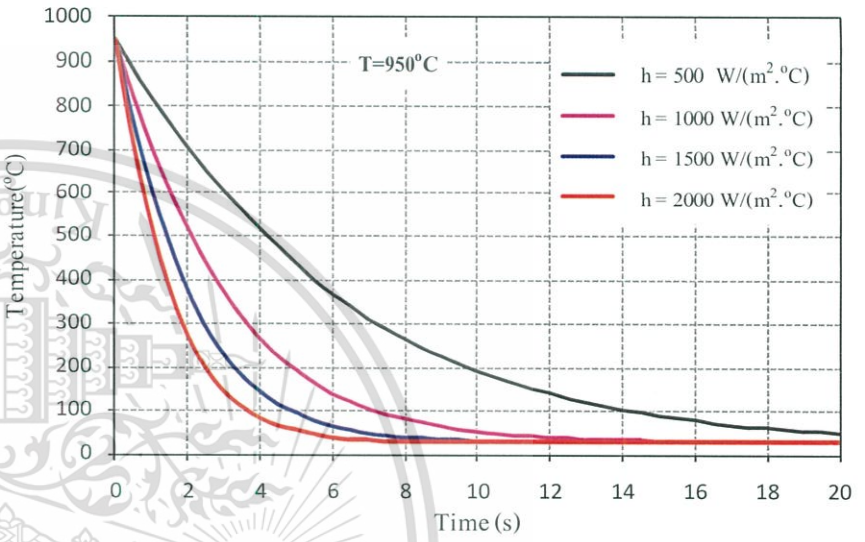

Figure 4.10 Quenching time of gold sheathed in SUS316L from 950°C in water.

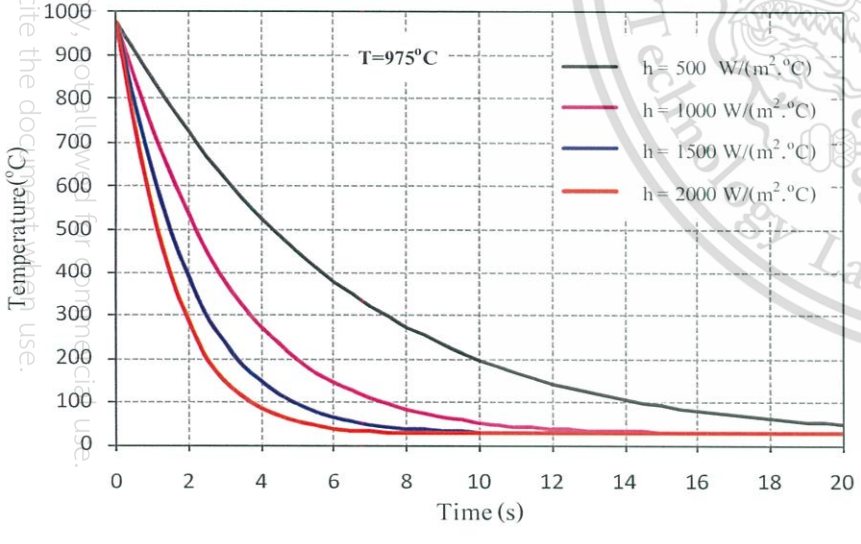

Figure 4.11 Quenching time of gold sheathed in SUS316L from 975°C in water.

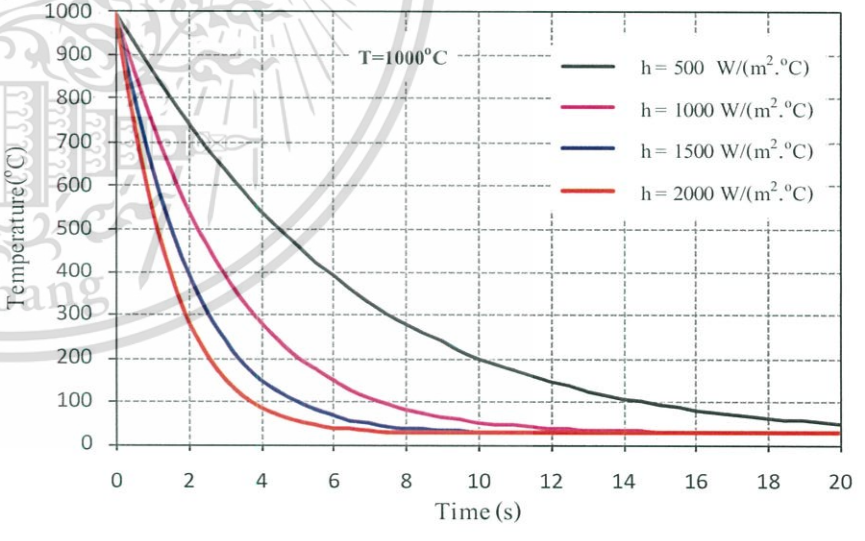

Figure 4.12 Quenching time of gold sheathed in SUS316L from 1000°C in water.

Figure 4.9 – Figure 4.12 show the quenching time of the electric conducting wire made of gold sheathed in SUS316L. The quenching time of gold sheathed in SUS316L is almost the same as silver sheathed in SUS316L although the thermal conductivity of gold sheathed in SUS316L is less than silver sheathed in SUS316L and the amount of heat for gold is a bit greater than silver due to high density of gold. However, if silver is not sheathed in SUS316L, its quenching time is lower than for gold because of high thermal conductivity of silver and a direct contact with water. In this case, SUS316L seems like an insulator for silver and gold owing to its lower coefficient of thermal conductivity.

However, the results are still based on the constant coefficient of heat convection transfer in this thesis. In practice, the heat transfer convection coefficient is not stable due to boiling point of water around the specimen. The boiling point of water has more effect when the specimen does not move and stays at the bottom of glass.

4.1.3 Specimen Sectioning

The specimen was cross - sectioned for SEM investigation as the inside of the specimen was not oxidized. The variation of the thermal stress was not significant and was assumed to be symmetry along z-axial within a few millimetres.

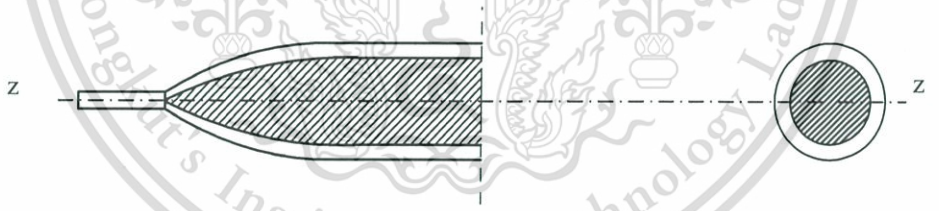

Figure 4.13 Position of cutting specimen.

Before the specimens were investigated using SEM, they were calculated gap area as a function of temperature using optical oscilloscope and Image-Pro Plus (Media Cybernetics Version 5.1) as shown in Figure 4.14.

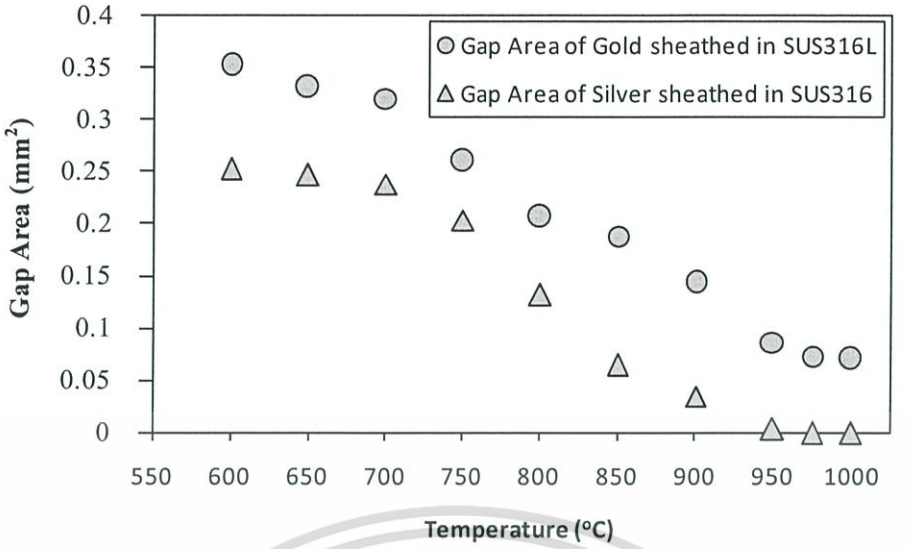

Figure 4.14 Gap Area at contact interface as a function of temperature.

Gap area at the contact interface decreases when the temperature of specimen was increased as shown in Figure 4.14. The gap area of silver sheathed in SUS316L is less than that of gold sheathed in SUS316L at every temperature. However, the real gap area of gold sheathed in SUS316L is not able to be calculated by using an optical microscope and Image-Pro Plus (Media Cybernetics Version 5.1) because it still has many areas which are porous. The less gab area increases the contact interface between inner and outside materials; the electric current can easily flow through between materials in case there are some spaces in inner material. The electric current can change flow direction of electric current from inner material to outside material and return back to inner material again as shown in Figure 4.15.

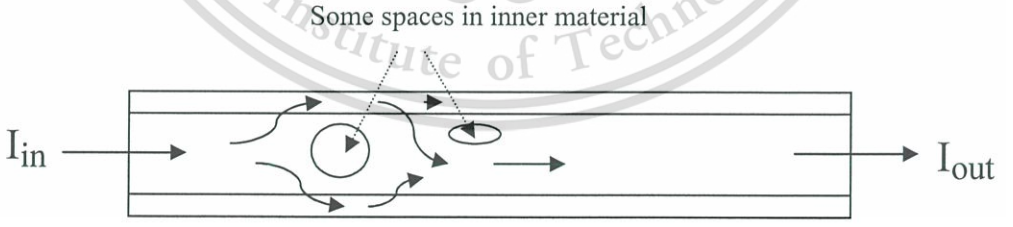

Figure 4.15 Changing flow direction in case of some space in inner material.

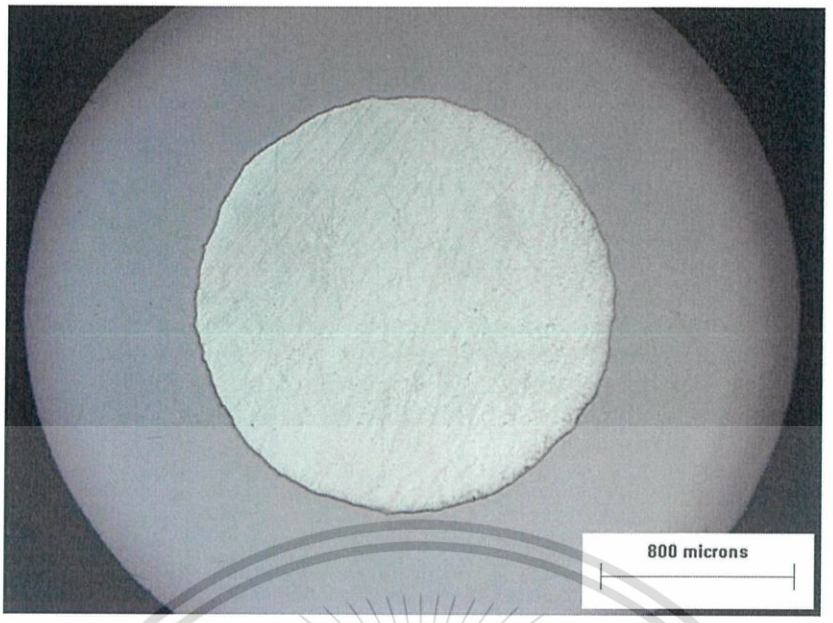

Figure 4.16 Optical microscope photograph of silver sheathed in stainless steel SUS316L at 900°C.

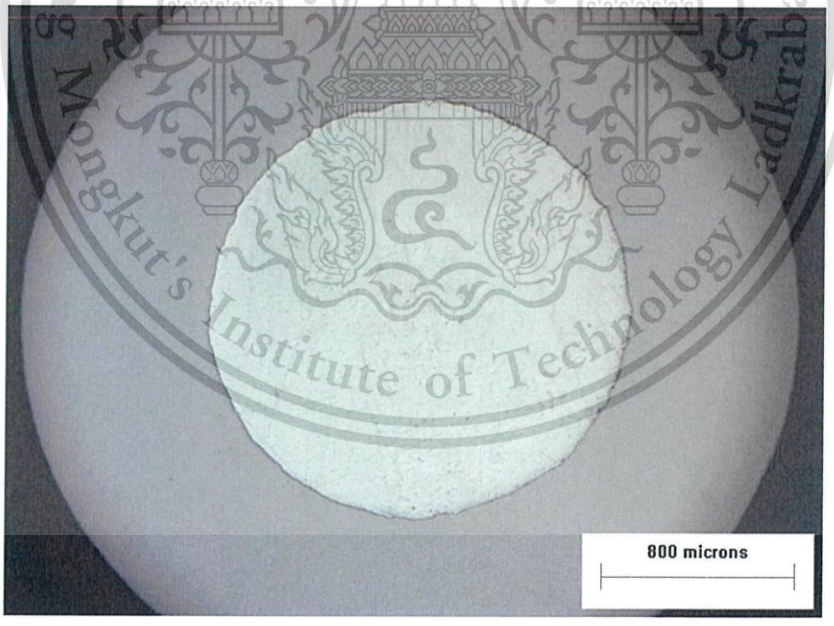

Figure 4.17 Optical microscope photograph of silver sheathed in SUS316L at 950°C.

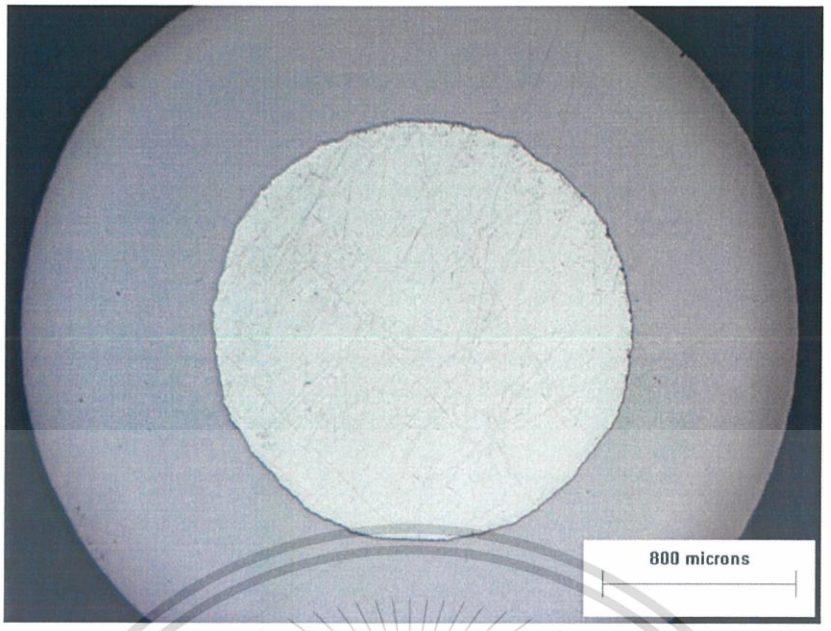

Figure 4.18 Optical microscope photograph of silver sheathed in SUS316L at 975°C.

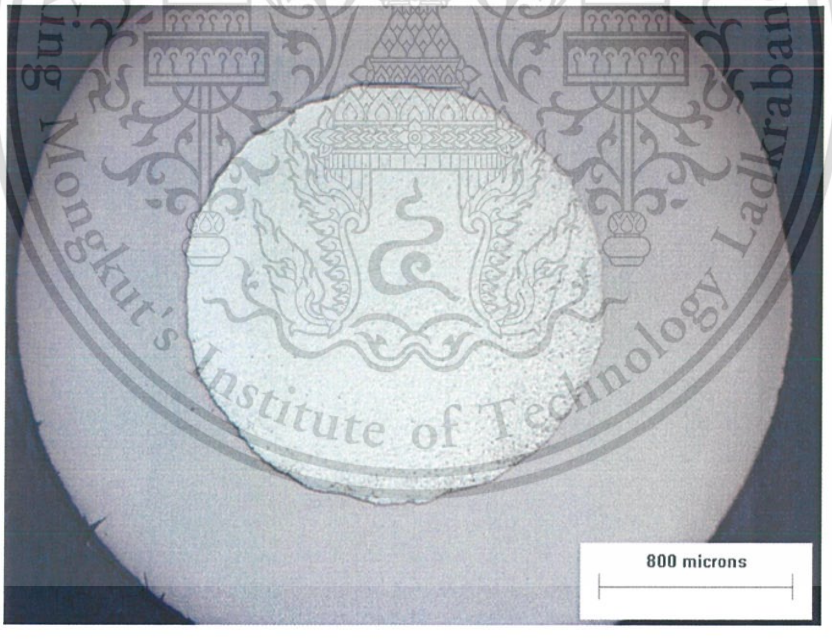

Figure 4.19 Optical microscope photograph of silver sheathed in SUS316L at 980°C.

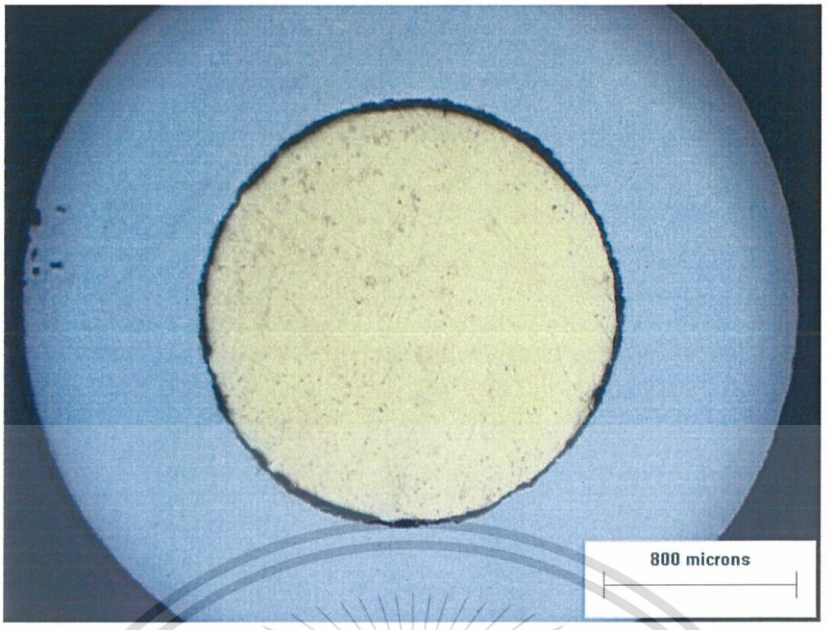

Figure 4.20 Optical microscope photograph of gold sheathed in SUS316L at 900°C.

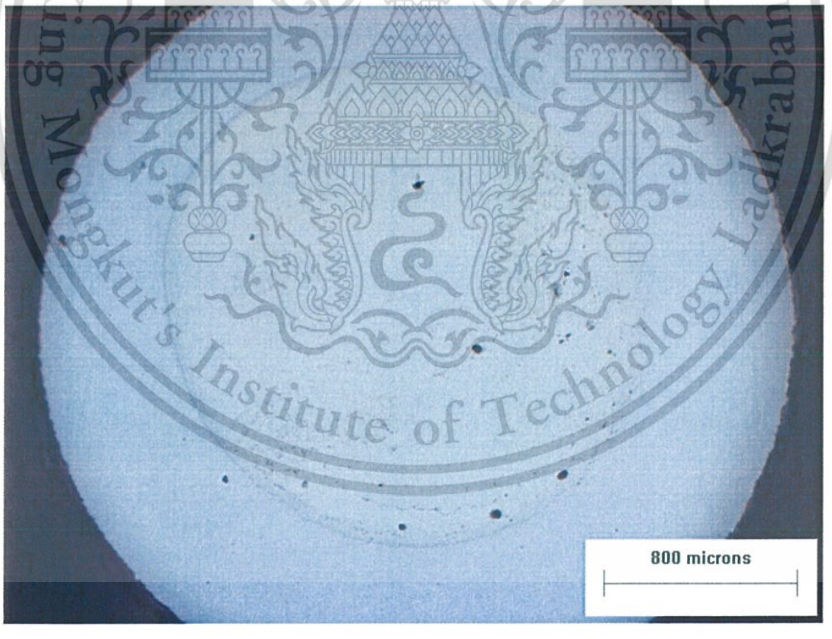

Figure 4.21 Optical microscope photograph of gold sheathed in SUS316L at 950°C.

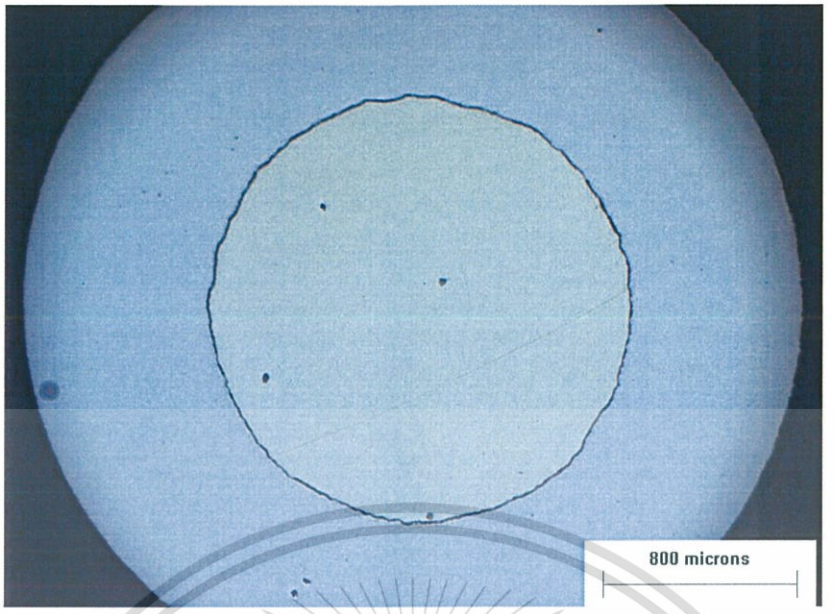

Figure 4.22 Optical microscope photograph of gold sheathed in SUS316L at 975°C.

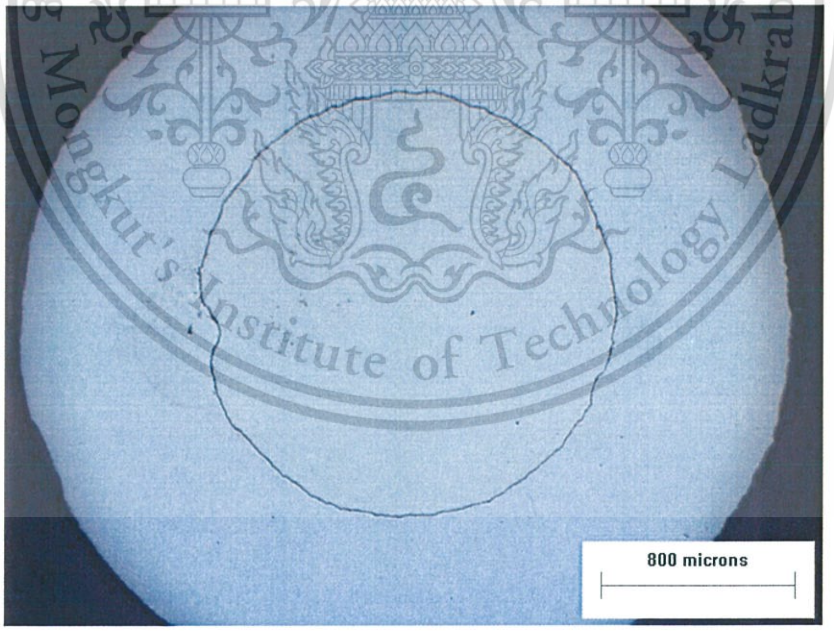

Figure 4.23 Optical microscope photograph of gold sheathed in SUS316L at 1000°C.

Figures 4.16-4.19 show optical microscope photographs of the silver sheathed at SUS316L in each quenching temperature. The photographs reveal that they have no alloy between silver and SUS316L. On the other hand, the optical microscope photographs of the gold sheathed in SUS316L as shown in Figures 4.20-4.23 have alloyed between the contact interfaces when temperature of the gold and SUS316L was heated to higher than 950°C; this could be explained by the typical alloy formation between Au and Ni as shown in Figure 2.24 in chapter 2.

4.1.4 Scanning Electron Microscope Investigation

For SEM investigation, the specimens were polished and coated if the specimen includes silver; it was coated with gold to be easily detected using an SEM (JEOL JSM-5410). For the specimen including gold, it was coated with carbon. All of the specimens are shown in Figure 4.24. The specimen on the left of Figure 4.24 is gold sheathed in stainless steel which was coated with carbon and the other specimen is silver sheathed in stainless steel that was coated with gold.

Figure 4.24 Specimens for SEM investigation.

The specimens heated at 900°C, 950°C, 975°C and 1000°C were taken photographs of microstructure using SEM while the linear EDS were used to investigate amount of diffusion at the contact interface.

4.2 Results and Discussion

The microstructure of the interfacial contacts between Ag and Au with SUS316L were observed using an SEM. The linear EDS was performed to investigate the diffusion of metals at the contact interfaces between Ag and Au with SUS316L.

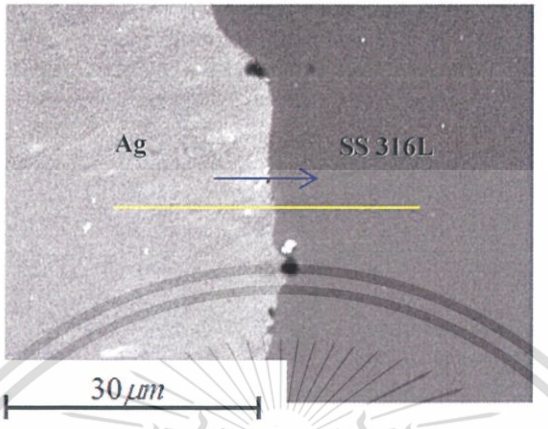

(a)

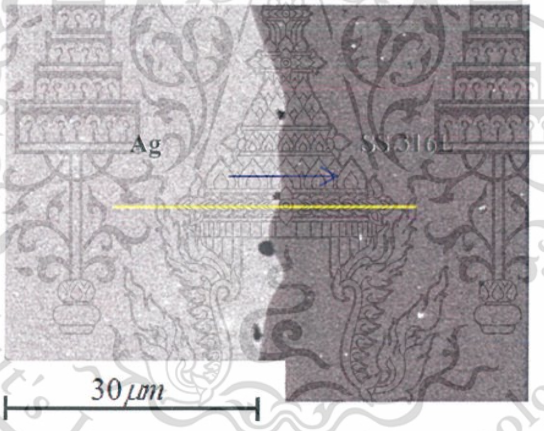

(b)

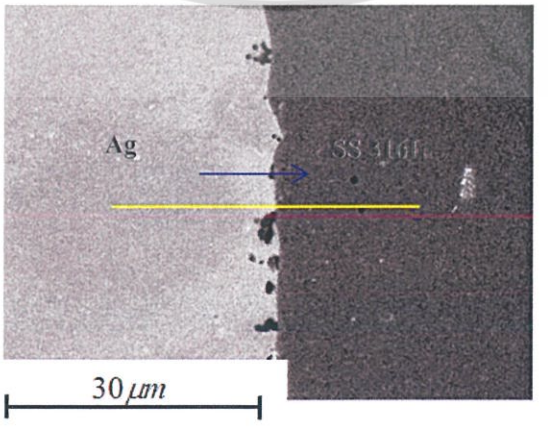

(c)

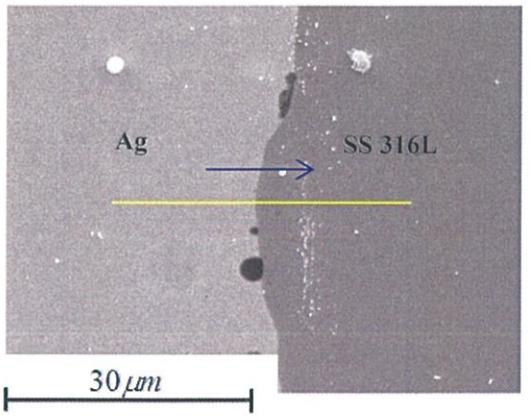

(d)

Figure 4.25 SEM micrographs of silver sheathed in SUS316L at 900(a), 950(b), 975(c) and 1000°C(d).

Figures 4.25 (a), (b), (c) and (d) show the microstructures at the interface between Ag and SUS316L at various temperatures. Figure 4.26 – Figure 4.29 show EDS line scans of each specimen from Figure 4.25 along the arrow direction. The line scans show that the diffusion at the interface contacts between Ag and SUS316L has not occurred.

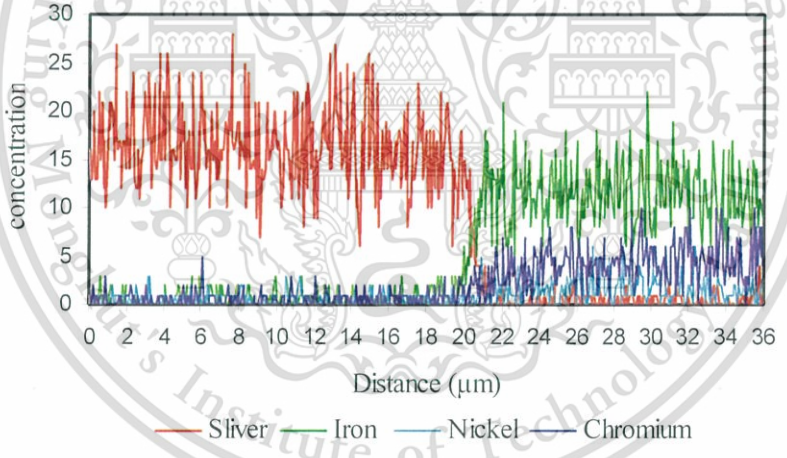

Figure 4.26 EDS of silver sheathed in SUS316L at 900°C.

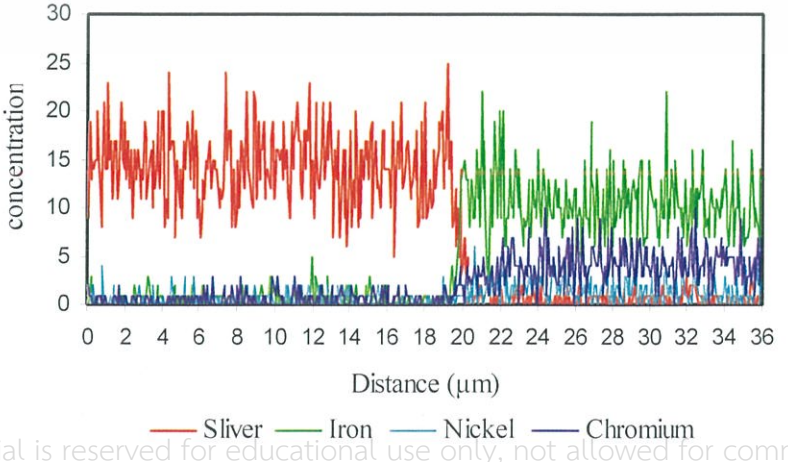

Figure 4.27 EDS of silver sheathed in SUS316L at 950°C.

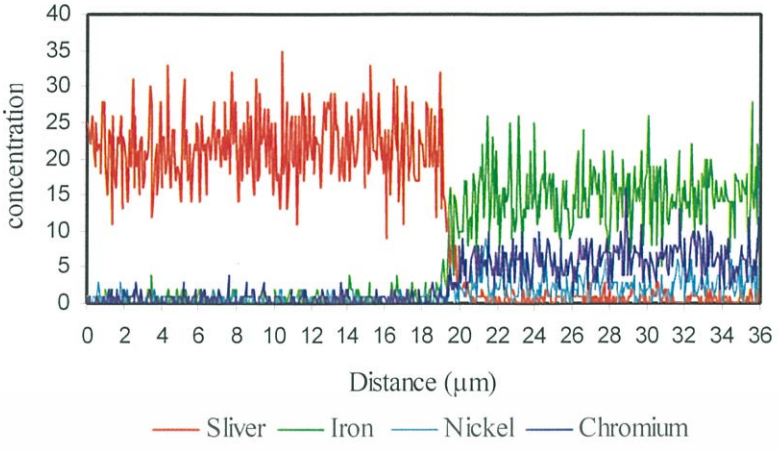

Figure 4.28 EDS of silver sheathed in SUS316L at 975°C.

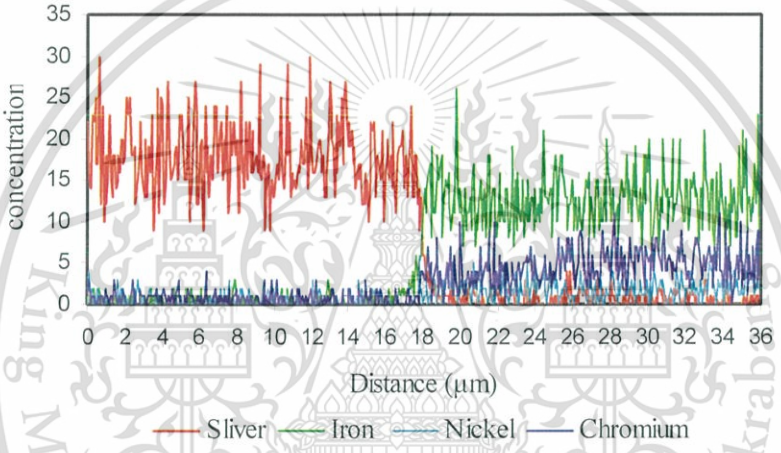

Figure 4.29 EDS of silver sheathed in SUS316L at 1000°C.

Figures 4.30 (a), (b), (c) and (b) show the microstructure at the interface between Au and SUS316L at various temperatures. Figure 4.31 – Figure 4.34 show the EDS line scans of each specimen from Figure 4.20 along the arrow direction. In the opposite, the line scans reveal that diffusion at the interface contacts between Au and SUS316L have occurred at every temperature examined.

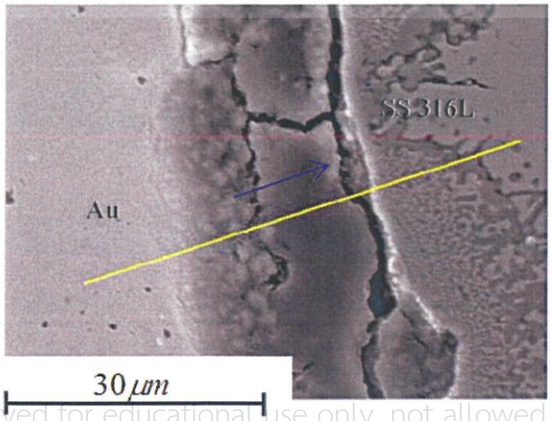

(a)

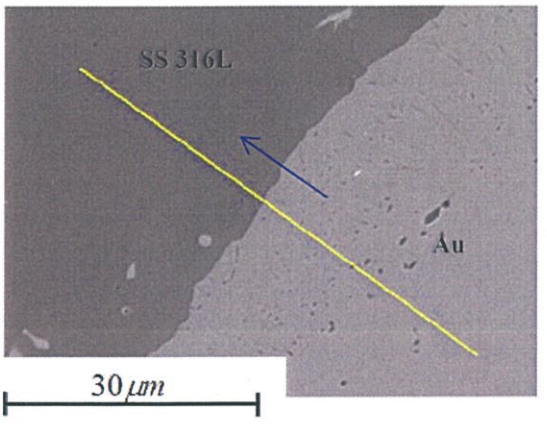

(b)

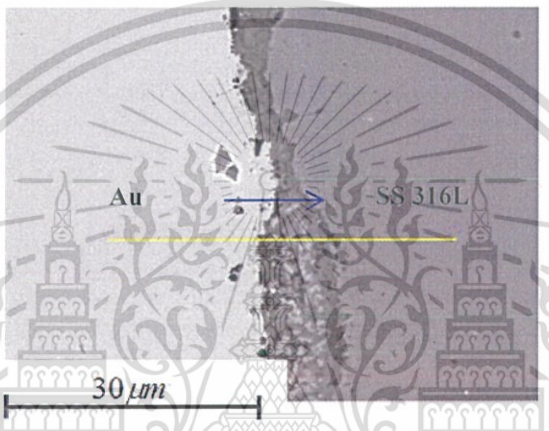

(c)

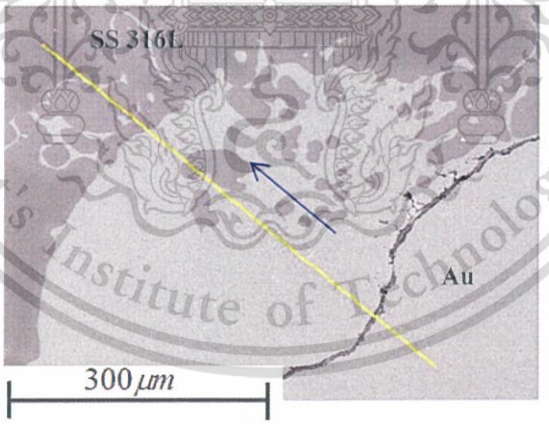

(d)

Figure 4.30 SEM micrographs of gold sheathed in SUS316L at 900(a), 950(b), 975(c) and 1000°C(d).

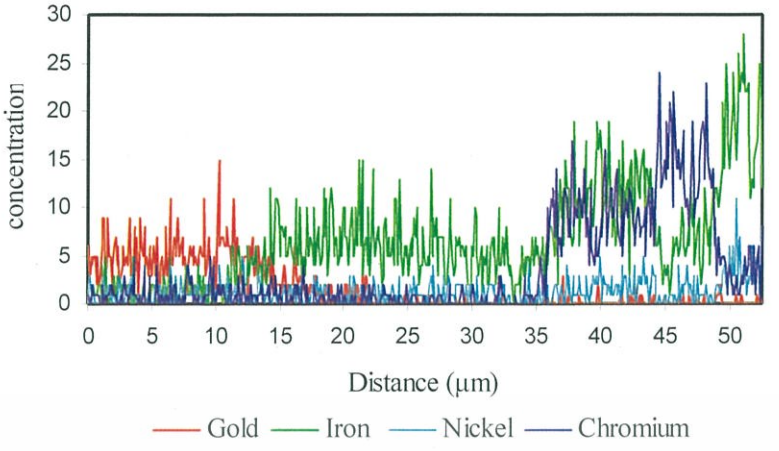

Figure 4.31 EDS of gold sheathed in SUS316L at 900°C.

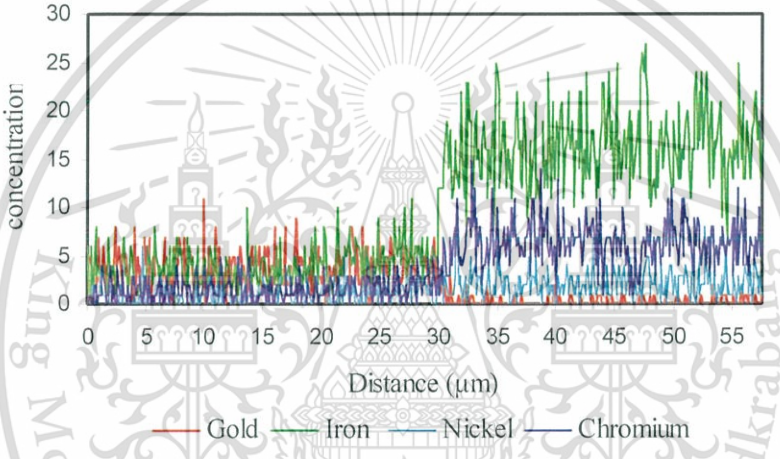

Figure 4.32 EDS of gold sheathed in SUS316L at 950°C.

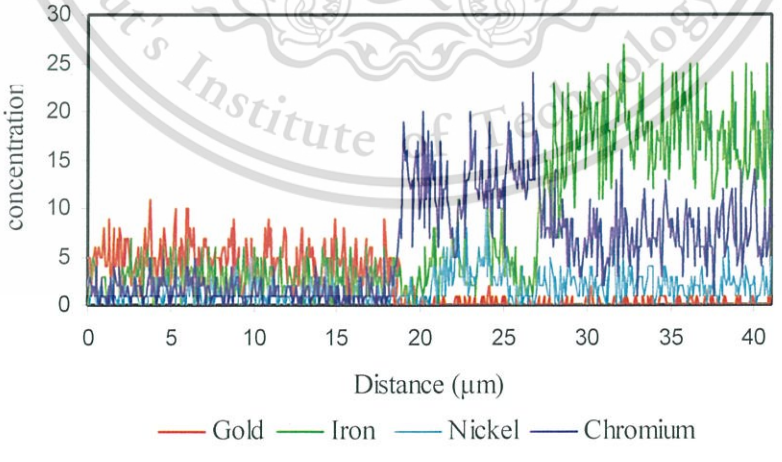

Figure 4.33 EDS of gold sheathed in SUS316L at 975°C.

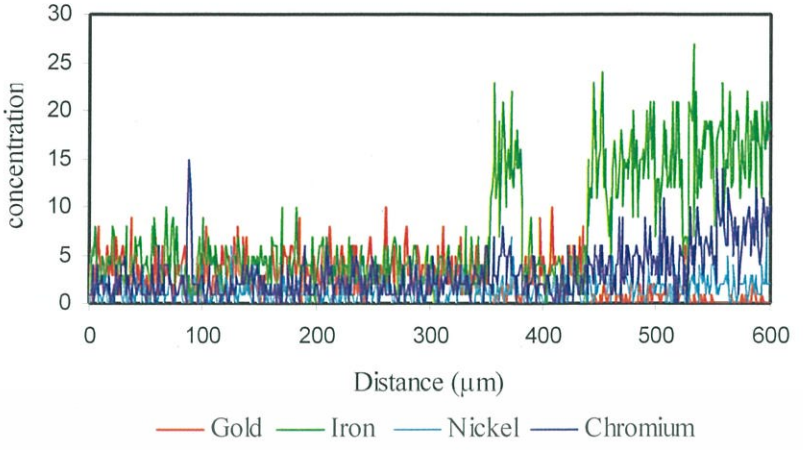

Figure 4.34 EDS of gold sheathed in SUS316L at 1000°C.

From literature review in chapter 2, the diffusion coefficients of iron, cobalt and nickel into otherwise pure gold is higher than the diffusion coefficients of iron, cobalt and nickel in silver, and an increase in temperature causes a large amount of diffusion. They are the reasons for EDS result as shown in Figures 4.26 - 4.29 and Figures 4.31 - 4.34 in that the diffusion at the contact interface of gold sheathed in SUS316L is greater than the diffusion of silver sheathed in SUS316L at high temperature. However, the principal purpose in covering silver and gold with SUS316L is to protect from oxidation, deformation and lower strength. Therefore, the gold sheathed in SUS316L has a chance of alloying metal at the contact interface and diffusion may occur outside of SUS316L in which is not practical in the long run.

4.3 Behaviour of the Contact Interface Using a Simulation Method.

The thermal stresses of silver and gold sheathed in stainless steel at each temperature were simulated automatically using a finite element COMSOL program (version 3.4). The properties of SUS316L are provided in COMSOL.

4.3.1 Geometry

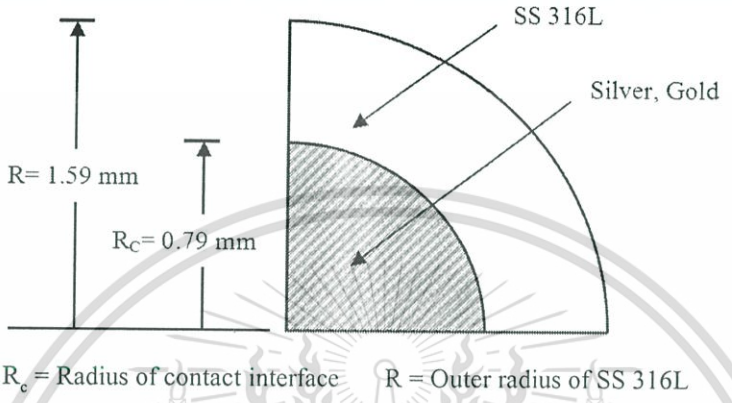

Figure 4.35 Geometries of specimen for numerical simulation.

The geometry in Figure 4.35 shows the dimension of model for 2D which was drawn in COMSOL. One quarter of a cross section of the electric conducting wire is used to be the model as the model is symmetrical.

4.3.2 Boundary Conditions

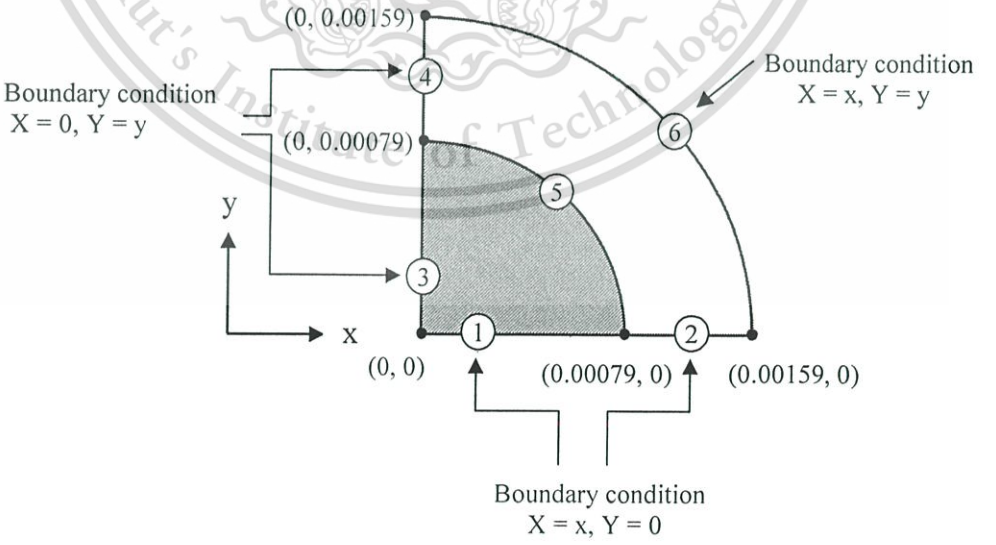

Figure 4.36 Boundary conditions of specimen for numerical simulation.

In a numerical simulation, there were six boundary conditions of lines as shown in Figure 4.36. The boundary conditions of line 1 and line 2 were able to extend in X-axis, but did not allow them to move in Y-axis. On the other hand, line 3 and line 4 were able to extend along in Y-axis, but did not allow them to move along in X-axis. The boundary condition of line 6 was able to move both X-axial and Y-axial independently. Besides, line 5 was a boundary condition of the contact interface between two materials; in which the two materials were assumed to expand together.

4.3.3 Material Property

In this thesis, the electric conducting wires were made of several materials including gold, silver and stainless steel 316 L. Their properties required for the simulation are shown in chapter 2 and some properties are provided in COMSOL. However, all the properties are a function of temperature for both the properties listed in Chapter 2 and the properties provided in COMSOL, such as thermal conductivity, specific heat capacity, electrical conductivity, thermal expansion, density, Poisson's ratio and Young's modulus.

Figure 4.37 shows the position of each domain. The materials in domain 1 are both gold and silver and the material in domain 2 is stainless steel 316 L.

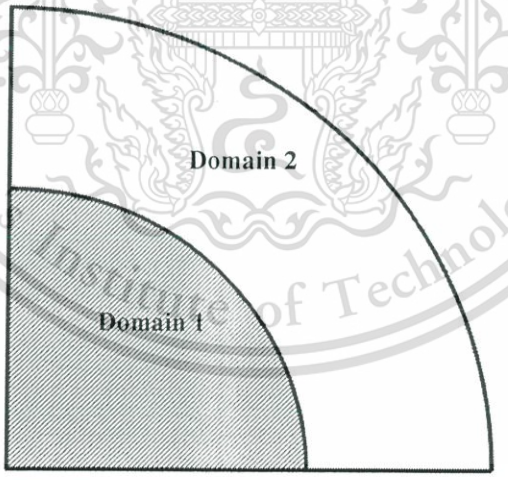

Figure 4.37 Position of each domain.

4.3.4 Mesh Generation

From Figure 4.38, the mesh model was generated using COMSOL program before setting the boundary condition. A number of elements were 2229 elements.

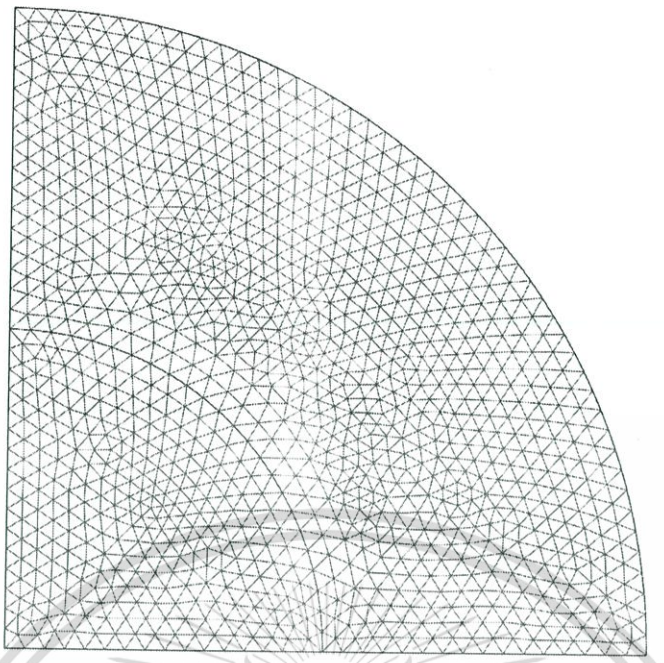

Figure 4.38 Mesh model of the specimen.

4.3.5 Simulation Results

The thermal stresses of silver and gold sheathed in stainless steel at each temperature were simulated using a finite element program COMSOL (version 3.4). The properties of SUS316L are readily provided in COMSOL.

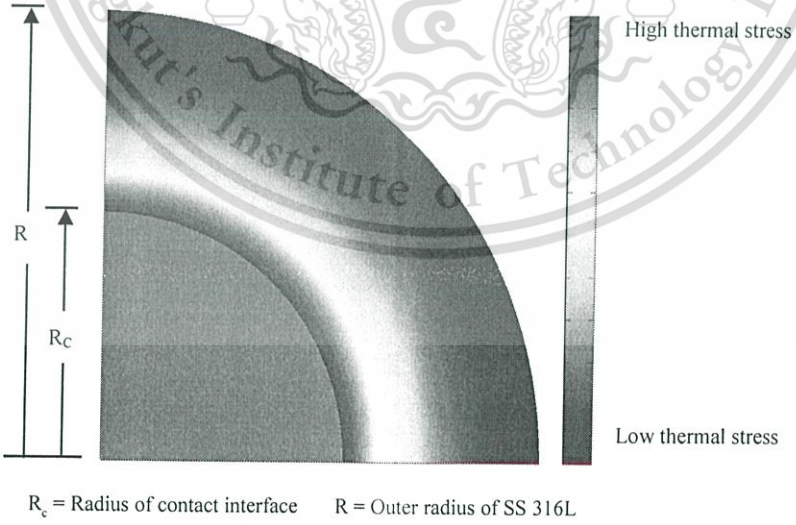

Figure 4.39 Thermal stress in a specimen at high temperature.

The simulation result from COMSOL has yielded the thermal stresses of Ag and Au from the center of the specimen (r=0mm) to the contact interface between Ag and Au with

SUS316L (r=0.79mm). The thermal stresses are constant at every temperature but rapidly increased at the contact interface. The thermal stress at the outer surface of SUS316L (r=1.59mm) is less than the inner diameter of SUS316L.

Silver/ SUS316L

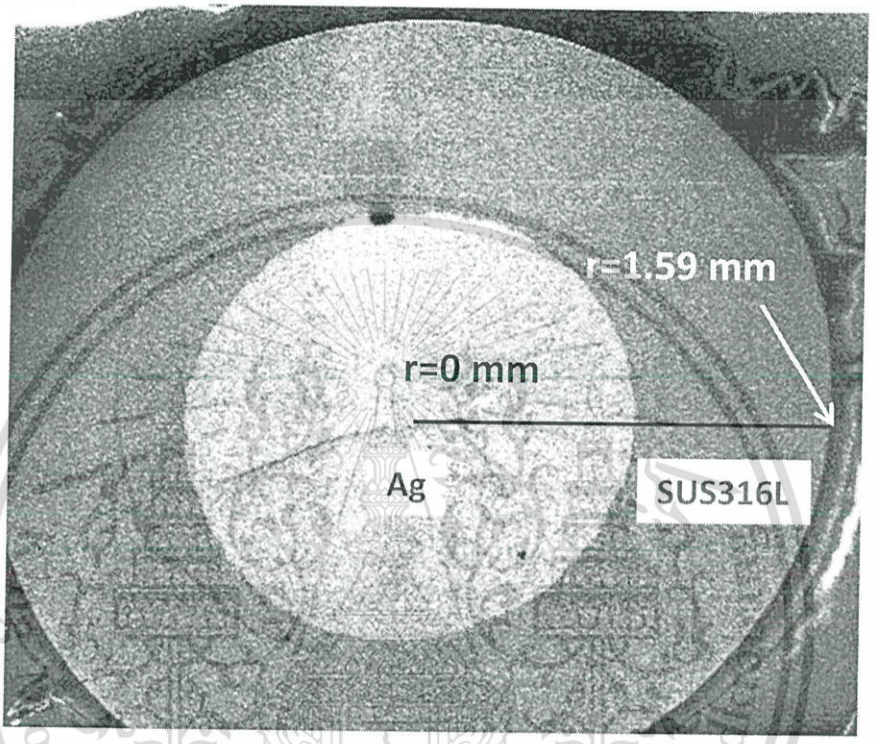

Figure 4.40 SEM micrograph of silver sheathed in SUS316L at 1000°C.

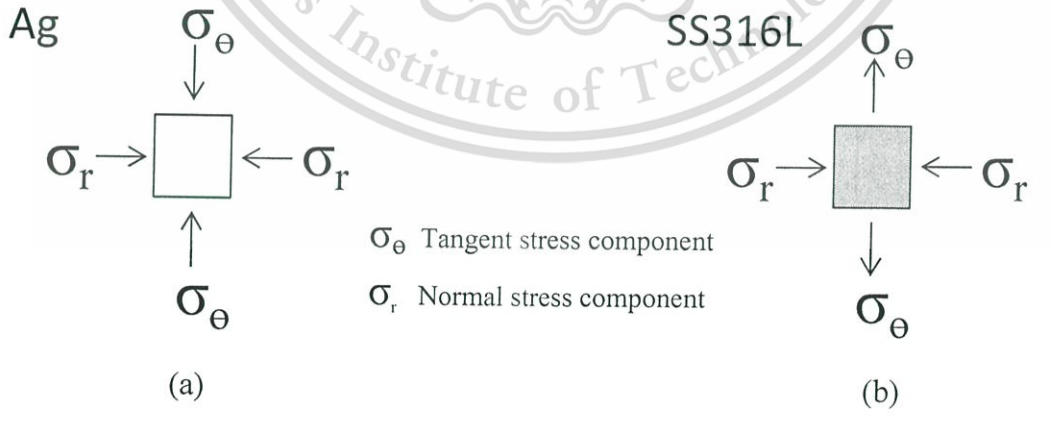

Figure 4.41 Stress components in the radial direction in silver (a) and SUS316L (b).

Figures 4.40 – 4.43 demonstrate the stresses, which are tangential stress component and normal stress component in the radial direction, acting within silver and SUS316L at 400°C, 700°C and 1000°C. For silver, both the normal stress component and the tangential stress

component in the radial direction are compressive stress which shows their minus sign as shown in Figure 4.42 and Figure 4.43, respectively. For SUS316L, the normal stress component in the radial direction is compressive stress and the tangential stress component in the radial direction is tensile stress, plus sign, as shown in Figure 4.42 and Figure 4.43.

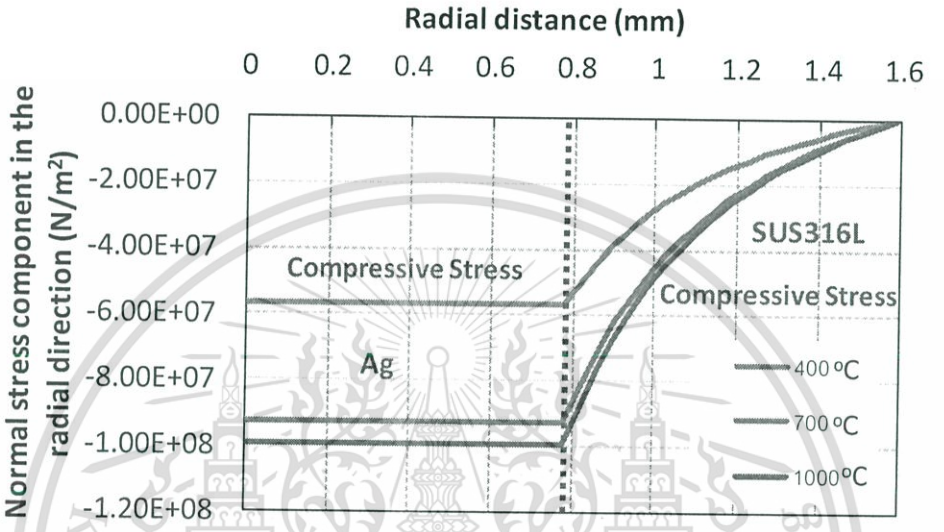

Figure 4.42 Normal stress component in the radial direction of silver sheathed in SUS316L at 400°C, 700°C and 1000°C.

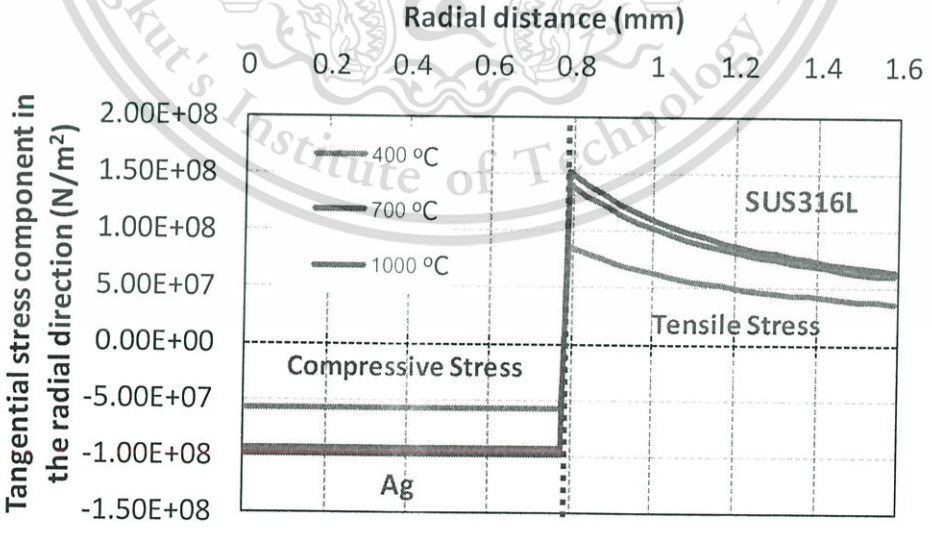

Figure 4.43 Tangential stress component in the radial direction of silver sheathed in SUS316L at 400°C, 700°C and 1000°C.

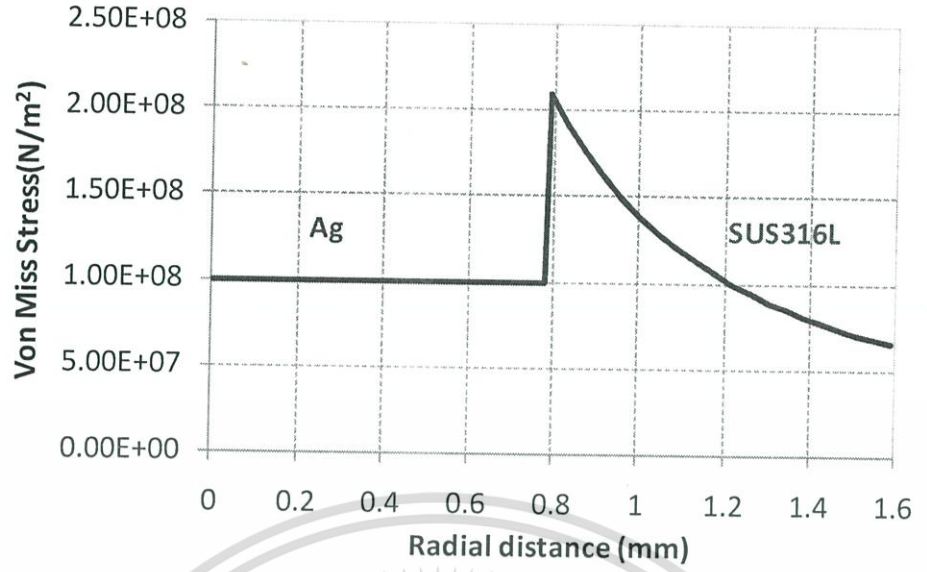

Figure 4.44 Von miss stress in the radial direction of silver sheathed in SUS316L at 1000°C.

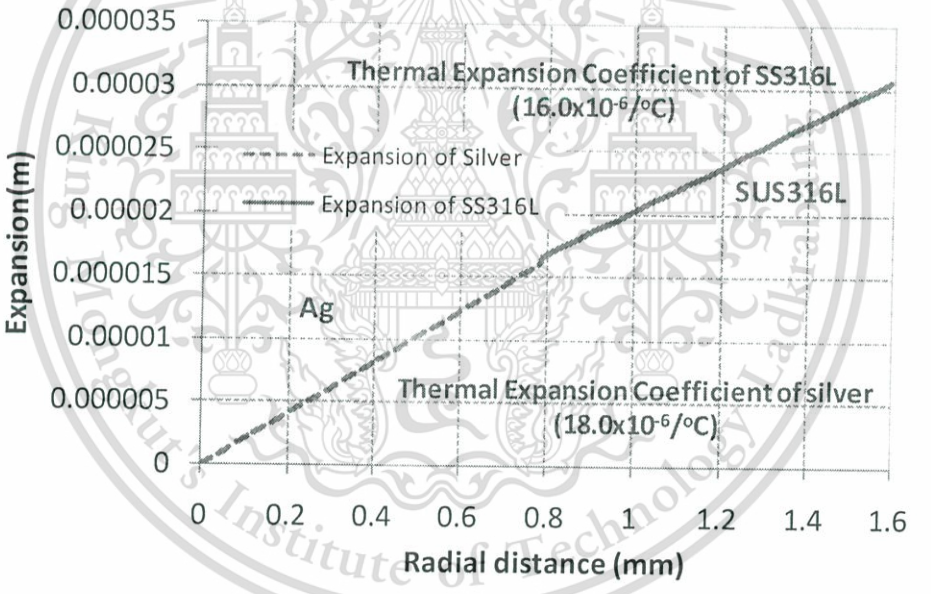

Figure 4.45 Expansion in the radial direction of silver sheathed in SUS316L at 1000°C.

Figure 4.44 demonstrates von miss stress in the radial direction of silver sheathed in SUS316L at 1000°C. Owing to higher expansion of silver as shown in Figure 4.45, a peak von miss stress is at the contact interface. The distribution of von miss stress from the center to the contact interface between silver and SUS316L is constant.

Gold/ SUS316L

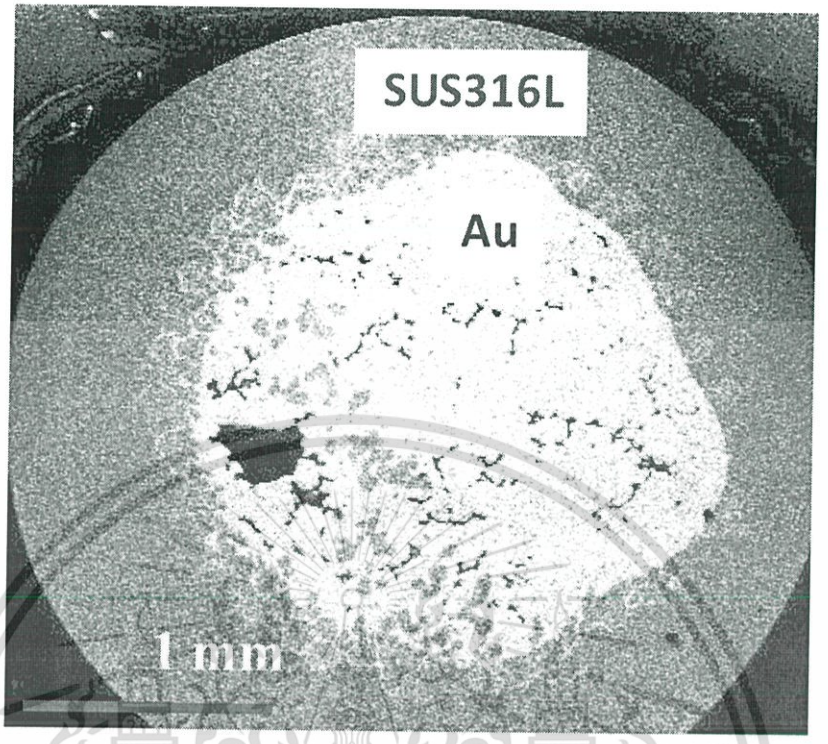

Figure 4.46 SEM micrograph of gold sheathed in SUS316L at 1000°C.

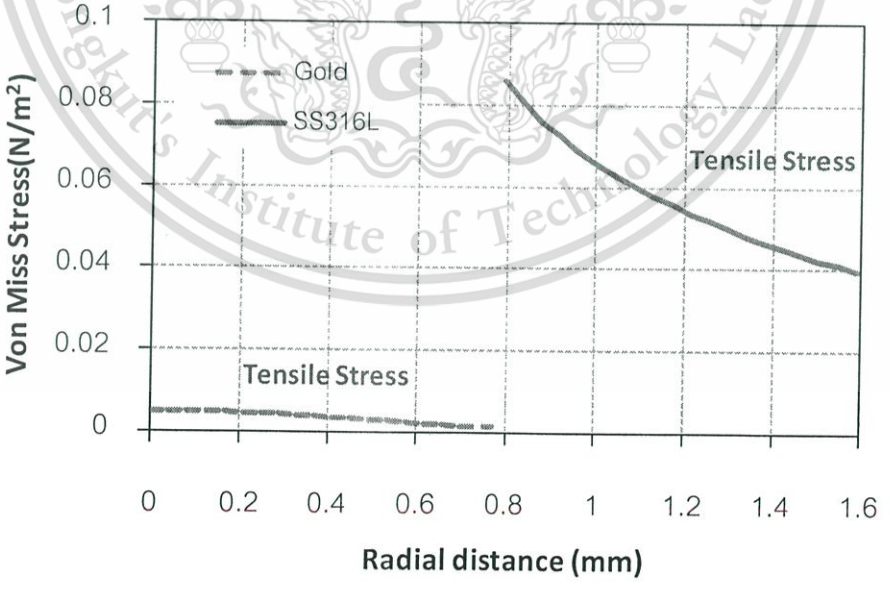

Figure 4.47 Von miss stress in the radial direction of gold sheathed in SUS316L at 1000°C.

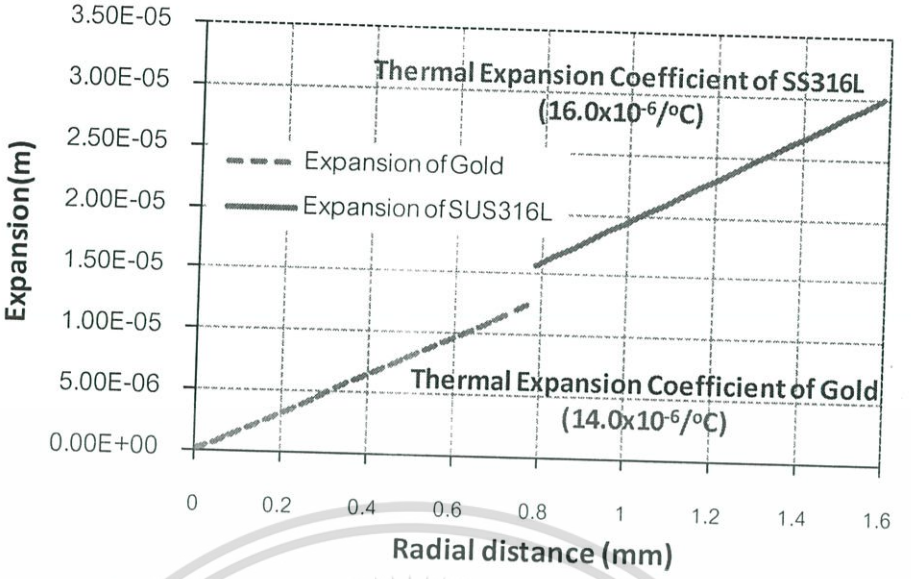

Figure 4.48 Expansion in the radial direction of gold sheathed in SUS316L at 1000°C.

The thermal stress of gold sheathed in stainless steel, von miss stress, is lower than that of silver sheathed in 316L stainless steel as shown in Figure 4.44 and 4.46. The main reason why the thermal stress of Au sheathed in SUS316L is lower because the expansion of gold cannot expand to contact with 316L stainless steel as shown in Figure 4.47. However, gold sheathed in 316L stainless steel have much damage which results from diffusion and metal alloying at the contact interface.

4.4 Conclusions

Experiments showed that inter-diffusion and occurring metal alloy at contact interface directly have much impact on damage of electrical conducting wire made of gold and 316L stainless steel. On the other hand, silver sheathed in 316L stainless steel has a little damage from result of diffusion although it has quite amount of thermal stress. Therefore, models made of silver sheathed in stainless steel succeed in operating at high temperature.

CHAPTER 5

CONCLUSIONS AND SUGGESTIONS

5.1 Conclusions

The newly invented technique for the electric current conducting wire can be applied for use in a solid oxide fuel cell. According to experimental on electrical conductivity and the behaviour of contact interface, the conducting wires are not only capable of conducting electric current but also succeed in operating at high temperature.

The electrical conductivity study of each model exhibited in chapter 3 has been compared with the electrical conductivity of commercial materials comprising of gold, silver and platinum at high temperature. The electrical conductivity for Ag_4625 and Ag_4968, which were made of silver and SUS316L, are lower than those of silver (99.99%) and gold (99.99%), but they are higher than a platinum and other models (Au_4625 and Au_4968). Furthermore, the manufacturing and material cost of Ag_4625 and Ag_4968 are also lower than Au_4625, Au_4968, gold and platinum despite their prices are higher than silver, but silver cannot be operated at high temperature because it is too close to its melting point.

For the behaviour of contact interface, Ag_4968 and Au_4968 have been investigated by using a scanning electron microscope investigation as shown in chapter 4. The result of SEM demonstrates Ag_4968, made of silver sheathed with SUS316L, have a little effect of diffusion between silver and SUS316L in every temperature. On the other hand, Au_4968 have a significant amount of diffusion and alloying at the contact interface at higher temperature. However, the diffusion effect of gold with stainless may be too much to be used as a electric current conducting wire because it has became metal alloy.

In addition, results in chapter 4 also present the thermal stress from numerical simulation which focuses at the contact interface. In our study, the model of silver sheathed with SUS316L and the model of gold sheathed with SUS316L were of the same geometry hence the effect of geometry was not considered. The simulation result was found that the silver sheathed with SUS316L has much thermal stress than the gold sheathed with SUS316L in every zone and every temperature. The contact interface zone of the silver sheathed with SUS316L has the highest thermal stress there any other zone because expansion in this zone of silver cannot expand fully owing to its location SUS316L blocking any movement as a result of accumulated thermal stress.

In summary, the new technique used to fabricate the conducting wire is possible to be implemented in a solid oxide fuel cell system or other areas which operate at high temperature as well as the cost of this technique has still suitability for commerce.

5.2 Suggestion

Although this work has finished, it was only the first step towards the electric current conducting wire technique. There are several suggestions to the work for further study towards material selection.

5.2.1 Material Selection

Several electrical conducting wires could be employed at high operating temperatures and increase the lifetime of the model. We could select the outside of material as shown in table 5.1. In addition, the cost of the wire could be reduced if we change the inner material to copper. However, changing both materials require the study of diffusion effects between materials

Table 5.1 Material selection for electric current conducting wire.

Operating temperature	Inner materials	Outside of materials
600-1300	Silver and Copper	Stainless steel grade 310S, 430 and Inconel 600
1300 -1900	Platinum	Ceramic

5.2.2 Electrical Conducting Wire Production

In this thesis, the electric current conducting wires were assembled by hand. This method is not suitable for commercial-scaled production because we cannot control the gap. Therefore, practical solution is extrusion process to make the electric current conducting wire as shown in Figure 5.1.

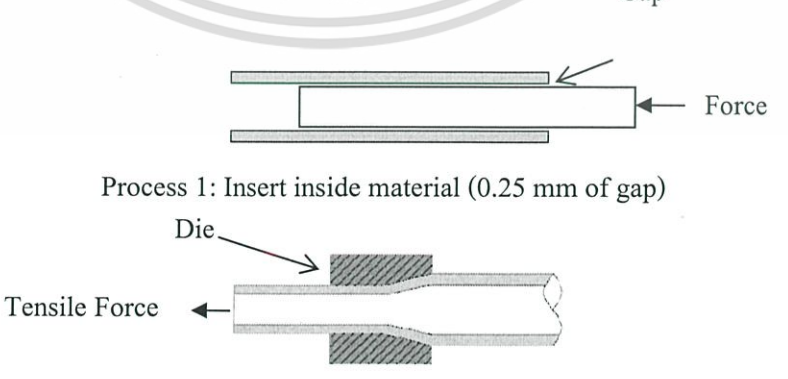

Figure 5.1 Extrusion process for producing electrical conducting wire.

REFERENCES

[1] Hirschenhofer, J.H., Stauffer, D.B., Engelman, R.R., Klett, M.G., 1998. **Fuel Cell Handbook. Fourth ed. US Department of Energy Federal Energy Technology Center**, Business Technology Books, Morgantown, WV, 1998

[2] G. Hoogers, **Fuel Cell Technology Handbook**, Boca Raton, FL: CRC Press, 2003

[3] **U.S. Department of Energy**, Hydrogen Program Annual Merit Review Proceedings, 2008 www.hydrogen.energy.gov/annual_review08_proceedings.html

[4] Ben Wiens Consulting Inc. Metro Vancouver BC Canada,www.benwiens.com/energy4.html #energy4.11

[5] SFC Smart Fuel Cell AG, www.sfc.com, 2009

[6] C.Y. Ho, R.W. Powell and P.E. Liley, **J. Phys. Chem. Ref. Data**, Vol. 1, pp. 279, 1972

[7] B.J. McBride, S. Gordon and M.A. Reno, **NASA Technical Paper 3287**, 1993

[8] D.R. Smith, F.R. Fickett, **J. Research National Institute Standards Technology,** Vol. 100, pp. 119, 1995

[9] L.B. Pankratz, US Bureau of Mines Bulletin 672, 1982

[10] G.T. Furukawa, M.L. Reilly and J.S. Gallagher, **J. Phys. Chem. Ref. Data**, Vol. 3, pp. 163, 1974

[11] F. Righini, A. Rosso, High Temperatures-High Pressures, Vol. 12, pp. 335, 1980

[12] R.A. Matula, **J. Phys. Chem. Ref. Data**, Vol. 8(4), pp. 1147, 1979

[13] W.L. Tew, G.F. Strouse, **NIST Special Publication**, pp. 260-139, 2001

[14] www.kitco.com, April 1, 2008

[15] N. Waterhouse and B. Yates, **Cryogenics**, Vol. 8, pp. 267, 1968

[16] F.C. Nix and D. MacNair, **Physical Review**, Vol. 60, pp. 597, 1941

[17] E.A. Owen and E.L. Yates, **Phil. Mag**. S7, Vol. 17, pp. 113, 1934

[18] T.A. Hahn and R.K. Kirby, Thermal Expansion - 1971, Editors M.G. Graham and H.E. Hagy, **Pub. American Institute of Physics**, pp. 87, 1972

[19] J. Valentich, **J. Materials Science**, Vol. 14, pp. 371, 1979

[20] E. Firzer, S. Weisenburger, **High Temperatures-High Pressures**, Vol. 4, pp. 559, 1972

[21] R.K. Kirby, in Thermal Conductivity 24, Eds. P.S. Gaal, D.E. **Apostolescu**, pp. 655, 1999

[22] A. Wolfenden, M.R. Harmouche, **J. Materials Science**, Vol. 28, pp. 1015, 1993

REFERENCES (Con.)

[23] http://www.exo.net/~jillj/activities/phasediagram.pdf

[24] S.M. Collard and R.B. McLellan, Acta metall. mater., Vol. 39(12), pp. 3143, (1991)

[25] W. Koester, Z. Metallkde., Vol. 39(1), pp 1, 1948 (in German)

[26] S. Sakai, H. Tanimoto, K. Otsuka, T. Yamada, Y. Koda, E. Kita and H. Mizubayashi, Scripta Materialia, Vol. 45, pp. 1313, 2001

[27] S.M. Collard and R.B. McLellan, Acta metall. mater., Vol. 39(12), pp. 3143, 1991

[28] R. Farraro and R.B. McLellan, Metall. Trans., Vol. 8A, pp. 1563, 1977

[29] S.M. Collard and R.B. McLellan, Acta Metall. Mater., Vol. 40(4), pp. 699, 1992

[30] Giorgio Rizzoni, **Principles and applications of Electrical Engineering**, McGraw Hill, 2005

[31] Kilowatt Classroom, LLC, www.kilowattclassroom.com

[32] http://www.four-point-probes.com/four-point_probe.html

[33] P.G. Shewmon, **Diffusion in Solids**, McGraw-Hill, NY, 1960.

[34] B. Tuck, **Introduction to Diffusion in Semiconductors**, Peregrinus, England, 1974

[35] R. Fowler and E.A. Guggenheim, **Statistical Thermodynamics**, Cambridge University Press, 1960

[36] O.F. Devereux, **Topics in Metallurgical Thermodynamics**, J. Wiley & Sons, NY, 1963

[37] L.S. Darken, Trans. AIME, 180 (1949) 430

[38] David Duhl, Ken-Ichi Hirano and Morris Cohen, **Diffusion of iron, cobalt and nickel in silver, Acta Metallurgica**, Vol.11(5), pp. 463-466, May 1963

[39] David Duhl, Ken-Ichi Hirano and Morris Cohen, **Diffusion of iron, cobalt and nickel in gold** , Acta Metallurgica, Vol. 11(1), pp. 1-6, Jan 1963

[40] J. Mimkes and M. Wuttig, **Diffusion and phase diagram in binary alloys**, Thermochimica Acta 282/283, pp 165-173, 1996

[41] Joseph R. Davis et al., **Metals Handbook**, Desk Edition (Second Edition), ASM International, The Materials Information Society, Dec 1998

[42] http://www.engineeringtoolbox.com/convective-heat-transfer-d_430.html

[43] http://www.azom.com/details.asp?ArticleID=1175

REFERENCES (Con.)

[44] David A.Porter and Kenneth E. Easterling, **Phase Transformations in Metals and Alloys**, CHAPMAN & HALL

[45] ASM Handbook, Vol.3 Alloy Phase Diagrams, ed. By H. baker, **ASM International**, Materials Park, Ohio (1992)

Appendix A: Journal

1. **M. Masomtob**, K. Wongtida,J. Charoensuk and S. Charojrochkul, "**Improved Electrical Conducting Wires for SOFCs**", Journal Advanced Materials Research Vols. 55-57(2008) pp 797-800 in www.scientific.net

2. **M. Masomtob**, K. Wongtida, K. Hanamura, J. Charoensuk and S. Charojrochkul **"High Temperature Behaviour of Contact Interface for Ag and Au with Stainless Steel 316L"**, Journal of Metals, Materials and Minerals, Vol.18 No.2 pp.71-75, 2008, www.material.chula.ac.th

Advanced Materials Research Vols. 55-57 (2008) pp 797-800
online at http://www.scientific.net

Online available since 2008/Aug/22

Improved Electrical Conducting Wires for SOFCs

M. Masomtob[1,a], K. Wongtida[2,b], J. Charoensuk[1,c] and S. Charojrochkul[2,d]

1 Department of Automotive Engineering, Faculty of Engineering, King Mongkut's Institute of Technology Ladkrabang, Bangkok 10520, Thailand

[2] National Metal and Materials Technology Center, Pathumthani 12120, Thailand

[a]manop_auto45@hotmail.com, [b]krisadew@mtec.or.th, [c]kcjarruw@graduate.kmitl.ac.th, [d]sumittrc@mtec.or.th

Keywords: electrical conducting wires, Solid Oxide Fuel Cells (SOFCs)

Abstract. Solid Oxide Fuel Cells (SOFCs) have attracted a number of researchers due to their efficiency as alternative energy devices. Studies have been conducted to investigate different components of the SOFCs to improve the performances. Current collecting wires are the components which have affected the overall performance. Since SOFCs are normally operated in the temperature range of 700-1000 °C in dual atmospheres, the wiring material must be able to function at this condition. Currently, the material used to make the wires is platinum because of its high electrical conductivity, high melting point and oxidation resistant. However, platinum is expensive, especially for the practical operation of SOFCs. Silver could be an alternative choice due to its very high electrical conductivity. Nevertheless, the melting point of silver is rather low (900-960 °C). In our study, a modified silver current collecting wire has been used in the temperature range of 100-1000 °C. Their conductivity curves have demonstrated higher performances in comparison with the systems employing Pt and gold wires. In addition, the cost is reduced approximately 800-1000 times from that of the traditional material used.

Introduction

Currently, gold, platinum and silver are the top electrical conducting wires. Their required properties are high electrical conductivity and oxidation resistant. The melting point of gold and platinum is higher than silver. In addition, silver deforms and melts at the temperature range of 900 -1000 °C [3]. On the other hand, the cost of silver is cheaper than gold and platinum. Thus, this research is aimed to exploit and develop a technique to apply silver to make wires to conduct electrical current for a high temperature application. In this research, the electrical conducting wires were developed for a high temperature operation (600 – 1000 °C) in dual atmospheres.

The electrical conducting wires are a part used in solid oxide fuel cell (SOFC). An SOFC is one of a highly promising fuel cell for small and large scale power generating station. Since an SOFC is normally operated in the temperature of 700 - 1000 °C, it probably is used as a power station for charging electrical vehicles in the future. Therefore, it is interesting to develop the electrical conducting wires for SOFCs. The development of electrical conducting wires include a study of the properties of materials (gold, platinum and silver) such as electrical conductivity, melting point, oxidation resistance and cost, design technique to use the silver for electrical conducting wires, a new technique in using the silver for electrical conducting wires operated from 700 to 1000 °C.

Experimental

Sliver, gold and platinum are commercially available materials. Ag_4625, Ag_4968, Au_4625 and Au_ 4968 are composite materials used in our study by changing the melting point and strength at various ratios and diameter of current collecting wires. The cost per gramme of each material has been calculated as shown in Table 1.

Table 1. Cost of materials

Materials	Cost (USD/g)
Sliver 99.99% (Ag)	0.542
Gold 99.99% (Au)	28.404
Platinum 99.99% (Pt)	61.792
Composite of sliver 0.4625 (Ag 4625)	0.657*
Composite of sliver 0.4968 (Ag 4968)	0.675*
Composite of gold 0.4625 (Au 4625)	34.479*
Composite of gold 0.4968 (Au 4968)	35.415*

www.kitco.com April 1, 2008
* calculated from material and production cost

Basically, the resistance of electrical conducting wires is measured through a two-point, four-wire probe approach [1]. The current was set from fifty to five hundreds mA and the voltage across the specimen was measured using a multimeter. In addition, the temperature is changed from 100 to 1,000°C as shown schematically in Fig. 1. Before collecting the data, the wire was heated up at the rate of 2.5 °C.min^{-1}.

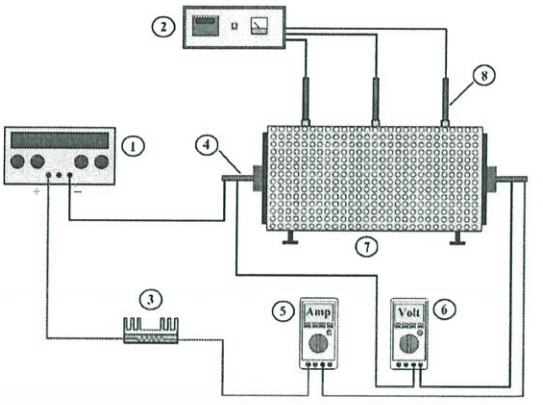

Equipment for mesuring 4 point probe
1. Power supply DC
2. Temperature control 30-1000°C
3. Resistor (1000 ohms) and heat exchange fin
4. Wire specimen
5. Amp meter
6. Voltage meter
7. Electrical Furnace
8. 3 sets of thermocouple

Figure 1. Equipment for a 4 point probe measurement

Results and Discussion

The electrical conductivity of composite material can be calculated from I-V curves and plotted to compare with commercial materials (Ag [4], Au [4] and Pt [5]) as a function of temperature shown in Fig. 2. The conductivities of composite materials as Au_4625, Au_4968, Ag_4625 and Ag_4968 are lower than silver and gold but higher than platinum. In addition, the conductivity of all these materials decrease at high temperature (form 100 to 1000°C) but the conductivity of silver composite materials increases as a result from changing the phase from solid to liquid at 900-1000 °C.

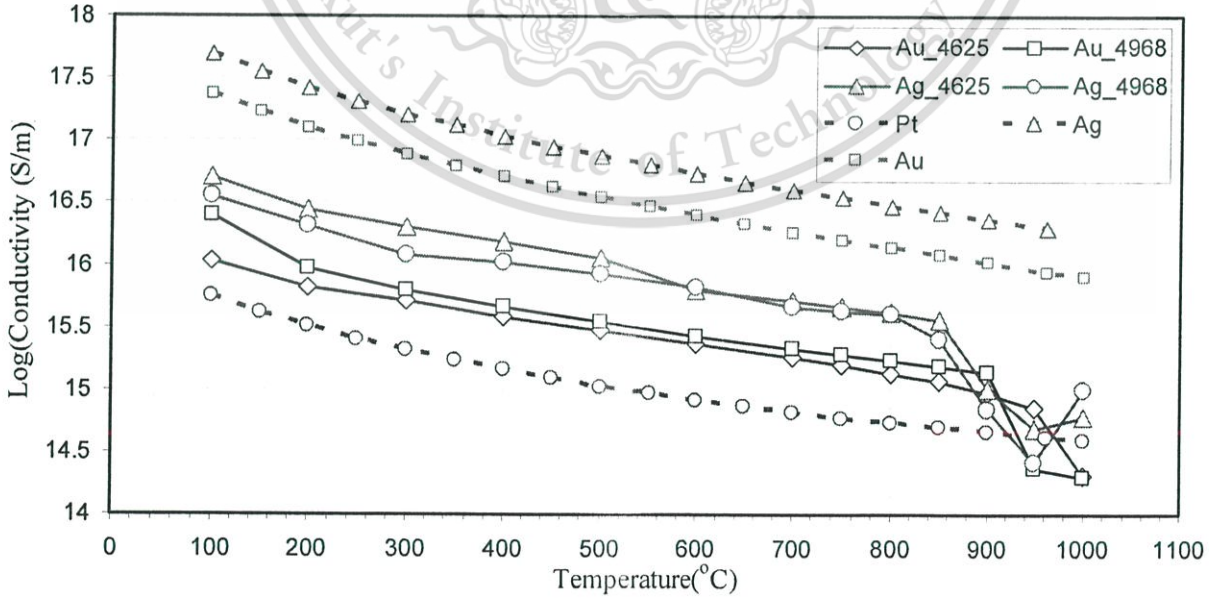

Figure 2. Electrical conductivity as a function of temperature

The conductivity of Ag is higher than other materials at every range of operating temperature. In practice, it cannot be used in SOFC because of deformation from low melting point. Ag_4625 and Ag_4968 were designed to prevent from the deformation from the low melting point. In addition, this method can also prevent the oxidation of silver wire. From Fig. 2, Ag_4625 and Ag_4968 can be used at high temperature.

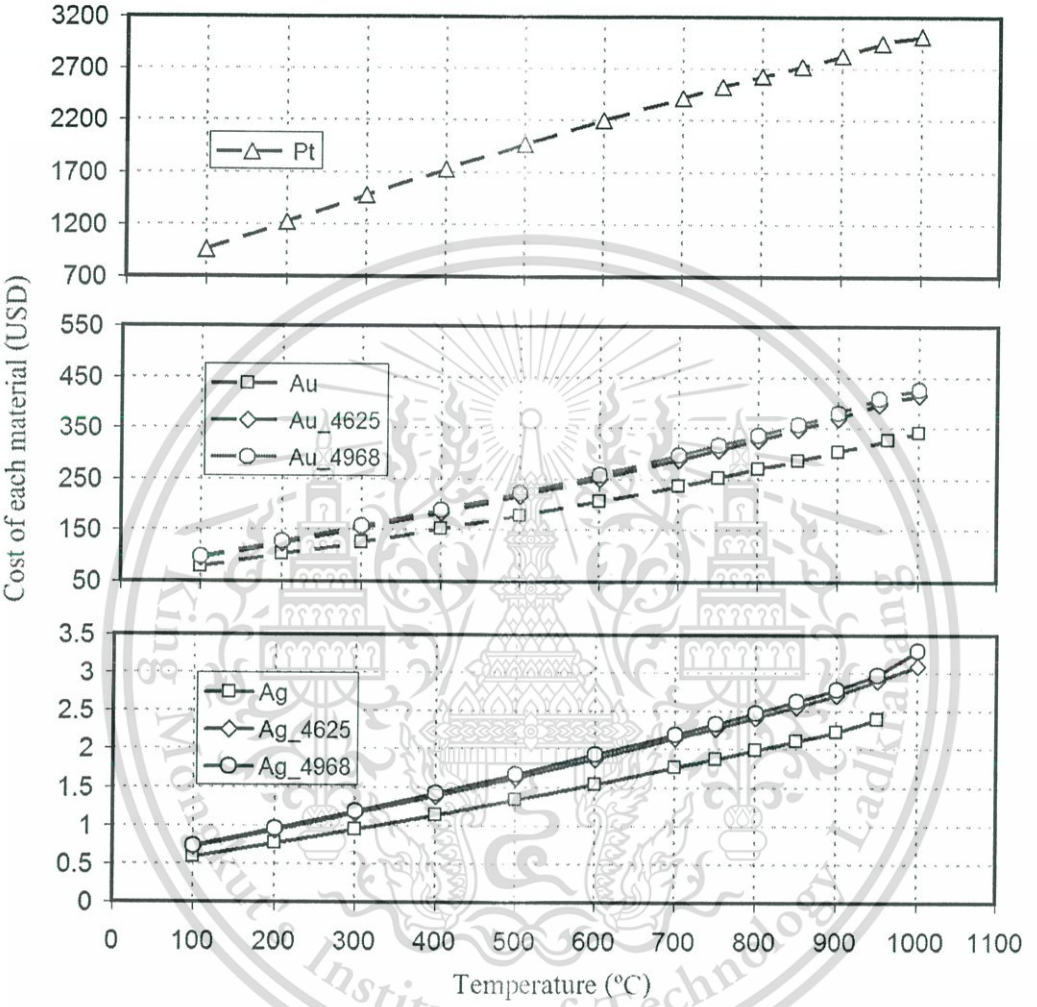

Figure 3. The cost of each material at various operating temperatures, compared at constant resistance of 0.2 Ω/m.

Fig. 3 shows the cost of material at various operating temperatures compared at constant resistance of 0.2 Ω/m. The cost of each material is approximately 2-3 times different while at high temperature the result from collecting wire is increased at the cross-section area for keeping constant resistance of 0.2 Ω/m.

The comparison between composite silver and composite gold, the cost of composite silver is cheaper than composite gold and the conductivity of composite silver is grater than the composite gold.

The cost of Pt is higher than the cost of Ag, Ag_4625 and Ag_4968 approximately 1200-1300 times at low temperature and 900-1000 times at high temperature. The cost of gold is higher than the cost of Ag, Ag_4625 and Ag_4968 about 100-150 times.

Summary

The conductivity curves are used to compare the performances of the systems employing various wiring composite materials. Ag_4625 and Ag_4968 are suitable for SOFC because their electrical conductivities are greater than those of Au_4625, Au_4968, Au and Pt. In addition, they are cheaper than Au_4625, Au_4968, Au and Pt. Therefore, they have a high potential to become commercialized. However, their production processes are more complicated than those of the wires made of pure Au, Ag and Pt.

Acknowledgment

This work was supported by National Metal and Materials Technology Center (MTEC), National Science and Technology Development Agency (NSTDA-Alternative energy cluster) and Thailand Advanced Institute of Science and Technology (TAIST Tokyo Tech)

References

[1] W.Z. Zhu, S.C. Deevi: Materials Research Bulletin Vol. 38 (2003), p. 957.
[2] T.Imaizumi, N.Yamamoto, M.Tomita, N.Sakai, M.Murakami, I. Hirabayashi and K. Sawa: Contact Resistance Characteristics of High Temperature Superconducting Bulk- III, IEEE
[3] www.kitco.com April 1, 2008.
[4] R.A. Matula: J. Phys. Chem. Vol. 8 (1979), p. 1147.
[5] W.L. Tew and G.F. Strouse: NIST Special Publication Vol. 260-139 (2001).
[6] F. Righini and A. Rosso: High Temperatures-High Pressures Vol. 12 (1980), p. 335.

Smart Materials
doi:10.4028/www.scientific.net/AMR.55-57

Improved Electrical Conducting Wires for SOFCs
doi:10.4028/www.scientific.net/AMR.55-57.797

Journal of Metals, Materials and Minerals, Vol.18 No.2 pp.71-75, 2008

High Temperature Behaviour of Contact Interface for Ag and Au with Stainless Steel 316L

Manop MASOMTOB[1], Krisadech WONGTIDA[2], Katsunori HANAMURA[3], Jarruwat CHAROENSUK[1] and Sumittra CHAROJROCHKUL[2]

[1]Department of Mechanical Engineering, Faculty of Engineering, King Mongkut's Institute of Technology Ladkrabang, Bangkok 10520,Thailand

[2]National Metal and Materials Technology Center, Pathumthani, 12120, Thailand

[3]Tokyo Institute of Technology, Tokyo, 152-8550, Japan

Received Nov. 14, 2008
Accepted Feb. 10, 2009

Abstract

The behavior of contact interface for Ag and Au with SS 316L at high temperature (600 to 1000°C) has been studied. The behaviors in each temperature of specimens were investigated using SEM for microstructure at interface. In addition, the thermal stress was simulated using a finite element COMSOL program for each temperature (600 to 900°C).

Key words : Contact Interface, Solid oxide fuel cell, COMSOL program, Thermal stress.

Introduction

The behaviors of contact interface for metals are important for an application in Solid Oxide Fuel Cells (SOFC) because a high electrical conductivity at high temperature (900°C to 1000°C) is desired. Metals of our interest for use in SOFC are platinum, gold, silver and stainless steel. They were selected because of their high electrical conductivity and potential for an application at high temperature. The contact behaviour of metals such as gold and silver sheathed in stainless steel (SS316L) has been studied. The properties of material from the simulation work which depend on temperature are thermal conductivity,[1] thermal expansion coefficient,[2, 3] density,[3] Poisson's ratio,[5, 6] and Young's modulus.[5-10] The thermal stress from a simulation and interfacial microstructure from SEM are reported.

Materials and Experimental Procedures

Experiments were conducted in these sequences.

Preparing Specimen

The geometries of investigated tube specimens were shown in Figure 1. Silver and gold were sheathed in stainless steel (SS 316L). The outer diameter and inner diameter of SS 316L were 3.18 mm and 1.58 mm, respectively. The gap of about 0.05 mm was observed between interfacial contacts.

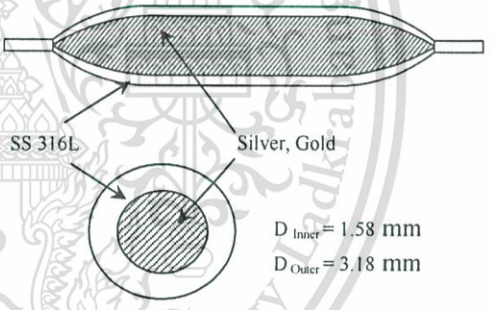

Figure 1. Geometries of investigated specimen

Heating and Quenching Specimen

The specimens were heated in a furnace at 600 °C, 650 °C, 700 °C, 750 °C, 800 °C, 850 °C, 900 °C, 950 °C, 975 °C and 1000°C and held at each temperature for 30 minutes in air and then quenched in water at room temperature.

Specimen Sectioning

The specimen was cut in half for SEM investigation because the inside of the specimen was not oxidized. The variation of the thermal

E-Mail: manop_auto45@hotmail.com, kcjarruw@graduate.kmitl.ac.th
Phone +66 (0) 2564-6500, Fax. +66 (0) 2564-6447, E-Mail: krisadew@mtec.or.th, sumittrc@mtec.or.th
Phone +81-3-5734-2975, Fax +81-3-5734-3661, E-mail: hanamura@mech.titech.ac.jp

stress was not significant and was assumed to be symmetry along z-axial within a few millimeters.

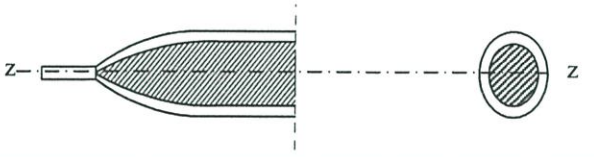

Figure 2. Position of cutting specimen

Scanning Electron Microscope Investigation

Before specimens were examined using a scanning electron microscope (JEOL JSM-5410) for the microstructure and linear EDS investigation, the specimens were polished and cleaned.

Results and Discussion

Experimentals

The microstructures of interfacial contacts between Ag and Au with SS 316L were observed using an SEM. The linear EDS was performed to investigate the diffusion of metals at the contact interfaces between Ag and Au with SS 316L.

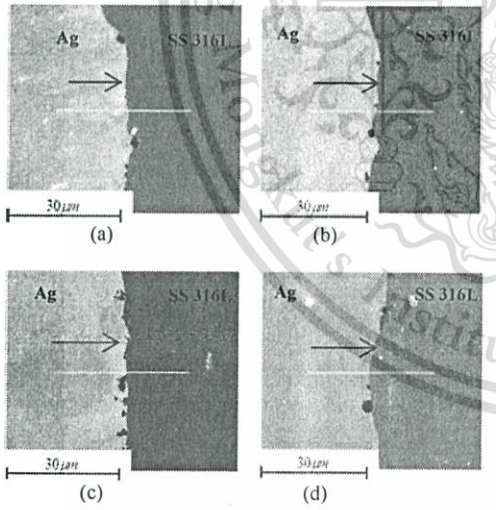

Figure 3. SEM micrographs of silver sheathed in SS 316L at 900, 950, 975 and 1000°C (a, b, c and d respectively)

Figure 3 (a), (b), (c) and (d) show microstructure at the interface of Ag and SS 316L at various temperatures. Figure 4 – Figure 7 show EDS line scans of each sample in Figure 3, along the arrows. The line scans show that diffusion of interface contacts between Ag with SS 316L has not occurred.

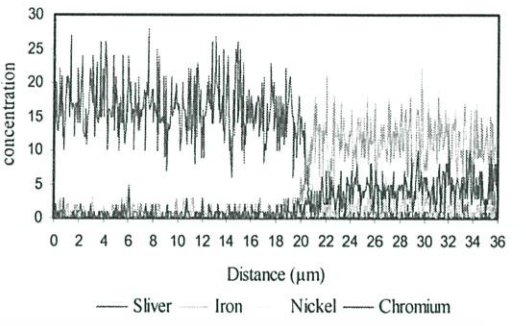

Figure 4. EDS of sliver sheathed in SS 316L at 900°C

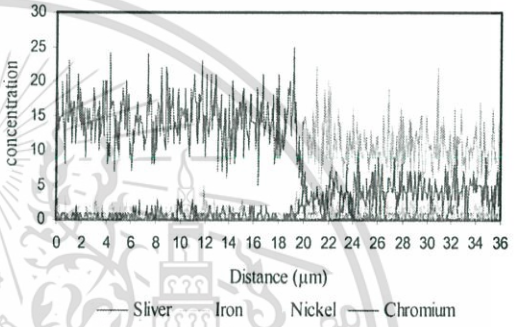

Figure 5. EDS of sliver sheathed in SS 316L at 950°C

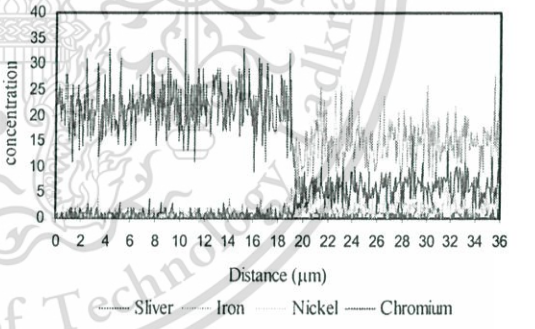

Figure 6. EDS of sliver sheathed in SS 316L at 975°C

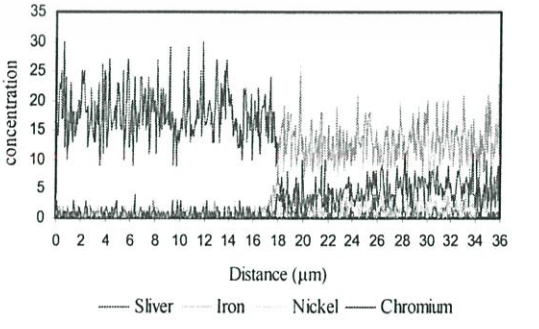

Figure 7. EDS of sliver sheathed in SS 316L at 1000°C

Figure 8 (a), (b), (c) and (b) show microstructure at interface Au and SS 316L at various temperatures. Figure 9 – Figure 12 show EDS line scans of each sample in Figure 8, along the arrows. In opposite, the line scans reveal that diffusion of interface contacts between Au with SS 316L has occurred.

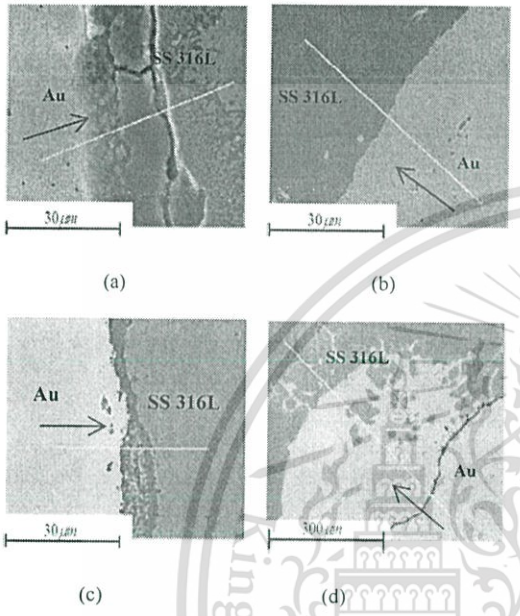

Figure 8. SEM micrographs of gold sheathed in SS 316L at 900, 950, 975 and 1000°C (a, b, c and d respectively)

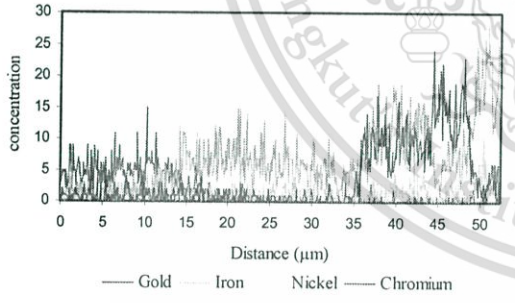

Figure 9. EDS of gold sheathed in SS 316L at 900°C

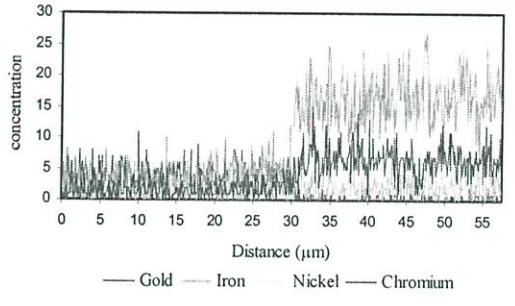

Figure 10. EDS of gold sheathed in SS 316L at 950°C

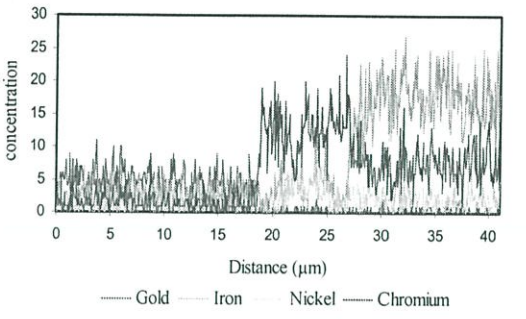

Figure 11. EDS of gold sheathed in SS 316L at 975°C

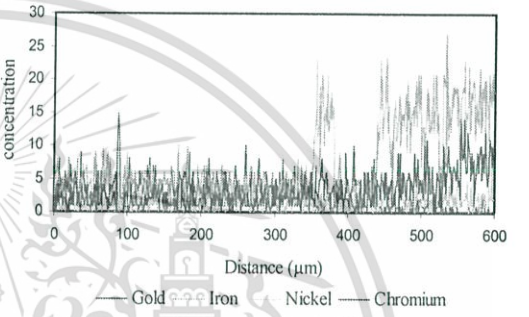

Figure 12. EDS of gold sheathed in SS 316L at 1000°C

Simulation

The thermal stresses of silver and gold sheathed in stainless steel at each temperature were simulated using a finite element COMSOL program (version 3.4). The properties of SS 316L are provided in COMSOL.

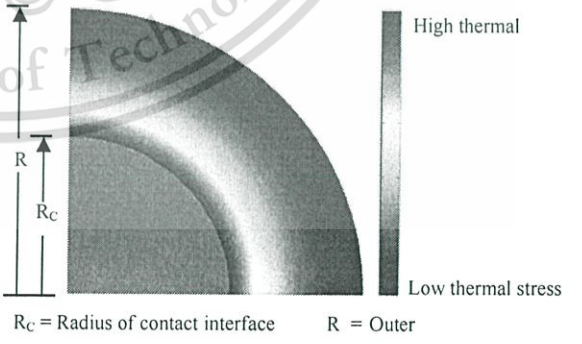

Figure 13. Thermal stress in a specimen at high temperature

The simulation result from COMSOL has yielded the thermal stresses of Ag and Au from the center of the specimen (r=0mm) to the contact interface between Ag and Au with SS 316L (r=0.79mm). The thermal stresses are constant at

every temperature but rapidly increased at the contact interface. The thermal stress at the outer surface of SS 316L (r=1.59mm) is less than inner diameter of SS 316L.

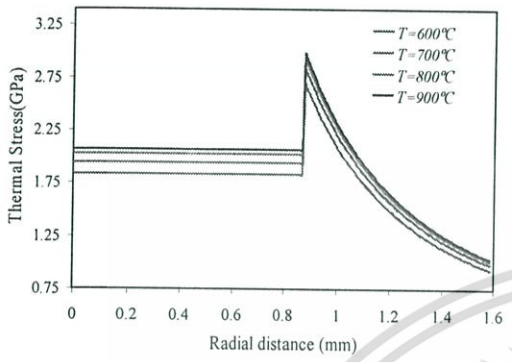

Figure 14. Thermal stress of silver sheathed in SS 316L.

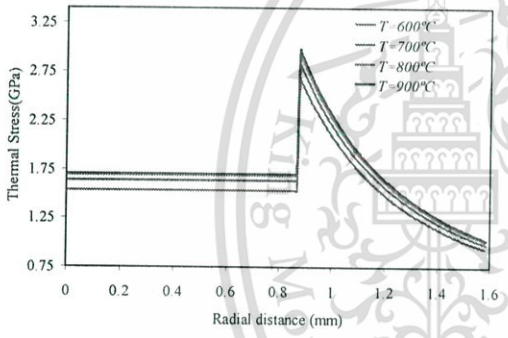

Figure 15. Thermal stress of gold sheathed in SS 316L.

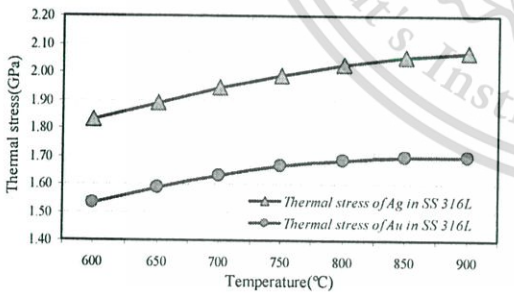

Figure 16. Thermal stress of Ag and Au in SS 316L as a function of temperature.

The thermal stress of Ag in SS 316L was continually increased when the temperature was increased as shown in Fig.16. In the same condition, the thermal stress of Au in SS 316L was found to be lower than the thermal stress of Ag in SS 316L.

Conclusions

Experiments showed that inter-diffusion of Fe, Au (Ag), Cr and Ni occur as investigated from Au sheathed in SS 316L at above 950°C. According to the simulation result, the thermal stress of Ag in SS 316L is higher than that of Au in SS 316L because Ag expands greater than Au. In addition, the thermal stress between Fe, Cr, Ni and Ag have a little effect on Inter-diffusion.

Acknowledgment

This work was supported by National Metal and Materials Technology Center (MTEC), National Science and Technology Development Agency (NSTDA-Alternative Energy Cluster) and Thailand Advanced Institute of Science and Technology (TAIST-Tokyo Tech).

References

1. Ho, S. C.Y., Powell, R.W. and Liley, P.E. 1972. Thermal conductivity of the elements. *J. Phys. Chem. Ref.* Data, **1** : 279.

2. Waterhouse, N. and Yates, B. 1968. The interferometric measurement of the thermal expansion of silver and palladium at low temperatures. *Cryogenics*. **8(5)** : 267-271.

3. Nix, F.C. and MacNair, D. 1941. The Thermal Expansion of Pure Metals : Copper, Gold, Aluminum, Nickel, and Iron. *Am. Phys. Society*. **60** : 597-605.

4. Owen, E.A. and Yates, E.L. 1934. *Phil. Mag.* **17** : 113

5. Wolfenden, A. and Harmouche, M.R. 1993. Elastic-constants of silver as a function of temperature. *J. Mater. Sci.* **28** : 1015-1018.

6. Smith, D.R. and Fickett, F.R. 1995. Low-Temperature properties of silver. *J. Res. Natl. Inst. Stand. Technol.* **100** : 119

7. Collard, S. M. and McLellan, R. B. 1948. High-temperature elastic constants of gold single-crystals. *Acta. Metall. Mater.* **39(1)** : 3143-3151.

8. Sakai, S., Tanimoto, H., Otsuka, K., Yamada, T., Koda, Y., Kita E. and Mizubayashi, H. 2001. Elastic behaviors of high density nanocrystalline gold prepared by gas deposition method. *Scripta Mater*. **45(11)** : 1313-1319.

9. COMSOL, Commercial Software. **3.4**

10. Bakker, H., Bonzel, H.P., Bruff, C.M., Dayananda, M. A., Gust, W., Horvath, J., Kaur, I., Kidson, G.V., Le Claire, A.D., Mehrer, H., Murch, G.E., Neumann, G., Stolica, N. and Stolwijk, N.A. Diffusion in Solid Metals and Alloys. Numerical Data and Functional Relationships in Science and Technology. *LANDOLT-BORNSTEIN*. **26**

BIOGRAPHY

Name: Mr. Manop Masomtob

Date of Birth: November 2, 1979

Place of Birth: Bangkok, Thailand

Education:

1994 – 1997	Vocational in Automotive, Samutprakran Technical College
1997 – 1999	Diploma in Mechanical Power, Rajamangala University of Technology Krungthep
2000 – 2003	B. Eng. in Mechanical Engineering, Faculty of Engineering, King Mongkut's Institute of Technology Ladkrabang (KMITL)
2003 – 2007	M. Eng. in Mechanical Engineering, Faculty of Engineering, King Mongkut's Institute of Technology Ladkrabang (KMITL)
2007 – 2010	M. Eng. in Automotive Engineering (International program), International College, King Mongkut's Institute of Technology Ladkrabang (KMITL)

Honour and Scholarships:

2006	Awarded 1st prize in "research, design and development vehicle use alternative energy type engine use Gasohol E-20" in Society of Automotive Engineers Thailand Auto Challenge 2006
2006	Awarded 2nd prize in "research, design and development vehicle use alternative energy type Electrical Vehicle" in Society of Automotive Engineers Thailand Auto Challenge 2006
2007-2009	Full scholarship for study in the master degree from National Science and Technology Development Agency (NSTDA)

Publications:

1. ***M. Masomtob***, N. Chaithanee, K. Suppavattanagool, S. Khuansaeng-arun, P. Chara, R. Suwanwarangkul and S. Charojrochkul "Use of Ultrasonic Humidifier to Increase Performance of Proton Exchange Membrane Fuel Cell (PEMFC)", orally presented in the National Conference on "The 23th Conference of Mechanical Engineering Network of Thailand", Chiang Mai University, 2008, Thailand.

2. ***M. Masomtob***, K. Wongtida,J. Charoensuk and S. Charojrochkul, "Improved Electrical Conducting Wires for SOFCs" orally presented in the International Conference on "Smart Materials Smart/Intelligent Materials and Nanotechnolgy (Smartmat-'08)", 22-25 April 2008, Chiang Mai, Thailand. And, Published in journal Advanced Materials Research Vols. 55-57(2008) pp 797-800 in www.scientific.net

3. ***M. Masomtob***, K. Wongtida, K. Hanamura, J. Charoensuk and S. Charojrochkul "High Temperature Behaviour of Contact Interface for Ag and Au with Stainless Steel 316L" orally presented in the National Conference on "5th Thailand Materials Science and Technology Conference", 2008, Bangkok, Thailand.

4. P. Onbhuddha, ***M. Masomtob*** and S. Charojrochkul "Characterization of $Ce_{0.8}Gd_{0.2}O_{1.9}$ catalyst support for solid oxide fuel cells", poster in the National Conference on "5th Thailand Materials Science and Technology Conference", 2008, Bangkok, Thailand.

5. ***M. Masomtob***, R. Suwanwarangkul, N. Chaithanee and S. Charojrochkul, "Stack Fabrication and Test Station Development of 500-W Proton Exchange Membrane Fuel Cell System for Commercial Production in Thailand", orally presented in the National Conference on "The 18th Thailand Chemical Engineering and Applied Chemistry Conference", 2008, Thailand.

6. N. Punbusayakul, ***M. Masomtob***, P. Onbhuddha, J. Charoensuk and S. Charojrochkul "Performances of proton Exchange Membrane Fuel Cell(PEMFC) from Increasing Inlet Pressure of Hydrogen", orally presented in the National Conference on "The 22th Conference of Mechanical Engineering Network of Thailand", Thammasat University, 2008, Thailand.

7. W. Boonjob, N. Punbusayakul, R. Beckett, ***M. Masomtob***, K. Wongtida, S. Charojrochkul and W.Veerasai, "Combination of Electrochemical Impedance Spectroscopy and Cyclic Voltammetry to Investigate Oxygen Ion Transport in YSZ Electrolyte of SOFC", Solid Oxide Fuel Cells 10 (SOFC-X), Japan.

Publications (con):

8. ***M. Masomtob***, J. Charoensuk, V. Jayranaiwachira and S. Gerdpratoom "Effect of the Geometry of Hollow Stirrers on Aeration into Water" orally presented in the National Conference on "The 19th Conference of Mechanical Engineering Network of Thailand", Prince of Songkla University, Thailand.